Karlsruhe Institute of Technology

Switchable Block Copolymer Systems for Reversible Membrane Encoding

Zur Erlangung des akademischen Grades eines
DOKTORS DER NATURWISSENSCHAFTEN
(Dr. rer. nat.)

von der KIT-Fakultät für Chemie und Biowissenschaften
Karlsruher Institut für Technologie (KIT)

genehmigte
DISSERTATION
von

Dipl. Chem. Marcel Langer

aus
Heidelberg, Deutschland

KIT-Dekan:	Prof. Dr. Willem M. Klopper
Referent:	Prof. Dr. Christopher Barner-Kowollik
Koreferent:	Prof. Dr. Michael A. R. Meier
Tag der Mündlichen Prüfung:	21.10.2016

Die vorliegende Arbeit wurde im Zeitraum von November 2012 bis August 2016 im Rahmen einer BMBF Kollaboration zwischen dem KIT und der Universität Jena (Prof. Dr. Schacher) unter der Betreuung von Prof. Dr. Christopher Barner-Kowollik angefertigt.

It Ain't Over 'Til It's Over

Rocky Balboa (Rocky Balboa)

Zusammenfassung der Doktorarbeit

Die vorliegende Arbeit beschreibt die Entwicklung eines neuartigen Konzepts zur Herstellung von nano-porösen Blockcopolymer-Membranen mit modifizierbarer Oberflächenchemie. Grundlage des Konzepts ist die modulare Synthese von amphiphilen Blockcopolymeren mit einer schaltbaren Verknüpfung. Bei der Verwendung solcher Blockcopolymere zur Membranherstellung kann im Anschluss der polare Block von der Oberfläche der Membran entfernt werden. Anschließend lassen sich die gewünschten Komponenten, entsprechend der jeweiligen Verwendung der Membran, wieder an die Oberfläche anbinden.

In diesem Zusammenhang wurde zum ersten Mal die thermoreversieble hetero-Diels–Alder (HDA) Chemie zur Herstellung von amphiphilen Blockcopolymeren verwendet. Außerdem konnte die HDA-Reaktion erstmals dazu verwendet werden, wasserlösliche Polymere in einem definierten Muster im µm-Bereich auf Oberflächen anzubinden. Des Weiteren wurde HDA und lichtinduzierte Konjugationschemie in einem neuen Kettentransfer-Agens (engl. chhain transfer agent, CTA) kombiniert, was die einfache Herstellung von triblockterpolymeren in drei Schritten ermöglicht.

Die reversible Addition-Fragmentierung-Kettentransfer-(engl. reversible addition-fragmentation chain transfer, RAFT) Polymerisationsmethode wurde benutzt, um die jeweiligen Bausteinpolymere herzustellen. Zur Herstellung des hydrophoben Bausteinpolymers wurde ein Brom-funktionales RAFT-Agens in einer Copolymerisation von Isopren und Styrol verwendet. Nach der Polymerisation wurde das Brom durch Cyclopentadien (Cp) substituiert, um ein reaktives Dien an einer Endgruppe einzuführen. Zur Herstellung der hydrophilen Bausteinpolymere wurden Triethylenglycol-methylether Acrylat (engl. triethylene glycol methyl ether acrylate, TEGA), Hydroxyethyl Acrylat (engl. hydroxyethyl acrylate, HEA) und Acrylsäure (engl. acrylic acid, AA) mittels eines HDA fähigen RAFT-Agens polymerisiert.

Zur Untersuchung des thermischen Verhaltens der HDA Verbindung zwischen der RAFT-Endgruppe der hydrophilen Bausteinpolymere und der Cp-Endgruppe des hy-

drophoben Bausteinpolymers wurde ein Poly(Isopren-*co*-Styrol)-*block*-Poly(Triethylenglycol-methylether Acrylat) (P(I-*co*-S)-*b*-PTEGA) Diblockterpolymer mit niedrigem Molekulargewicht (M_n = 16 000 g mol^{-1}) hergestellt und ausführlichen Hochtemperatur-Kernspinresonanzspektroskopie- (engl. high temperature nuclear magnetic resonance, HT-NMR), Hochtemperatur-Größenausschluss-Chromatographie- (engl. high temperature size exclusion chromatography, HT-SEC) und Hochtemperatur dynamischer Lichtstreuungs- (engl. high temperature dynamic light scattering, HT-DLS)-analysen unterzogen. Desweiteren wurde ein P(I-*co*-S)-*b*-PTEGA Diblockterpolymer mit hohem Molekulargewicht (M_n = 68 000 g mol^{-1}) hergestellt und in einem makroskopischen Spaltungsexperiment verwendet.

Um die Vielfalt der möglichen Membranmodifikationen weiter zu erhöhen, wurde ein doppel-funktionelles RAFT-Agens entwickelt, welches in der Lage ist, α,ω-funktionelle Polymere zu generieren, die wiederum dazu fähig sind, nacheinander effektive, thermisch- und lichtinduzierte Konjugationsreaktionen einzugehen. Durch eine HDA Reaktion mit Cyclopentadien kann die C=S-Doppelbindung der RAFT-Endgruppe geschützt werden. Anschließend wird durch die lichtinduzierte Konjugationsreaktion ein zweiter Polymerblock an das α,ω-funktionelle Polymer geknüpft. Nach der Entfernung der Cyclopentadien-Schutzgruppe durch Erhitzen entsteht ein Diblockcopolymer, welches sich mittels der wieder verfügbaren HDA fähigen RAFT-Endgruppe auf Cp-funktionelle (Membran-)Oberflächen anbringen lässt. Zur Demonstration der Einsatzvielfalt des doppel-funktionellen RAFT-Agens wurde ein amphiphiles Triblockquaterpolymer, Poly(Isopren-*co*-Styrol)-*block*-Poly(Ethyl Acrylat)-*block*-Poly(Ethylenoxid) (P(I-*co*-S)-*b*-PEA-*b*-PEO), hergestellt.

Nano-poröse Blockcopolymer-Membranen wurden durch Verwendung des P(I-*co*-S)-*b*-PTEGA Diblockterpolymer mit hohem Molekulargewicht, mittels des Selbstorganisations- und nicht-Lösungsmittel induzierten Phasenseparations- (engl. self-assembly and nonsolvent induced phase separation, SNIPS) Prozesses hergestellt. Jedoch waren die erhaltenen Membranen sehr fragil und wiesen nur sehr kleine Poren auf. Deshalb wurde ein weiteres Diblockterpolymer mit einem kleineren PTEGA-Block synthetisiert und der Membran-

herstellung durch SNIPS unterzogen. Auf diese Weise ließen sich dickere Membranen mit größeren Poren generieren.

Das Abspalten des polaren Blocks von der Oberfläche der Membran wurde durch Eintauchen in 50 °C heißes Wasser erreicht. Die Morphologie der Membran wurde durch das Verfahren nicht beeinflusst. Die Kinetik der Abspaltung wurde mittels NMR Spektroskopie verfolgt.

Die Fähigkeit der hydrophilen Bausteinpolymere (PTEGA, PHEA und PAA) im wässrigen Medium an Cp-funktionelle Oberflächen in einer poren-ähnlichen Umgebung zu knüpfen, wurde durch Mikroabformung in Kapillaren (engl. micromolding in capillaries, MIMIC) getestet. Die erfolgreiche, kovalente Bindung der Polymere in den entsprechenden Mustern der angewendeten Kapillarstempel wurde mit Wasserkontaktwinkel-Messungen, Wasserdampfabscheidungs-Bilder, Röntgen-Photoelekronen-Spektroskopie (engl. X-ray photoelectron spectroscopy, XPS), Rasterkraftmikroskopie (engl. atomic-force microscopy, AFM) und Flugzeit-Sekundärionenmassenspektrometrie (engl. time-of-flight secondary ion mass spectrometry, ToF-SIMS) nachgewiesen.

Abstract

The development of a new concept for the preparation of nanoporous block copolymer membranes with adjustable surface chemistry is reported. The foundation of the concept is the modular synthesis of amphiphilic block copolymers with a switchable linkage between the individual blocks. After membrane formation, employing these kind of block copolymers, the polar block on the surface of the membrane can be cleaved off and new components with any desired functional group can subsequently be grafted onto the surface.

In this context, the thermo switchable hetero Diels–Alder (HDA) chemistry was used for the first time to prepare an amphiphilic block copolymer. Moreover, it was accomplished to employ the HDA reaction for the grafting of water soluble polymers on surfaces in defined patterns in µm scale. Furthermore, HDA and light induced ligation chemistry was combined in a novel chain transfer agent (CTA), which enables the facile preparation of triblock terpolymers within three steps.

The reversible addition-fragmentation chain transfer (RAFT) polymerization technique was used for the preparaton of the building block polymers. A bromine functional RAFT agent was employed for the copolymerization of isoprene and styrene, generating the unpolar building block after substitution of the bromine with a cyclopentadiene (Cp) moiety. A HDA capable RAFT agent was used to polymerize triethylene glycol methyl ether acrylate (TEGA), hydroxyethyl acrylate (HEA) and acrylic acid (AA), yielding the polar building blocks.

For the investigation of the thermal behavior of the HDA linkage between the RAFT end group of the polar blocks and the Cp moiety of the unpolar block, a low molecular weight (M_n = 16 000 g mol^{-1}) poly(isoprene-*co*-styrene)-*block*-poly(triethylene glycol methyl ether acrylate) (P(I-*co*-S)-*b*-PTEGA) diblock terpolymer was prepared and employed in detailed high temperature nuclear magnetic resonance (HT-NMR) spectroscopy, high temperature size exclusion chromatography (HT-SEC) and high temperature dynamic light scattering (HT-DLS) analyses. Moreover, a high molecular weight (M_n =

68 000 g mol^{-1}) analogue of the P(I-*co*-S)-*b*-PTEGA diblock terpolymer was prepared and subsequently subjected to a macroscopic cleavage experiment.

In order to further increase the variety of possible membrane modifications, a dual functional RAFT agent, capable of highly efficient sequential thermal and photo induced ligation, generating α,ω-functional polymers, was developed. A HDA reaction with cyclopentadiene can be used as protection of the reactive C=S-double bond. After photo ligation of the α,ω-functional polymers with a second polymer block, the cyclopentadiene can be removed at elevated temperatures and the HDA capable RAFT end group is accessible again. Thus, the so generated block copolymers can be grafted onto a Cp-functionalized (membrane) surface. To exemplarily demonstrate the versatility of the dual functional RAFT agent, an amphiphilic triblock quaterpolymer poly(isoprene-*co*-styrene)-*block*-poly(ethyl acrylate)-*block*-poly(ethylene oxide) (P(I-*co*-S)-*b*-PEA-*b*-PEO) was prepared.

Nanoporous membranes were generated from the high molecular weight P(I-*co*-S)-*b*-PTEGA diblock terpolymer *via* the self-assembly and nonsolvent induced phase separation (SNIPS) process. The resulting membranes were very fragile and featured only small pores. Thus, another diblock terpolymer with a smaller PTEGA block was synthesized and subjected to membrane formation. In this way, thicker membranes with larger pores could be generated.

Cleaving off the polar polymer from the surface of both generated membranes was achieved by immersion in 50 °C hot water. Importantly, the morphology of the membranes was not affected by the cleaving procedure. The kinetics of the reaction was followed by NMR spectroscopy.

The ability of the generated polar polymer blocks (PTEGA, PHEA and PAA) to attach to a cyclopentadienyl functional surface in aqueous media in a pore like environment was tested by micromolding in capillaries (MIMIC) on silicon wafers. The successful covalent functionalzation in the patterns of the applied stamps was confirmed *via* water contact angle measurements, vapor deposition analysis, X-ray photoelectron spectroscopy (XPS), atomic-force microscopy (AFM) and time-of-flight secondary ion mass spectrometry (ToF-SIMS).

Contents

1

Motivation and Aims

The access to clean water is of critical significance for every civilization. In industrialized countries, porous filtration membranes play a key role in meeting the ever-increasing demand for water.[1,2] Filtration membranes are utilized in urban water supplies to ensure viral clearance as well as in the pretreatment of seawater prior to desalination by reverse osmosis.[3,4] Another increasingly established application is the use in bioreactors for waste water treatment processes.[5] Besides the use in environmental applications, membranes find use in many other fields, for example in biological processes such as pharmaceutical separations, controlled release of therapeutic drugs or in biomedical engineering devices.[6] However, there are still challenges to overcome and future applications to be developed. Membrane reactors (the use of membranes as catalyst support) are one example of these future possibilities.[7] However, nonspecific adhesion and deposition of solutes on the surface of the membrane (fouling) is an ever-present problem for membrane processes.[8–10] Until now, the complete prevention of fouling has not been achieved for any type of membrane.[11] Indeed, for each specific feed stream encountering a membrane, the surface chemistry must be tailored accordingly.[12–14] The

complexity of this matter is further demonstrated by studies showing that a moiety on the surface of a membrane can reduce fouling for one feed stream, but reinforce it for another.[15–17]

Stating the importance of tailored surface chemistry for filtration membranes, the motivation and aim of the current thesis becomes clear. A novel concept for the preparation of recodable nanoporous block copolymer membranes *via* modular chemical ligation is developed (see Figure 1.1). The fundamental concept of the strategy is the

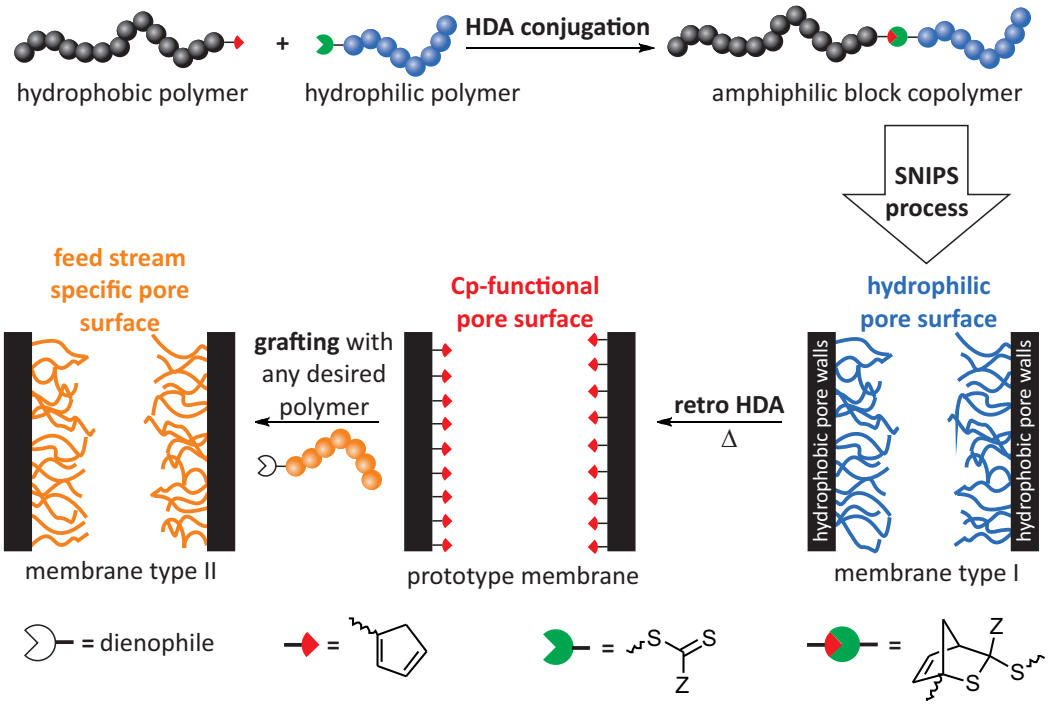

Figure 1.1 Concept for the preparation of nanoporous block copolymer membranes with feed stream specific pore surface *via* modular ligation chemistry.

modular synthesis of an amphiphilic block copolymer with a cleavable linkage, i.e. the reversible hetero Diels-Alder (HDA) reaction of a cyclopentadienyl (Cp) moiety with an electron deficient C=S-double bond from a chain transfer agent (CTA).[18–20] The polymer is employed in a self-assembly and nonsolvent induced phase separation (SNIPS) procedure (see Section 2.2.1) to generate a nanoporous filtration membrane (membrane type I). Subsequently, hot water (50 °C) is percolated through the membrane, inducing the retro HDA reaction and cleaving off the hydrophilic polymer chains on the pore surface. Thus, a prototype membrane with highly reactive Cp moieties on the surface

is generated. Consequently, any kind of polymer or molecule containing a dienophile (or even mixtures) can now be grafted onto the pore surface, generating a membrane whose surface chemistry features are tailored to the feed stream employed when in use (membrane type II). This method has the perspective to function as a new archetype for the preparation of nanoporous block copolymer membranes with application prospects in multiple areas.

2

Theoretical Background

The development of a modular strategy for the preparation of nanoporous block copolymer membranes combines multiple topics of polymer chemistry. The current chapter provides the theoretical background needed and describes the selection criteria for the chosen methods.

2.1 Modern Radical Polymerization Techniques

The preparation of polymers with a specific molecular weight, a narrow distribution and defined end groups is crucial for reaching the aims of the current thesis. According to these requirements, anionic polymerization is the most powerful technique.[21] However, anionic polymerization suffers from substantial restrictions such as a limited monomer choice associated with the required demanding experimental conditions.[22] Within the last decades, polymer chemists developed controlled radical polymerization (CRP) techniques that benefit from fewer limitations regarding the monomer choice and reaction conditions.[23] The International Union of Pure and Applied Chemistry (IUPAC)

uses the term reversible-deactivation radical polymerization (RDRP) for these techniques. In general, the control over the free radical polymerization (FRP) is gained by introducing a fast reaction that reversibly traps the radicals in a dormant state, competitive to the radical termination reactions (k_t). It needs to be mentioned that radical termination can never be completely suppressed, but in a contolled polymerization it is reduced to a non-significant rate. A rapid exchange between dormant species and propagating radical allows all polymer chains to grow simultaneously. A growing radical species ideally reacts, within a few milliseconds, only with a few monomer units (depending on the polymerization rate coefficient (k_p)), before it is trapped again in the dormant state for several seconds. The lifetime of growing chains during a polymerization is extended from nearly a second (in FRP) to several hours. Moreover, the generated polymers can be used for re-initiated chain growth in a subsequent polymerization. Besides these living characteristics, the rapid exchange between dormant and active species results in polymers with narrowly distributed molecular weight (typically a polydispersity index ($Đ$) below 1.5 is achieved) and high end group fidelity.

The most common CRP techniques, namely the nitroxide mediated polymerization (NMP), atom transfer radical polymerization (ATRP), and reversible addition-fragmentation chain transfer (RAFT) polymerization, are described in more detail in the following chapters.

2.1.1 Nitroxide-Mediated Radical Polymerization

Although other attempts were reported previously in the patent literature,[24] the first successfully conducted example of a CRP was reported by Georges in 1993.[25] Styrene was polymerized in the presence of the stable free radical 2,2,6,6-tetramethyl-1-piperidynyl-*N*-oxy (TEMPO), using benzoyl peroxide as initiator. A linear increase of molecular weight with conversion and polydispersities below 1.3 were observed. The explanation for this observation is the established equilibrium in NMPs (see Scheme 2.1). Nitroxide

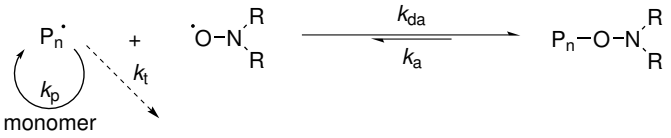

Scheme 2.1 Reaction equilibrium of the NMP process. Propagating radical chains are reversibly trapped by combination with persistent nitroxide radicals, generating dormant alkoxyamine species that are not affected by termination.

radicals react with the propagating chain radicals ($P_n^{\cdot}$) of the polymerization and generate a deactivated (dormant) alkoxyamine species. In order to suppress termination, the equilibrium of this reaction needs to be shifted strongly to the side of the dormant species. Therefore the deactivation rate coefficient (k_{da}) needs to be significantly larger than the activation rate coefficient (k_a). As a result, the concentration of the growing chain radicals is much smaller, compared to FRP. A termination reaction with two propagating chains is less likely to occur and the fast exchange between dormant and growing polymers induces the linear increase of molecular weight with conversion. Besides the addition of a free nitroxide control agent to a conventional radical polymerization, NMP can be induced *via* dissociation of a previously synthesized alkoxy amine as well. However, in order to effectively control the polymerization, the employed nitroxide radical has to meet certain criteria. Most important, it should not initiate the growth of new polymer chains nor react with itself. Moreover, the nitroxide radical should not induce any side reactions such as the abstraction of β-H atoms. The molecular structures of four commonly used nitroxides in NMP are depicted in Figure 2.1. Initially, NMP required high temperatures (up to 130 °C) and was limited to monomers that withstand the heat. Over time the

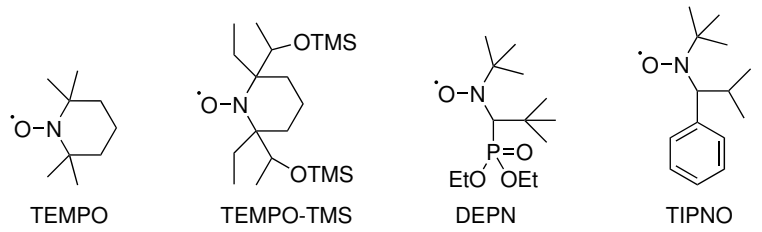

Figure 2.1 Molecular structures of commonly used nitroxides for NMP.

development of nitroxides like 2,2,5-trimethyl-4-phenyl-3-azahexane-*N*-oxyl (TIPNO) or 4-(diethoxyphosphinyl)-2,2,5,5-tetramethyl-3-azahexane-*N*-oxyl (DEPN, also known as SG-1) improved the selection of monomers and enabled polymerizations at more moderate temperatures.[26–28] By lowering the bond dissociation energy of the alkoxyamine with the introduction of significant steric bulky moieties to TEMPO derivatives such as *trans*-2,6-diethyl-2,6-bis(1-trimethylsilanoxyethyl)-1-(1-phenylethoxy)piperidine-*N*-oxyl (TEMPO-TMS), the temperature needed for a successful mediation could be reduced to 70 °C.[29,30] Furthermore, NMP at ambient temperature was achieved *via* photo-induced radical polymerization.[31,32] However, a major drawback of NMP is the long reaction time compared to FRP, caused by the lower radical concentration.

2.1.2 Atom Transfer Radical Polymerization

ATRP is based on a frequently used reaction in organic synthesis known as the atom transfer radical addition (ATRA, see Scheme 2.2).[33] Organic halides (X) are transferred

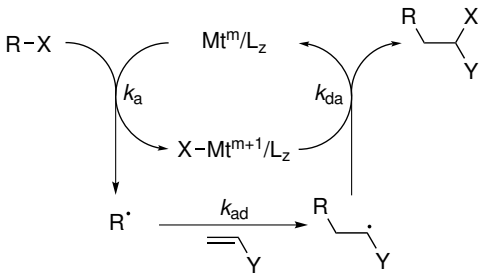

Scheme 2.2 Mechanism of an ATRA reaction. L = ligand.

to transition metal (Mt) complexes, generating radicals (R$^{\cdot}$). After reacting with an individual vinyl species the radical is terminated rapidly by back-transfer of the halide from the transition metal complex. Although the possibility of a vinyl polymerization was already stated in 1975 as a potential side reaction, it took 20 more years until Matyjaszewski and Sawamoto used this concept for CRP in 1995.[34,35] The key feature of ATRP is similar to NMP, although achieved in a different manner. An equilibrium between growing polymer chain radicals and reversibly halide (typically bromine) terminated polymer chains (dormant species) is established by a transition metal mediated redox system (see Scheme 2.3). Again, to achieve a good control over the polymerization,

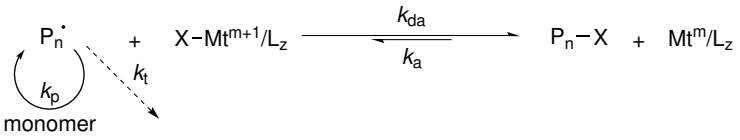

Scheme 2.3 Reaction equilibrium of the ATRP process. Propagating radical chains are reversibly trapped by combination with a halide provided by a transition metal complex, generating dormant polymer chains with a halide terminus that are not affected by termination.

the deactivation rate coefficient needs to be significantly larger than the activation rate coefficient.[36] Therefore, the equilibrium has to be shifted strongly to the side of dormant chains. Over time, many transition metals (Ti,[37] Mo,[38] Re,[39] Fe,[40] Ru,[35] Os,[41] Rh,[42] Co,[43] Ni,[44] Pd[45]) were employed in ATRP. However, copper complexes

proved to be most efficient and versatile.[46] To adjust the conditions for different types of monomers, the initiator (an alkyl halide), ligands and solvent are chosen appropriately. A major advantage compared to other CRP techniques was that since at the time of its invention all necessary reagents were already commercially available. However for a long time, ATRP also suffered from two major drawbacks, compared to the other CRP techniques. It was much more sensitive towards oxidants, such as oxygen, and the removal of employed transition metals from the produced polymers was sophisticated. Modern modifications of ATRP such as the activator regenerated by electron transfer (ARGET) alternative improved the control of polymerization and reduced the sensitivity towards oxygen, as well as the amount of copper that is required, to a minimum.[47,48] This is achieved by addition of an appropriate reducing agent that constantly regenerates the oxidized catalyst species. Furthermore, an efficient and versatile method to remove copper completely has been developed.[49] However, among other reasons presented in the following section, ATRP was not employed in the current project because it cannot provide good control for the polymerization of isoprene.[50] As explained in section 3.1, isoprene is an important component for the hydrophobic polymer block.

2.1.3 Reversible Addition-Fragmentation Chain Transfer Polymerization

In 1998, researchers of the Commonwealth Scientific and Industrial Research Organization (CSIRO) in Australia invented the RAFT polymerization.[51] They reported that FRP can be controlled by the addition of dithioesters. At the same time a similar method was developed by a French research group, using xanthates as control agents (MADIX).[52] However, the RAFT concept is more general, includes xanthates in a broader sense and is based on dithioester compounds - so called RAFT agents (see Figure 2.2). In general, the moiety of the RAFT-agent which is bonded to the carbon of the C=S-double bond is called Z-group (-OR for xanthates). The moiety which is connected with the sulfur of the dithioester is termed R-group. Purpose and influence of these groups on the RAFT process and employed structures are discussed later in this section.

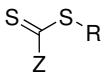

Figure 2.2 General structure of a RAFT agent.

The control of the polymerization is based on the establishment of an equilibrium between active and dormant species obtained by reversible transfer reactions (see Scheme 2.4). In the pre-equilibrium phase at the beginning of the polymerization, polymer chain radicals add to the sulfur of the C=S-double bond of the dithioester of the RAFT agent and form an intermediate radical. Now two options are available for the intermediate radical to fragment. Either the addition is reversed, or the R-group of the RAFT agent is expelled *via* β-scission, generating a macro RAFT agent. For a well controlled RAFT polymerization the β-scission rate coefficient (k_β) is larger than the fragmentation rate coefficient (k_{frag}). Thus, the R-group should be a better leaving group than the attached polymer chain. Moreover, the expelled R-group radical has to be able to re-initiate polymer chain growth. For an efficient fragmentation and re-initiation, the radical formed after β-scission of the R-group should be slightly more stable than the radical of the growing polymer chain. Otherwise the polymerization will either be inhibited (*i.e.* R-group radical to stable to re-initiate) or the polymerization does not proceed in a

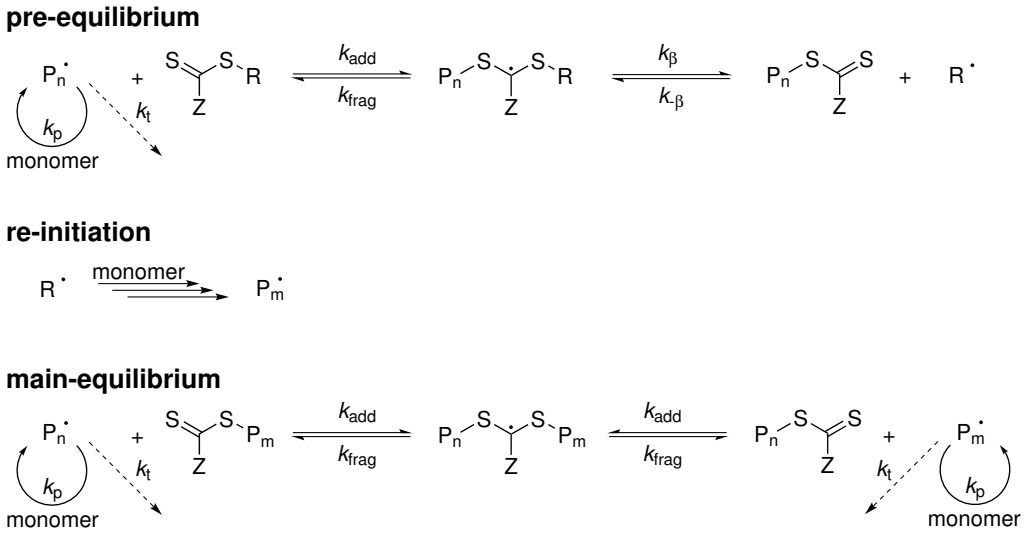

Scheme 2.4 General mechanism of the RAFT process. The transfer reactions in the pre-equilibrium and the main-equilibrium phase of the polymerization compete with the termination reactions.

controlled manner (no β-scission fragmentation takes place, polymer chain radicals are not transformed to dormant state). However, often the initial inhibition is overcome after a while, when all RAFT agents have their R-group substituted by a polymer chain and there is still sufficient initiator left in the polymerization mixture.[53] A series of R-groups with different leaving abilities is depicted in Figure 2.3. After a certain time, all RAFT

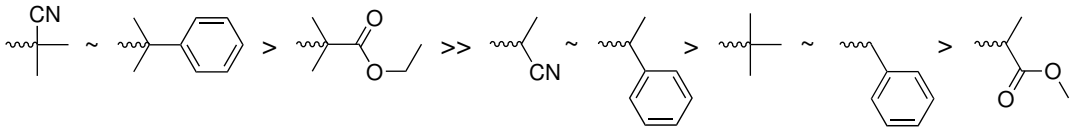

Figure 2.3 Series of R-groups in order of leaving ability.

agents in the polymerization mixture carry polymer chains instead of the initial R-group and the main-equilibrium is established. Now, after addition of a polymer chain radical to a macro RAFT agent, the formed intermediate radical expels the two attached polymer chains with equal probability. All polymer chains with a RAFT agent end group can be considered as dormant species. For every growing chain that is trapped, another polymer chain radical is released. For a well controlled RAFT polymerization the concentration of growing chain radicals is equal to FRP conditions. This is a major advantage of RAFT

compared to the CRP techniques described before. Moreover the technique is applicable to a wide range of monomers. The vast majority of the generated polymers carries the dithioester moiety at α- and the R-group at ω-position. Termination is not suppressed by a low radical concentration, but by the implementation of the transfer reaction, or rather the addition to the (macro) RAFT agent, which is a several magnitudes faster competing reaction. The addition rate coefficient (k_{add}) strongly depends on the Z-group and has to be adjusted respectively to the selected monomer.[54] Fast propagating monomers, such as vinyl esters, require weakly stabilizing Z-groups such as O-alkyl in xanthates. The use of strong stabilizing groups, like phenyl (Ph), inhibits the polymerization of these type of monomers. In contrast, slow propagating monomers such as styrene or methacrylates demand a good stabilization of the intermediate radical, otherwise the addition rate coefficient is not sufficient large to compete with the termination reaction. A series of common Z-groups with different stabilization abilities is shown Figure 2.4.

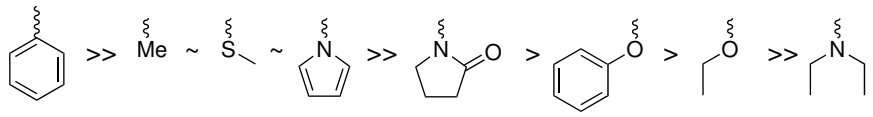

Figure 2.4 Series of Z-groups in order of stabilizing ability.

Besides inhibition and loss of control, the phenomena of retardation can be observed for ill chosen RAFT agent/monomer combinations, especially at high CTA concentrations. As an example, significant retardation occurs at the polymerization of acrylates with dithiobenzoate esters, but not when dithioacetates or other alkyl dithioesters are employed as transfer agent.[55,56] The origins of this effect were debated intensively and are still point of ongoing discussion.[57–60] In principle, two hypotheses (based on simulation results) are discussed how a lower total macroradical concentration can originate and thus, induce a retardation. One of them is the *slow fragmentation* hypothesis which relates to the observation that a too low fragmentation rate of the RAFT intermediate radical leads to an accumulation of this species and, hence, to a rate retardation.[61] The *intermediate radical termination* hypothesis states that such a rate retardation can also be obtained by a higher fragmentation rate of the RAFT intermediate radical in

combination with cross-termination events, resulting in the formation of (multi-arm) dead species and thus lowering the total macroradical concentration.[62] Both hypotheses have been tested for the relevant RAFT polymerization systems with a broad range of analytical methods, including mass spectrometry,[63,64] size exclusion chromatography (SEC),[65] nuclear magnetic resonance (NMR)[66,67] and electron paramagnetic resonance (EPR) spectroscopy.[60,68–71] Yet, existing discrepancies prevent a clear confirmation of one of the theories. For instance, although certain experimental studies[57,63] indicated that the cross-termination should be a valiable reaction pathway, the expected amount of dead multi-arm species is not observed in the obtained material of retarded RAFT polymerizations. On the other side, the combination of EPR with spin trapping has indicated that the lifetime of the RAFT intermediate radical species can be long while the concentration of intermediate radicals measured by EPR is overestimated upon consideration of slow RAFT fragmentation.[72,73]

To overcome this issue, several modified theories[74–76] were put forward, including modeling efforts in which only small radical species are involved in the cross-termination of the RAFT intermediate radical,[77–79] which was supported by experimental measurements of Ting *et al.*[80] However, thioketone mediated polymerization was utilized by Junkers *et al.* to demonstrate the viability of long living RAFT intermediate radicals even if cross-termination events are observed.[81] Moreover, Junkers and Barner-Kowollik highlighted the possible occurence of cross-propagation events that should be considered.[82] Furthermore, *ab initio* calculations were performed by Coote *et al.*, indicating a slow fragmentation for dithiobenzoate systems,[83,84] which is contrary to the findings of Meiser *et al.* by EPR-based kinetic modeling.[74,75] However, Junkers *et al.* noted in later studies that EPR data should be interpreted with care,[85] which is consistent with the report that the discrepancy between ab initio calculations and experimental data could be smaller than initially thought.[86]

RAFT agents with stability switchable Z-groups have been developed with the intention to create an universal RAFT agent for fast and slow propagating monomers.[87] However, block copolymers *via* sequential polymerization can only be prepared when the slower propagating monomer (with more stable chain radicals) is polymerized first.

An inverse order would not lead to block copolymers, because the formed intermediate radical of the macro RAFT agents would always expel the more stable radical. Thus, the polymer chains from the first polymerization with the less stable radicals would not be able to re-initiate a polymerization.

The number average molar mass (M_n) of the generated polymers can be adjusted and calculated by the ratio of RAFT agent to monomer and the conversion of the polymerization (see Equation 2.1).[88]

$$M_\mathrm{n} = conversion \cdot \frac{n_\mathrm{monomer}}{n_\mathrm{CTA}} \cdot M_\mathrm{monomer} + M_\mathrm{CTA} \tag{2.1}$$

Limitations for high molecular weights are reached when the concentration of CTA becomes so low that the transfer process cannot compete with the termination reaction any more and FRP prevails. Comparison of the calculated M_n with experimental data can indicate if a polymerization proceeds in a controlled fashion. Proof of control is achieved when, in addition to consistent values of calculated and experimental M_n, a linear evolution of M_n over the conversion is observed.

With the prospect of possible industrial application of the developed concept, RAFT was found to be the most suitable CRP technique, due to the wide range of accessible monomers, the rapid polymerization times and the convenient reaction conditions. An additional advantage in relation to ligation of polymers is described in Section 2.3.

2.2 Amphiphilic Block Copolymers

Amphiphilic block copolymers consist of at least one hydrophobic and one hydrophilic block. Two general approaches are possible for the preparation of linked polymer blocks. In the modular approach, pre-synthesized polymer building blocks are conjugated *via* efficient ligation techniques. A collection of conjugation methods employed in literature is presented in Section 2.3. In the second approach, polymerization techniques with living characteristics are used to polymerize several monomers sequentially. However, the choice of monomers in the sequential approach is (in general) limited by their reactivity. A chain extension is only possible when the precursor polymer is able to efficiently initiate a polymerization with the subsequently employed monomer. As an example, the preparation of a styrene and vinyl acetate block copolymer by using common RAFT agents is not possible.[89] In comparison, the modular approach does not feature such limitations. Thus, the range of monomer combinations and possible architectures is higher.

Regardless of the preparation approach, the different nature in polarity of the chosen monomer (or polymer) combination (which is essential to create amphiphilicity) can be problematic because of the solubility. For a successful block addition all components need to be in solution. Hence, the difference in polarity of the building blocks is limited. However, some strategies were developed to prepare block copolymers with components that are usually not soluble in the same solvent. One example is the successive aqueous solution and aqueous emulsion RAFT polymerization. Charleux *et al.* employed it for the preparation of poly(methacrylic acid-*co*-poly(ethylene oxide) methyl ether methacrylate)-*block*-polystyrene diblock terpolymers (see Scheme 2.5).[90] Both polymerizations can be performed in one-pot, isolation and purification of the first block is not necessary, making it a very feasible method for preparation of amphiphilic block copolymers.

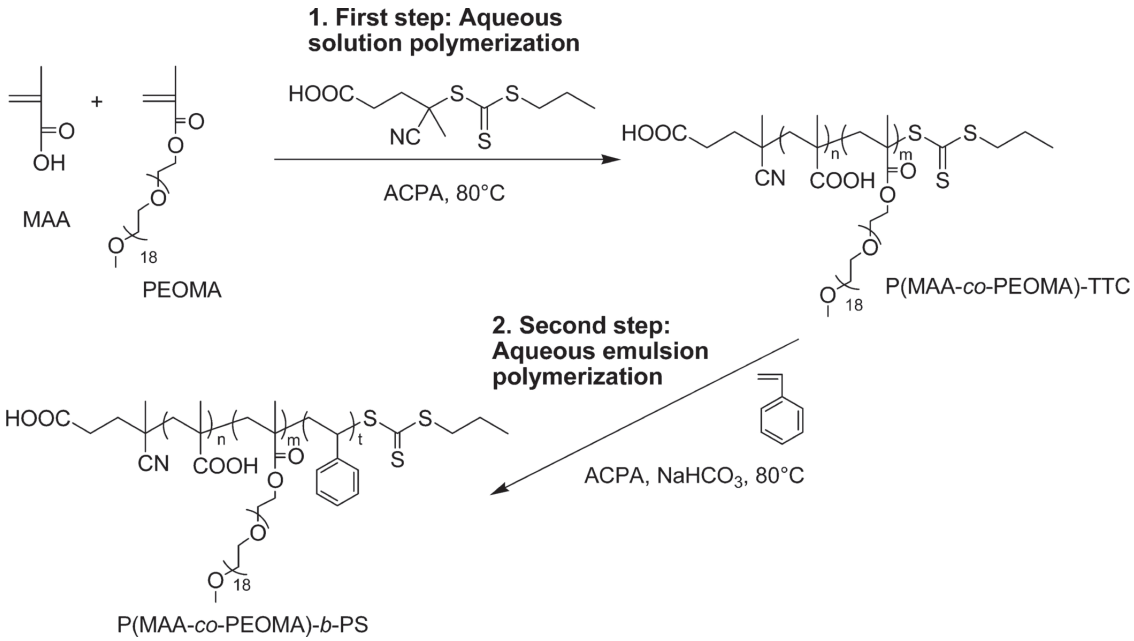

Scheme 2.5 Schematic representation of the one-pot synthesis of poly(methacrylic acid-*co*-poly(ethylene oxide) methyl ether methacrylate)-*block*-polystyrene, P(MAA-*co*-PEOMA)-*b*-PS, copolymers *via* successive aqueous solution and emulsion polymerizations. Reprinted with permission from [90]. Copyright 2011 American Chemical Society.

Another option is the use of host-guest complexation with cyclodextrin (CD) to make hydrophobic components water soluble.[91] The CD has a hydrophilic outer shell and a hydrophobic inner cavity that can enclose other hydrophobic moieties and thereby change their solubility. However, the approach is limited to hydrophobic monomers that are suitable guests for CDs. Moreover, Ritter and barner-Kowollik showed that due to the steric hindrance caused by the inclusion complex, the molecular weigt of the hydrophobic blocks that can be achieved is limited.[92] An additional method to generate block copolymers with a high amphiphilicity is to modify the polarity of a building block after the block copolymer formation.[93]

In general, an array of different architectures can be realized for (amphiphilic) block copolymers (see Figure 2.5). Linear AB, ABA, ABC, different star shaped or brush-like polymers represent only some examples.

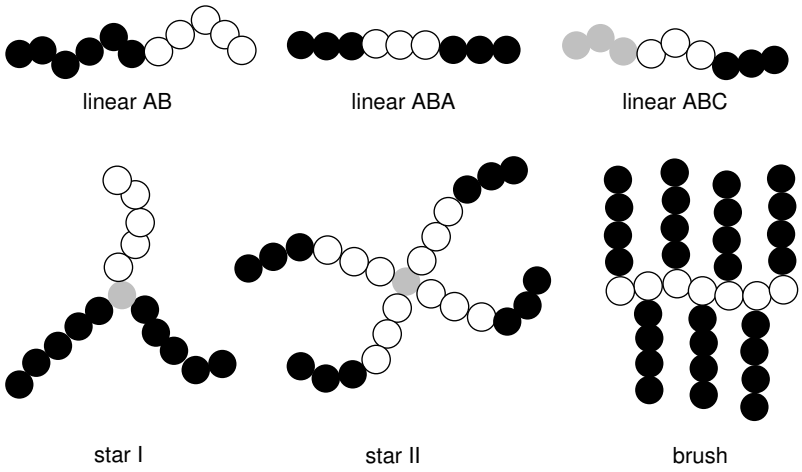

Figure 2.5 Examples for possible block copolymer architectures. The colors white, gray and black represent moieties with different polarities.

A characteristic property of all (amphiphilic) block copolymers is the tendency to self assemble in supramolecular structures. The reason for this behavior is the propensity of unlike polymers to separate in individual phases. However, the linkage between the segments prevents a macroscopic phase separation. Thus, block copolymers undergo microphase separation on the length scale of the constituting building blocks, creating supramolecular structures.[94,95] As the simplest representative, linear AB diblock copolymers have been studied extensively. It was found that in bulk the materials form spherical (S), cylindrical (C), gyroid (G), or lamellar (L) nanostructures, depending on the volume fraction of the blocks (see Figure 2.6). Block copolymers with a more

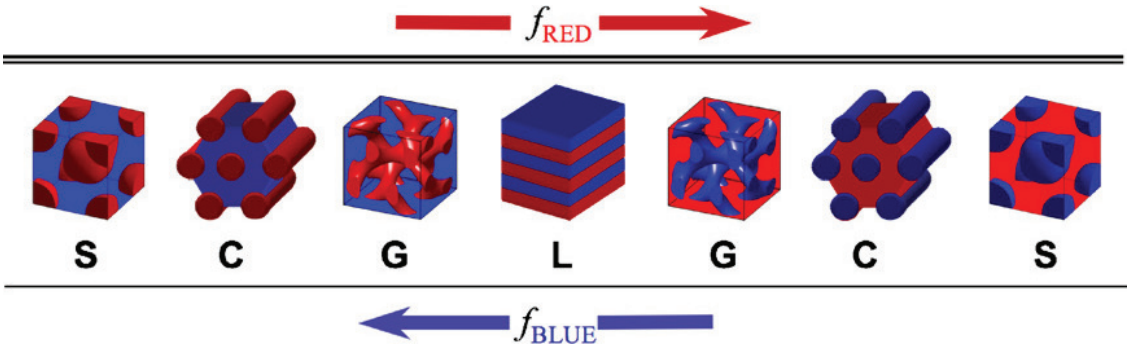

Figure 2.6 Diblock copolymer morphologies accepted to represent the equilibrium ordered states. Morphologies are shown in increasing red-block (decreasing blue) composition of a red-blue diblock copolymer. (S) Spheres, (C) hexagonally packed cylinders, (G) gyroid, (L) lamellae. Reprinted from [96] with permission from Elsevier.

complex architecture can form even more sophisticated nanostructures. Already only linear ABC triblock terploymers can form a myriad of structures.[97,98] For example, Abetz *et al.* demonstrated by transmission electron microtomography analysis that polystyrene-*block*-polybutadiene-*block*-poly(methyl methacrylate) (PS-*b*-PB-*b*-PMMA) triblock terpolymers can form double helical structures, arrayed in a honeycomb board perpendicular to the film plane (see Figure 2.7).[99] External stimuli, like an electric field,

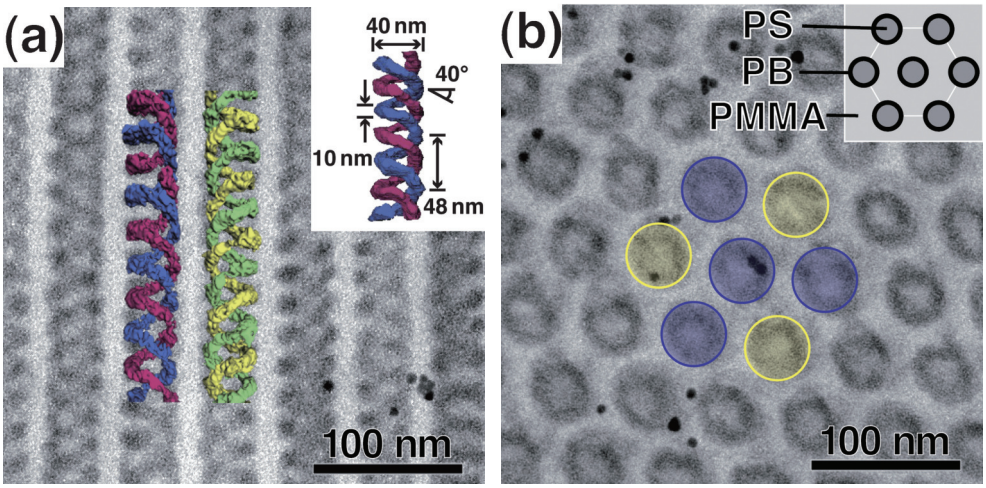

Figure 2.7 TEM micrographs of the SBM triblock terpolymer. OsO_4-stained PB microdomains appear in black. Two representative morphologies of the SBM terpolymer are shown in parts (a) and (b). As schematically shown in the inset of part (b), the PS cylinders with the PB helical microdomains are hexagonally packed in the PMMA matrix. 3D structures of the double helical structures are displayed on top of the TEM image in part (a). Left-handed and right-handed double helical structures were found and are shown by blue–red and green–yellow helices, respectively. The spatial arrangements of the left- and right-handed helices are also shown in part (b) by blue and yellow circles, respectively. Structural dimensions, *e.g.*, the helical pitch, *d*, diameter of the helix, *D*, etc., are demonstrated in the inset of (a). Reprinted from [99] with permission from Royal Society of Chemistry.

can guide the orientation of the nanostrucures in a macroscopic dimension.[100]

In aqueous solution, amphiphilic block copolymers can form various kinds of aggregates in order to achieve a state of minimum free energy (see Figure 2.8). At a low concentration, the polymer chains exist as unimers. When a certain concentration of polymer is exceeded (termed the critical micelle concentration, CMC), several unimers will aggregate into colloidal sized particles (10 - 100 nm) called micelles.[101] The hydrophilic part of the amphiphiles forms a corona while the hydrophobic part in the

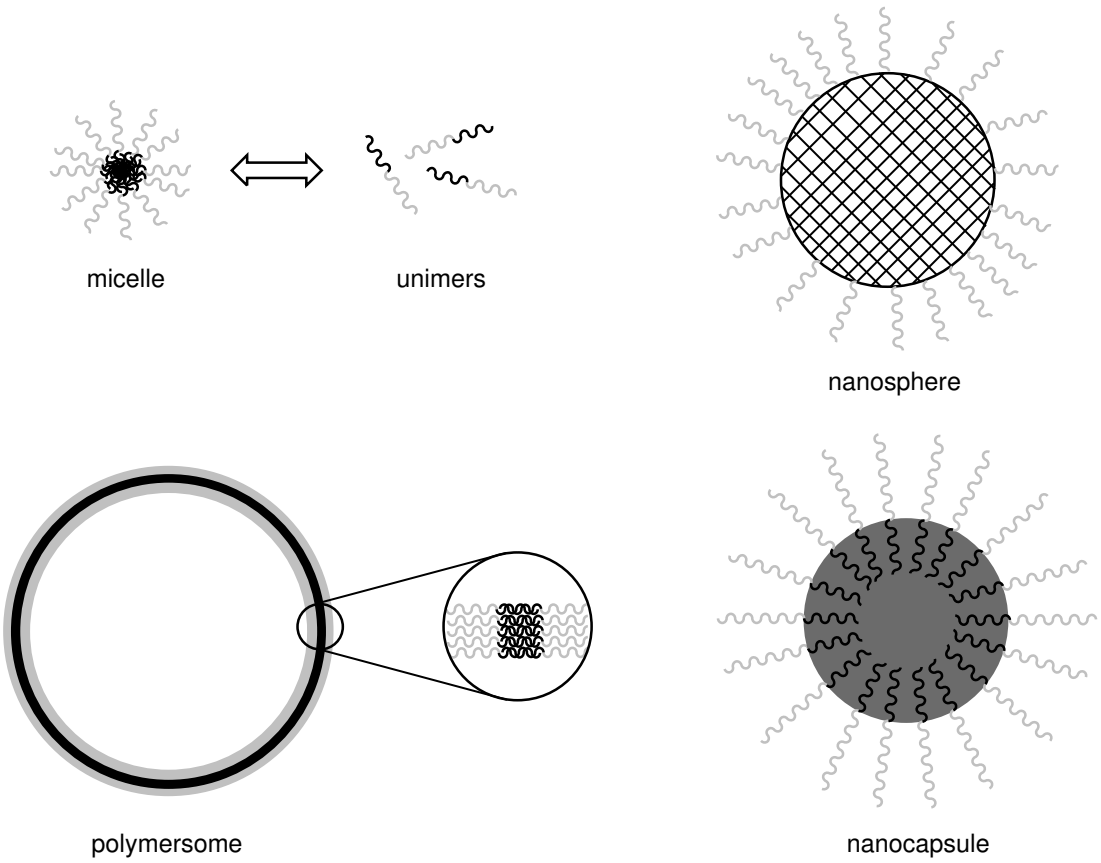

Figure 2.8 Aggregates formed by amphiphilic block copolymers in water. The black and dark gray color imply a hydrophobic character of the polymer chain/material, the light gray implies a hydrophilic character.

center is effectively protected from unfavorable interactions with the surrounding water molecules. Micelles are in a dynamic equilibrium with unimers in solution and should not be considered as solid particles.[102,103] However, due to the interactions between the chains in the hydrophobic core, in some cases micelles can persist even when the polymer concentration falls below the CMC, at least for some period of time.[104]

When phase separated structures with a solid core are formed, the term nanosphere is used.[105] The solid core of the nanosphere can be generated in different ways. Either another compound is chemically bound or adsorbed to the constituting polymer matrix, or the hydrophobic polymer block itself has a considerable high molecular weight and is the major component of the amphiphile.[106–109] Although the size of nanospheres

is typically larger than the size of micelles (100 - 200 nm), for block copolymer based nanoparticles a clear distinction between both forms is not always possible.[101]

Polymersomes and nanocapsules are vesicular systems in which a liquid reservoir is surrounded by a polymer membrane or coating (see Figure 2.8).[107] In case of nanocapsules, a core of hydrophobic liquid is surrounded by a single layer of polymer, whereby the hydrophilic part of the amphiphile forms the corona of the vesicle.[110] Typically the size ranges between 100 and 300 nm. If the core of the particle is water and the surrounding coating consists of a polymer bilayer, the vesicle is referred to as a polymersome (analog to liposomes).[111] The size of polymersomes can vary between 5 nm and 5 µm.

The self assembling nature of amphiphilic block copolymers in bulk and in solution is the basis for the broad range of possible application areas, *e.g.* in drug delivery systems,[112,113] separation and filtration systems[114] and electronic materials.[115] Especially in lithography applications, the selective removal of one of the polymer blocks (after nanostructuring) is often required.[116] Thus, several strategies have been developed, e.g. chemical etching[117], ozonolysis,[118] or degradation *via* UV radiation.[119] An example for the utilization of such removal strategies is the preparation of nanoporous SiO_2 gyroid structures reported by the group of Thomas (see Figure 2.9).[120] First, a polystyrene-

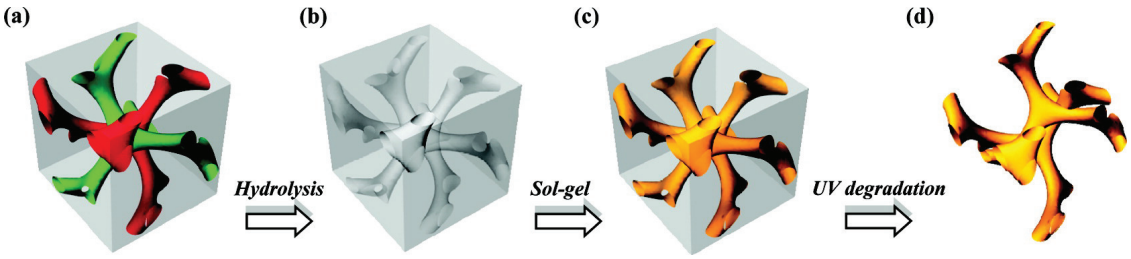

Figure 2.9 Schematic illustration for the creation of well-defined nanoporous gyroid SiO_2 from block copolymer templating. (a) PS-PLLA gyroid morphology (skeleton of double gyroid structure with two identical networks (green and red)). (b) Gyroid-forming nanoporous PS template after the removal of minority PLLA network. (c) PS/SiO_2 gyroid nanohybrids *via* the templated sol-gel process. (d) Nanoporous gyroid SiO_2 after the UV removal of PS template. Reprinted with permission from [120]. Copyright 2010 American Chemical Society.

block-poly(*L*-lactide) (PS-*b*-PLLA) block copolymer was used in a self-assembly process to generate a gyroid structured film. Subsequently, the PLLA block was removed *via* hydrolysis, obtaining a PS gyroid template. Then, the template was utilized in a sol-gel

process to prepare a SiO_2 gyroid network. In the end, the PS template was removed by UV radiation.

However, either the method is limited to specific materials or relatively harsh reaction conditions are required. The introduction of an efficiently cleavable junction between the polymer blocks and the use of distinct differences in solubility (in case of amphiphilic block copolymers) can remove such limitations and alleviate the required conditions. Russell *et al.* synthesized a polystyrene-*block*-poly(ethylene oxide) (PS-*b*-PEO) block copolymer with a triphenylmethyl (trityl) ether linkage, which can readily be cleaved under acidic conditions, between the individual polymer blocks (see Figure 2.10 (a)).[121] The block copolymer was used to generate thin films with highly ordered PEO cylinders

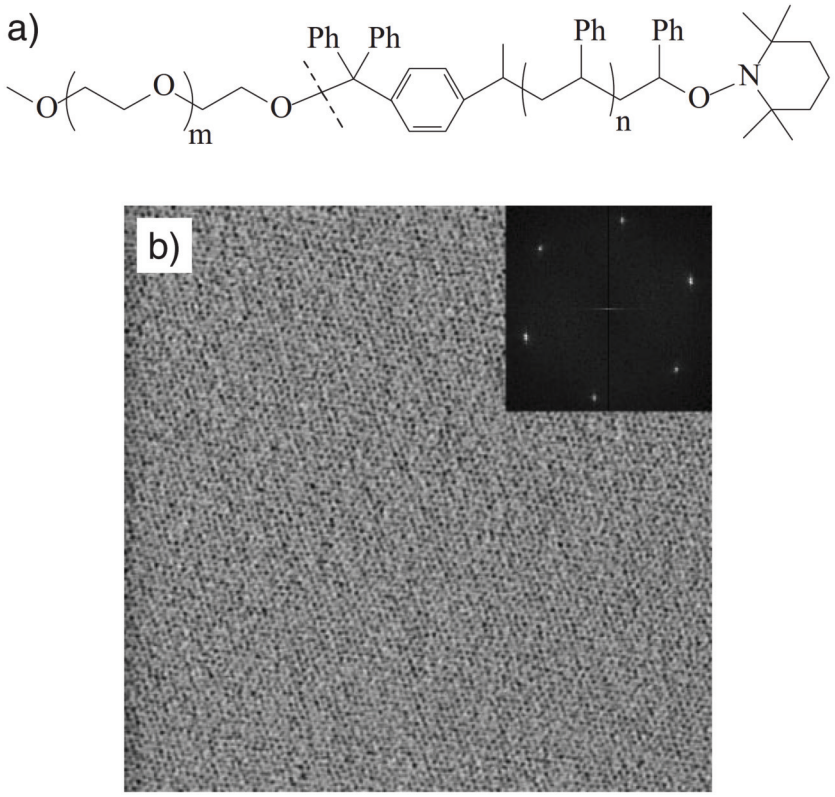

Figure 2.10 a) Chemical structure of cleavable PS-*b*-PEO (the dash line shows the point where scission occurs); b) Scanning force microscopy (SFM) phase image (2 lm×2 lm) of PS-b-PEO thin film (ca. 25 nm) containing KI (O/K = 64) on silicon wafer after solvent-annealing for 48 h. The inset shows the corresponding Fourier transform. Reprinted from [121] with permission from John Wiley and Sons.

(see Figure 2.10 (b)). Subsequently, the PEO block was removed by exposure of the thin

film to TFA vapor and washing with methanol, yielding highly ordered nanoporous thin films.

Another facile method for the preparation of highly orderen nanoporous thin films *via* amphliphilic block copolymers was demonstrated by Theato *et al* (see Figure 2.11).[122] This time the linkage of the synthesized PS-*b*-PEO block copolymer contained a photocleavable moiety. After thin film annealing simply followed a very mild UV exposure

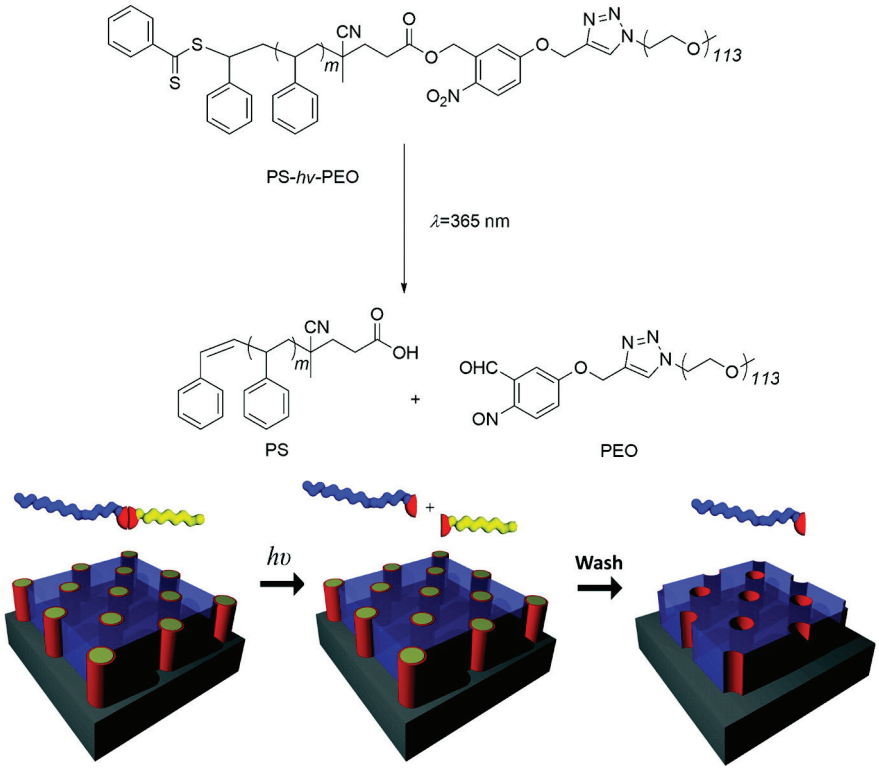

Figure 2.11 Photolysis of PS-*b*-PEO in solution (top). Schematic representation of the self-assembly of photocleavable block copolymers and the subsequent removal of one domain after UV irradiation (bottom). Adapted with permission from [122]. Copyright 2011 American Chemical Society.

and successive washing with water, to generate the nanoporours PS films.

In this context and in course of the current thesis, a temperature triggered linkage, as presented in Section 3.3, was added to the list of covalent but reversible conjugations of amphiphilic block copolymers. The conjunction is stable at ambient temperature, while elevated temperatures (starting above 45 °C) induce a shift of the reaction equilibrium towards the initial building blocks.

2.2.1 Self Assembly and Nonsolvent Induced Phase Separation Process

For the preparation of block copolymer based nano structured membranes, the self assembly and nonsolvent induced phase separation (SNIPS) process proved to be the most successful methodology.[123–125] The fabrication protocol expands the often used membrane fabrication procedure of NIPS with the thermodynamically driven self assembly of block copolymers in solution. The first reported and most often used block copolymer system is poly(styrene)-*block*-poly(4-vinylpyridine) (PS-b-P4VP).[125] Meanwhile, many other polymer systems were introduced such as poly(isoprene)-*block*-poly(styrene)-*block*-poly(4-vinylpyridine) (PI-*b*-PS-*b*-P4VP),[126,127] poly(styrene)-*block*-poly(2-vinylpyridine)-*block*-poly(ethylene oxide) (PS-*b*-P2VP-*b*-PEO),[128] PS-*b*-PEO,[129] PS-*b*-P2VP,[130] poly(styrene-*co*-isoprene)-*block*-poly(*N*,*N*-dimethylaminoethyl methacrylate) (P(I-*co*-S)-*b*-PDMAEMA),[131] poly(tert-butylsytrene)-*block*-poly(4-vinylpyridine),[132] and poly(trimethylsilylstyrene)-*block*-poly(4-vinylpyridine),[132] all in binary or ternary solvent mixtures containing DMF, dioxane or THF. Figure 2.12 illustrates the general procedure of the SNIPS process. First of all, the block copolymer is dissolved in an organic solvent (or solvent mixture) which is miscible with water. The concentration of polymer in solution typically ranges between 15 wt% and 20 wt%. The solution is cast into a thin film on a substrate with a smooth surface (*e.g.* a polished glass plate). Although any casting technique could be used, such as drop casting or dip coating, the application of an doctor blade is most common. The reason for the success of this technique is probably due to the fact that it is facile to reproduce and to upscale. After the film casting, the solvent is allowed to evaporate for a predetermined time (usually between 10 s and 2 min, depending on the employed solvent and polymer system). The evaporation of the solvent creates an increase in polymer concentration at the interface of air and solution. As a result, the block copolymers self assemble in the top layer of the solution.[130,133] After the self assembly time, the substrate with the partially evaporated film on top is immersed into a nonsolvent bath, which is typically water. The polymer precipitates in a membrane micro structure with its hydrophilic blocks at the surface.

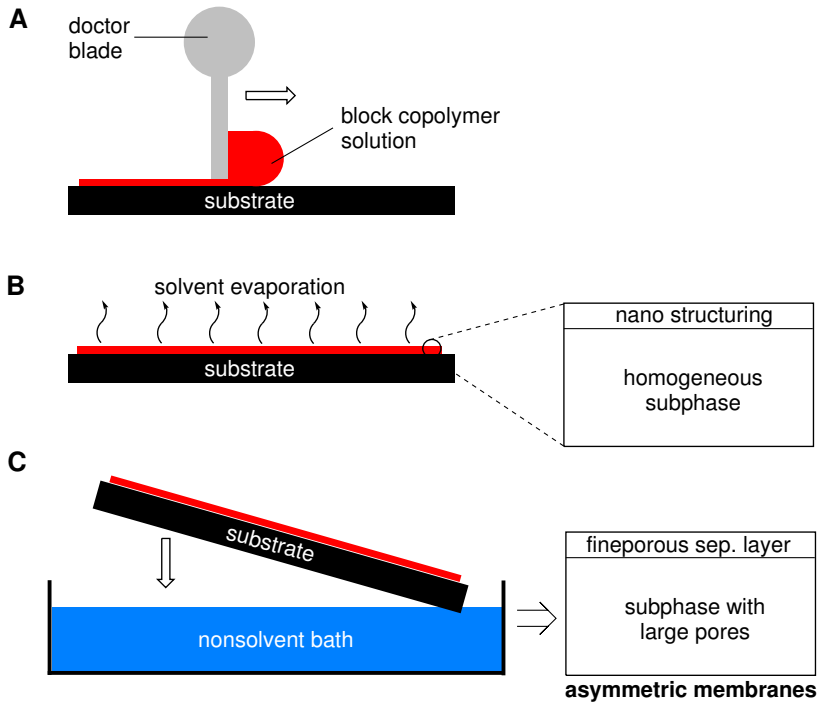

Figure 2.12 Schematic of the SNIPS process. **A** An amphiphilic block copolymer solution is drawn into a thin film by using a doctor blade (or another simple casting technique) on a plain substrate (*e.g* a polished glass plate). **B** The solvent is allowed to evaporate in a controlled manner for a predetermined time. At the interface of air and liquid the locally high concentration of block copolymers induces nano structuring by self assembly (self assembly time). **C** The substrate, with the thin film on top, is immersed in a nonsolvent bath (typically water). The polymer precipitates and the nano structure is kinetically trapped. An asymmetric membrane with a fine porous layer on top and a gutter layer beneath it is generated.

Due to the locally elevated concentration and previous self assembling, the top layer is fine porous and highly selective. Since the lower part of the thin film contains polymer at approximately the same concentration as that of the original solution, this portion of the film precipitates in nonordered structures with large pores, similar to that seen in the usual NIPS procedure.[123,125] Thus, an asymmetric membrane is generated combining the high throughput of a thin selective layer with the mechanical stability of a thick support/gutter layer. As an example, SEM images of three asymmetric membranes prepared from P(I-*co*-S)-*b*-PDMAEMA *via* the SNIPS process are depicted in Figure 2.13. The only difference in the applied process conditions for the individual membranes was the varied self assemble time with 15 s (**A**, **B**) 30 s (**C**, **D**) and 45 s (**E**, **F**). Besides the self assemble time, the employed solvents, the employed nonsolvent for precipitation

and the polymer concentration, the morphology of the generated membranes is also influenced by the rel. humidity, the temperature and the height of the casted film.

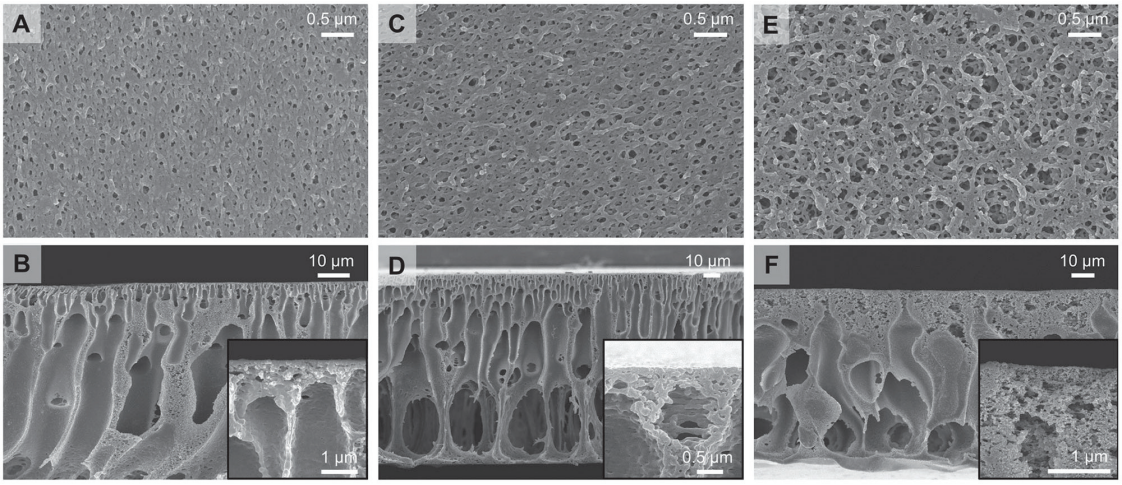

Figure 2.13 SEM images of membranes prepared *via* SNIPS processes from P(I-*co*-S)-*b*-PDMAEMA. Images **A**, **C**, **E** show top views and **B**, **D**, **F** cross sectional views of membranes prepared with self assemble times of 15 s (**A**, **B**) 30 s (**C**, **D**) and 45 s (**E**, **F**). Reprinted from [131] with permission from WILEY.

2.3 Modular Polymer Ligation Techniques

For a successful polymer conjugation, the employed reaction typically needs to be highly efficient. In 2001, Sharpless introduced the term *click* chemistry and defined the criteria a reaction needs to fulfill to be rightfully called a *click* reaction:

"*The reaction must be modular, wide in scope, give very high yields, generate only inoffensive byproducts that can be removed by nonchromatographic methods, and be stereospecific (but not necessarily enantioselective). The required process characteristics include simple reaction conditions (ideally, the process should be insensitive to oxygen and water), readily available starting materials and reagents, the use of no solvent or a solvent that is benign (such as water) or easily removed, and simple product isolation. Purification — if required — must be by nonchromatographic methods, such as crystallization or distillation, and the product must be stable under physiological conditions. [...] Click processes proceed rapidly to completion and also tend to be highly selective for a single product: we think of these reactions as being 'spring-loaded' for a single trajectory*".[134]

Although Sharpless intended mainly to influence the synthesis of biologically active molecules, the *click* concept had a much greater impact in polymer chemistry and material science.[135] The reason for this is that the efficiency, combined with the lack of side products and facile purification, proved to be a strong practical value for polymer chemists. Only a few methods, such as precipitation, can be used to purify a polymer. Especially the removal on unreacted polymer material is often impossible. Thus, the modular *click* concept enabled the design an synthesis of complex macromolecular architectures that would not have been achievable otherwise.[136] However, the undeniable success also lead to a misuse of the term *click*.[137] Successful conjugations with polymers were called *click* reactions, although the reactions often did not fulfill all the criteria, *e.g.* they did not proceed in short time or required tedious purification procedures.

In the following, a selection of conjugation methods is given that were successfully employed to generate irreversible and reversible linkages in polymer chemistry. Some fulfill the *click* criteria, some do not and for others it depends on the reaction conditions.

Since it was the method of choice, the (hetero)-Diels–Alder reaction is discussed in more detail in a separate subsection (Section 2.3.3).

2.3.1 Irreversible Linkages

2.3.1.1 Azide-Alkyne Cycloaddition

The most prominent *click* reaction is the cooper(I)-catalized azide-alkine cycloaddition (CuAAC).[138] Although the Huisgen 1,3-dipolar cycloaddition was reported 35 years before,[139] it was not until Sharpless introduced the copper(I) catalyzed version in 2002 that this reaction became increasingly relevant for polymer chemistry and material science.[140] Due to the mild reaction conditions, quantitative yields and tolerance towards a wide range of solvents, it found application in various fields, such as drug discovery, chemical biology and materials design.[141–146] However, the copper catalyst leads to several problems, including denaturation of proteins, cytotoxicity and reduction of the quantum yield of quantum dots.[147–149] Consequently, researchers were looking for strategies to avoid copper. Bertozzi developed the strain-promoted azide-alkine cycloaddition (SPAAC), where the (typically terminal) alkine is replaced with a cyclooctyne derivative.[150] The intramolecular strain of the 8-membered ring lets the cyclooctyne react readily with an azide without the need of a metal catalyst, reaching high yields at ambient temperature.[151–153] A selection of frequently used cyclooctyne derivatives in order of their reactivity towards azides is depicted in Figure 2.14. The SPAAC reaction

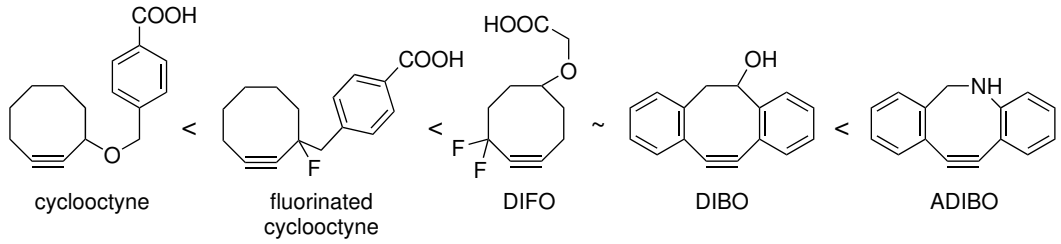

Figure 2.14 Chemical structures of cyclooctyne derivatives frequently used in SPAAC in order of their reactivity towards azides.

kinetics of cyclooctyne and fluorinated cyclooctyne are slower than the CuAAC. Difluorinated cyclooctyne (DIFO) however, shows an equal reactivity towards azides as in

CuAAC under the same conditions.[151] The dibenzocyclooctyne (DIBO) features approximately the same reaction rate as DIFO.[153] By replacing a carbon atom of the ring with a nitrogen, the reaction kinetics could be improved even further (aza-dibenzocyclooctyne, ADIBO).[154,155] However, cyclooctynes are expensive and difficult to synthesize. Thus, in some cases it is a better option to perform the CuAAC and subsequently remove the copper (if necessary) completely *via* electrolysis.[49]

2.3.1.2 Thiol-Ene Reaction

The thiol-ene reaction is the most common thiol based conjugation method. The reaction may proceed *via* two distinct pathways (see Scheme 2.6).[156,157] Either radical mediated

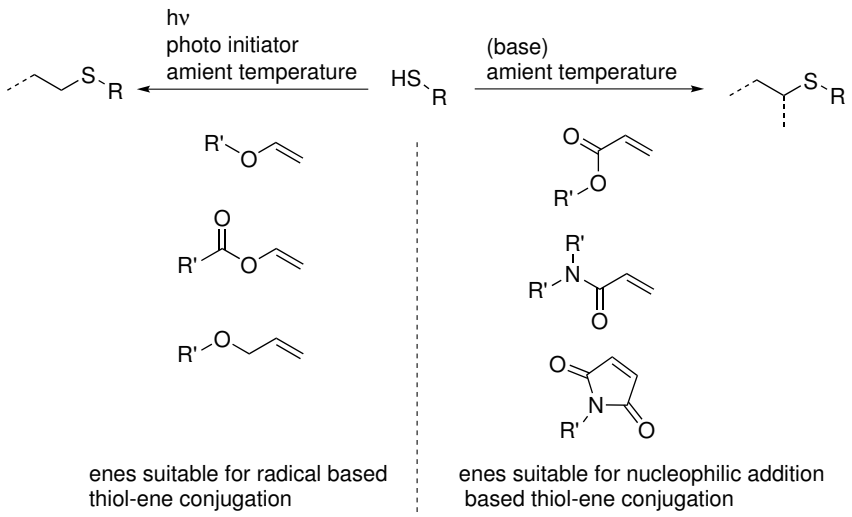

Scheme 2.6 General scheme for thiol-ene reactions with examples for suitable enes, corresponding to a radical or nucleophilic addition based conjugation.

or *via* a nucleophilic (Michael-type) addition.[158] The choice of the utilized ene is largely responsible for the favored reaction path and thus the reaction conditions that should be applied.[159] At this point it is important to note that whenever the radical based thiol-ene reaction is shown to perform very well, at least one of the components (typically the thiol) is a small molecule and used in excess. Barner-Kowollik and Du Prez demonstrated that the radical based thiol-ene reaction is not able to conduct an efficient polymer-polymer conjugation.[160] Besides alkenes, thiols are known to react readily with other functional groups, including terminal alkynes (*thiol-yne*),[161] organic bromides (*thio-bromo*),[162]

isocyanates (*thio-isocyante*)[163] and pentafluorostyrene groups.[164] Thus, thiol based reactions are not very selective and susceptible to side reactions.

2.3.1.3 Nitrile Imine Mediated Tetrazole-Ene Coupling (NITEC)

In 1967 Huisgen and coworkers found that under radiation with UV light 2,5-tetrazoles undergo a cycloreversion to form molecular nitrogen and a 1,3-dipole, which can react in a pericyclic reaction with suitable dipolarophiles, including many double bonds (see Scheme 2.7).[165] The resulting product exhibits fluorescence properties. Hence, it is

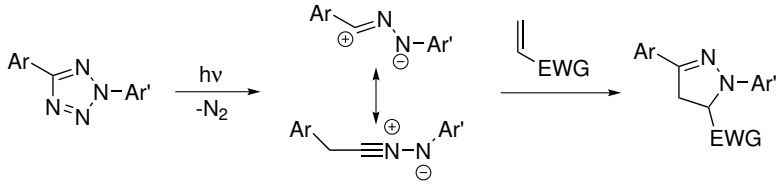

Scheme 2.7 General scheme of a NITEC reaction. EWG = electron withdrawing group; Ar, Ar' = general aromatic substituents.

possible to follow the conversion of the reaction *via* fluorescence spectroscopy. The aromatic substituents of the tetrazole determine the wavelength of radiation that needs to be applied to promote the reaction. Paul Lederhose *et al.* developed an aromatic system which allows the reaction to proceed by application of visible light (410 - 420 nm) and used it for block copolymer formation.[166] NITEC is a robust conjugation method and neither sensitive towards oxygen, nor to water. Thus, it is applicable in biological systems.[167]

2.3.2 Reversible Linkages

2.3.2.1 Hydrogen Bonding

Hydrogen bonding is one of the most commonly employed supramolecular conjugation methods.[168,169] It is based on the interaction between hydrogen bond donors (D) and acceptors (A). Donor motifs are typically positive polarized hydrogen atoms that are covalently bound to electronegative hetero atoms, such as nitrogen and oxygen. Correspondingly, the acceptor motifs are negative polarized hetero atoms (again, typically nitrogen and oxygen) with a lone pair of electrons. Prominent examples of hydrogen bonding structures are ureidopyrimidinone (A-A-D-D arrangement), the thymine/diaminopyridine system (A-D-A/D-A-D arrangement) and the Hamilton-wedge/cyanuric acid system (D-A-D-D-A-D/A-D-A-A-D-A arrangement)(see Figure 2.15). While the

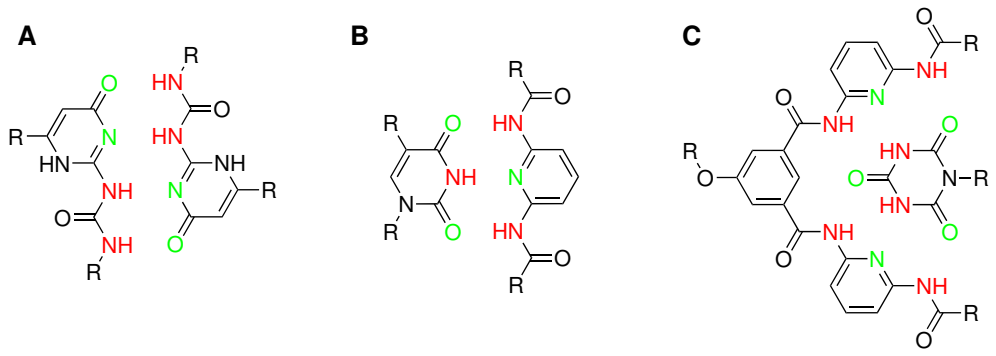

Figure 2.15 A Selection of hydrogen bonding structures, the hydrogen donor motifs are coloredin red and the acceptors in green. **A** ureidopyrimidinone dimer (A-A-D-D). **B** thymine/diaminopyridine system (A-D-A/D-A-D). **C** Hamilton-wedge/cyanuric acid system (D-A-D-D-A-D/A-D-A-A-D-A).

donor/acceptor arrangement of ureidopyrimidinone is forming dimers, the thymine/diaminopyridine system and the Hamilton-wedge/cyanuric acid system specifically connect with their counterpart. Furthermore,the systems are orthogonal to each other.[170] The strength of the linkage strongly depends on the number of hydrogen donor/acceptor pairs. However, by addition of a polar protic solvent (*e.g.* methanol) or by increasing the temperature, the conjugation can readily be cleaved.[171]

2.3.2.2 Metal Coordination

The use of metal complexes for polymer chemistry has been exploited extensively due to the additional functional properties that can be imparted to polymers, such as conductivity, catalysis, light emission, and gas binding.[172–174] The strength of the linkage is depending on the choice of metal (its oxidation state), ligand and solvent.[175] The preparation of AB diblock copolymers, without the formation of AA and BB homopolymers as side product, can be realized *via* subsequent coordination procedures.[176] Scheme 2.8 shows an example employing terpyridine functionalized polymers and Ruthenium. The

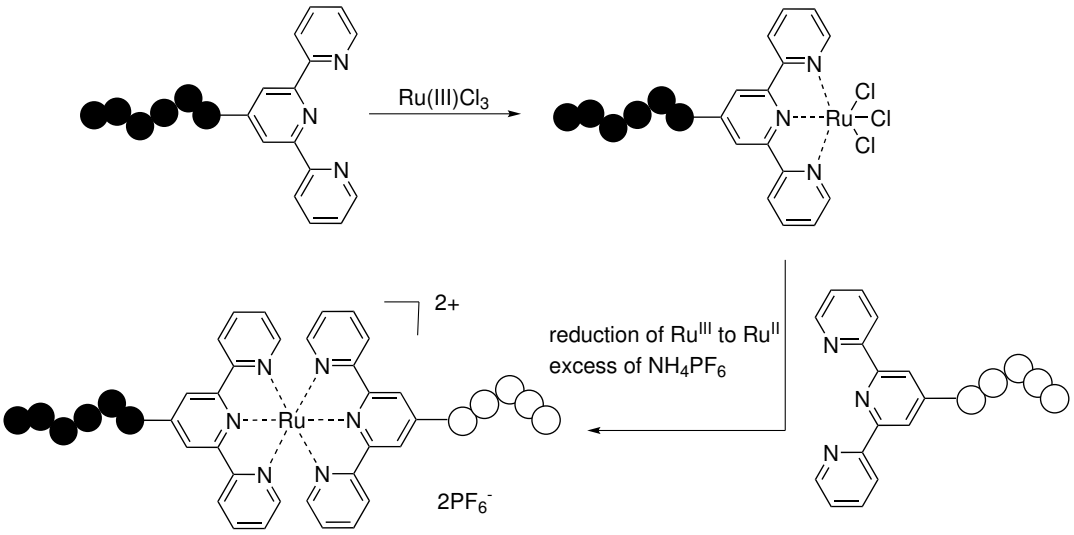

Scheme 2.8 Strategy for the preparation of AB diblock copolymers *via* subsequent metal complex coordination.

first polymer block is treated with $Ru(III)Cl_3$, which results exclusively in the formation of a monocomplex. Subsequently, the Ru^{III} ions are reduced to Ru^{II} ions and the second, terpyridine terminated polymer block is added, resulting in the formation of AB diblock copolymers.

2.3.2.3 Inclusion Complexes

An inclusion complex is formed when a ”host” compound has a cavity in which a second (”guest”) compound is located. The linkage between host and guest is based on van der Waals’ interaction. In polymer science, cyclodextrins (CDs) are the best-known

representatives of hosts.[177] They can form inclusion complexes with hydrophobic guest molecules primarily in aqueous solution and found applications in various areas, such as nano structures,[178] drug delivery,[179] self healing materials[180] or bioactive materials.[181] Over time, several guests were developed that are released from the cavity of the CD by application of an external stimuli such as temperature, light or voltage.[182,183]

2.3.3 (Hetero) Diels–Alder Reactions

The Diels–Alder (DA) reaction was first described in 1928 and corresponds to a pericyclic [4+2] cycloaddition between dienes and alkenes or their hetero atom analogues (in this context called "dienophiles").[184–186] It belongs to the most widely used reactions in organic synthesis and was honored with the Nobel prize in 1950.[187–189] The driving force of the reaction is that two of the π-bonds are transformed into two, energetically more favorable, σ-bonds, resulting in unsaturated six-membered rings as conjugation product (see Figure 2.16 **A**).[185,190] In order to explain why some diene/dienophile pairs react readily, while others require high temperatures or do not react at all, the empiric frontier molecule orbital (FMO) theory was developed. In this theory, only the FMO, *i.e.* the highest occupied molecular orbital (HOMO) and the lowest unoccupied molecular orbital (LUMO) are considered. For a successful reaction, the two overlapping molecular orbitals (MO), which form the new σ-bonds between the corresponding c-atoms, need to be in phase. For thermally allowed pericyclic reactions (such as the DA reaction is, following the Woodward–Hoffmann rules),[191] the bond formation proceeds suprafacial (on the same plane of the molecule). Thus, the HOMO of dienes and the LUMO of dienophiles (or vice versa) are overlapping for the σ-bond formation (see Figure 2.16 **B**).[186,192] Therefore, efficient DA reactions require a small HOMO-LUMO gap. That is the case for the combination of electron poor dienophiles and electron rich dienes, (normal electron demand) or electron rich dienophiles and electron poor dienes (inverse electron demand)(see Figure 2.16 **C**).[185] However, DA reactions with *normal* electron demand are more common.

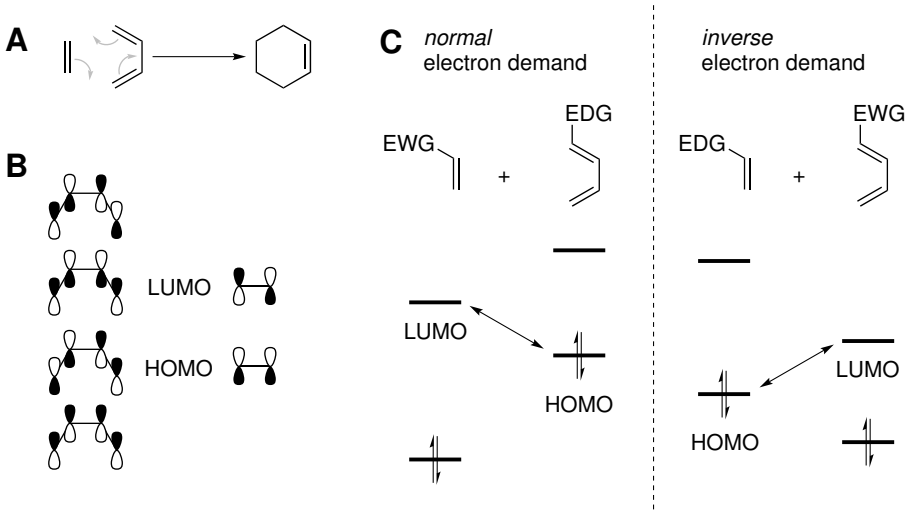

Figure 2.16 **A** Formal scheme of a pericyclic [4+2] cycloaddition of a diene with a dienophile resulting in an unsaturated six-membered ring. **B** MO diagram of the π-system from the diene (left side) and the dienophile (right side). **C** FMO interactions in DA reactions with normal electron demand (left side) and inverse electron demand (right side). EWG = electron withdrawing group, EDG = electron donating group.

The concerted mechanism of the cycloaddition leads to a high stereospecifity, *i.e.* the stereochemical information of the starting materials is transferred into the product. However, in DA reactions that are able to form two diastereomers, both products are formed (see as example the reaction of cyclopentadiene and maleic anhydride in Scheme 2.9).[186,192] The endo adduct (representing the kinetic produkt) is often, but not always, the

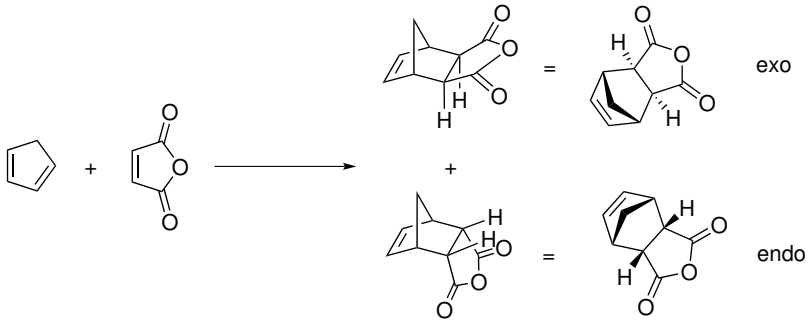

Scheme 2.9 DA reaction of cyclopentadiene and maleic anhydride with the resulting exo and endo products.

major product. Bulky substituents can give direction to the generation of the sterically and thermodynamically favored exo product.[185,193] This observation is often explained with secondary orbital interactions but solvent effects, steric interactions, hydrogen

bonds, electrostatic forces, and other effects can be argued as well.[194] For polymer conjugations stereo- and diastereospecific control are irrelevant. Nevertheless, chiral auxiliaries can be employed to enable enantioselective reaction control.[195]

Thermally allowed cycloadditions, including DA, are able to perform a cycloreversion at elevated temperatures.[185] The retro Diels–Alder (rDA) temperature depends on the employed reactants. Although the bonding/debonding on demand *via* DA/rDA found applications in various fields, such as adaptable networks, protecting groups or macromolecular architectures, only a few DA systems are known that can be cycled in a reasonable temperature range (i.e. below the materials degradation temperature).[196] The most commonly used DA system for bonding/debonding on demand is the pairing of furan and maleimide moieties (see Scheme 2.10). A typical forward reaction proceeds

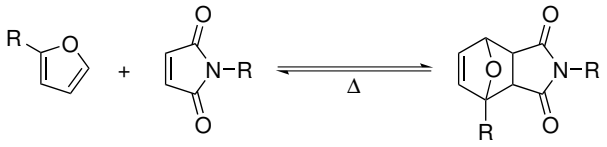

Scheme 2.10 DA reaction of cyclopentadiene and maleic anhydride with the resulting exo and endo products.

within hours at 60 °C to 80 °C or up to several days at ambient temperature. The rDA reaction becomes favored at temperatures above 120 °C.[197–199]

The groups of Barner-Kowollik and Stenzel pioneered the utilization of dithioester terminated polymers (prepared *via* RAFT polymerization) as dieneophiles in HDA reactions. In order to undergo an efficient HDA reaction, the employed RAFT agents require a strong electron withdrawing Z-group. In this context, two CTAs, one with a pyridinyl and one with a phosphoryl Z-group, were identified which are able to perform a CRP and to quantitatively react with sorbic alcohol based dienes (see Scheme 2.11 **A**).[200] The HDA reaction proceeded at 50 °C within 2 - 24 h employing $ZnCl_2$ (for the phosphoryl Z-group) or trifluoroacetic acid (TFA, for the pyridinyl Z-group) as catalyst. $ZnCl_2$ coordinates onto the phosphoryl moiety, while TFA protonates the pyridinyl moiety. In each case the electron withdrawing character of the Z-group, and therefore also the reactivity of the C=S-double bond towards dienes, is increased. The introduction

of cyclopentadiene (Cp) as reaction partner for the HDA-RAFT agents lead to even more moderate reaction conditions (see Scheme 2.11 **B**). Reaction times of less than 10 min

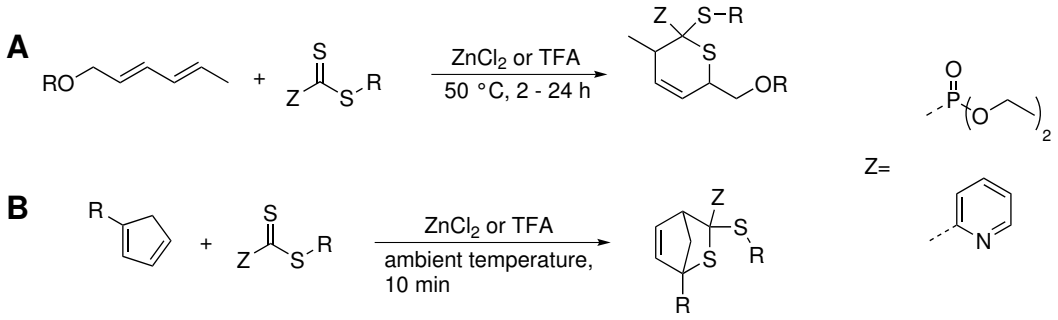

Scheme 2.11 RAFT-HDA reactions with sorbic alcohol (**A**) and cyclopentadiene (**B**) based dienes.

for a polymer conjugation at ambient temperature were observed.[201] While solvent polarity has no substantial effect on DA kinetics, reactions in water proceed significantly faster due to hydrophobic interactions and thus a closer proximity of the reactants.[202] It was demonstrated that a polymer conjugation in aqueous conditions, employing the RAFT-HDA Cp pair as reaction partners, proceeds within 15 min at ambient temperature without the need of any catalyst.[19] Thus, under the right conditions the Cp-RAFT-HDA reaction can be rightfully termed *click* reaction. Even when the less reactive sorbic alcohol moiety was used as diene, a complete polymer conjugation without catalyst was observed after 4 h at ambient temperature in water. The potential of the RAFT-HDA conjugation concept was demonstrated by the construction of various polymer architectures, including block copolymers,[18] (multi-arm) star polymers,[203,204] and combs,[205] or the Modifications of microspheres[206] and biosurfaces.[207]

Furthermore, the required temperatures for the rHDA reactions have been determined. For the 3,6-Dihydro-2*H*-thiopyran rings, formed by HDA cycloadditions between sorbic alcohol based diene functionalized PEO and RAFT agents with phosphoryl or pyridinyl Z-groups, a complete disappearance of the HDA adduct in mass spectrometric analysis was observed above 160 °C and 180 °C respectively.[208] When Cp was used as diene, a complete cleavage was achieved at 100 °C.[209] However, following investigations showed that the rDA (and temperature triggered linkages in general) temperature for

polymer-polymer linkages is not just reliant on the employed diene/dienophile pair, but also depends on entropic effects originating from the polymer chains.[171,210–212] Thus, each new polymer system can have a different cleavage temperature, although the conjugation method is always the same. When a precise knowledge about the cleaving conditions is needed, investigations for each employed polymer system is inevitable.

The ability of bonding/debonding on demand was demonstrated by the generation of a thermally reversible network, employing a trifunctional pyridinyl HDA-RAFT agent cross linker and a biscyclopentadienyl poly(methyl methacrylate) polymer.[213] A source of inspiration for the proposed concept in this thesis was the reversible grafting of HDA-RAFT end group terminated polymers onto Cp functionalized silicon substrates (see Scheme 2.12).[20] The grafting of the polymers onto the surface proceeded within

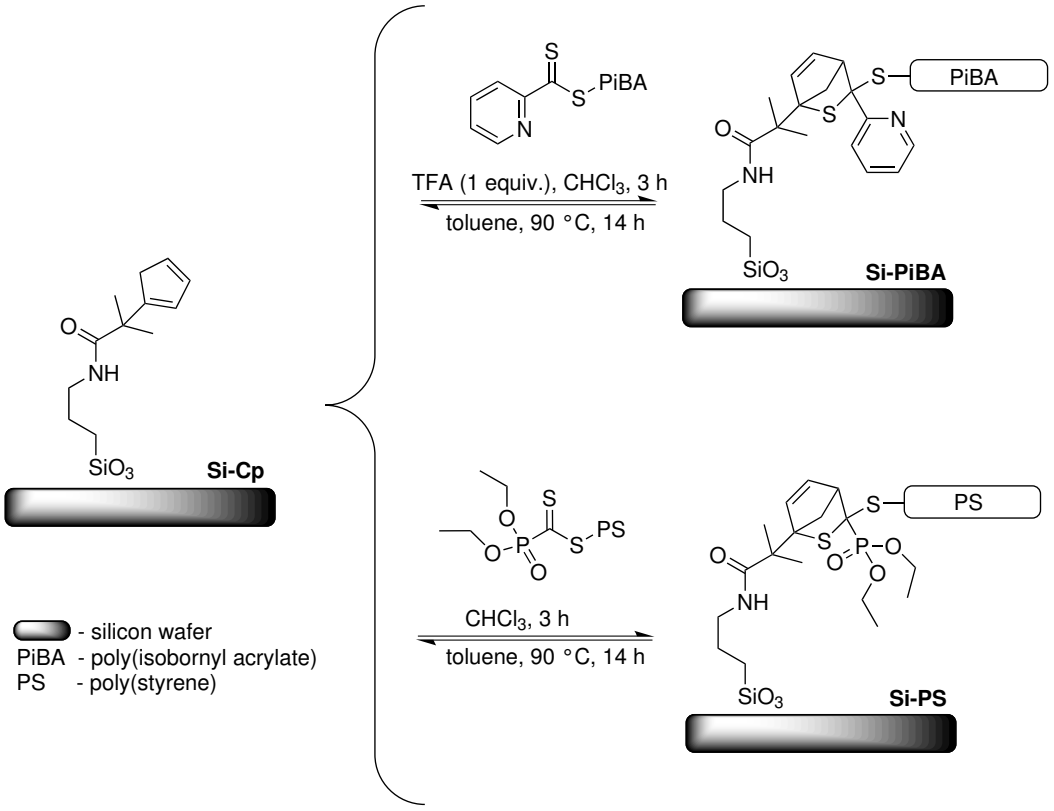

Scheme 2.12 Reversible grafting of HDA-RAFT end group terminated polymers onto Cp functionalized silicon substrates. Adapted from [20] with permission from John Wiley and Sons.

3 h at ambient temperature. The removal of the covalent bound polymer chains from the surface was achieved by immersing the substrates in 90 °C hot toluene for 14 h.

Subsequently, the same Cp-functionalized substrate was coated again with polymer, analogue to the first grafting procedure, proving that the Cp functionality remained intact after cleaving conditions.

Since it combines the most versatile CRP technique with the ability to reversibly conjugate polymers without the need of any post-polymerization modifications, the RAFT-HDA concept has the potential for a wide range of (industrial) applications. That is also the reason why it is the conjugation method of choice for the realization of the proposed concept in this thesis. The only limitations that have to be kept in mind is the limited monomer choice accompanying the utilization of RAFT agents with strong electron withdrawing Z-groups.

Light Activated Diels–Alder Reactions

Although DA reactions are always thermally triggered, it is possible to generate reactive dienes or dienophiles *via* irradiation. An example is the light induced formation of thioaldehydes from phenacyl sulfides, which can react as dienophile with corresponding dienes (see Scheme 2.13). For the release of acetophenone and the generation of the

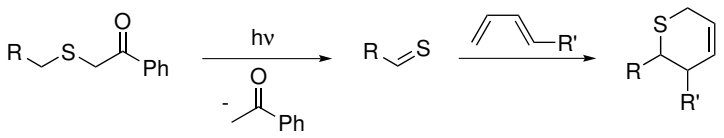

Scheme 2.13 General reaction scheme for the photo activated HDA reaction of phenacyl sulfides.

reactive thioaldehyde, radiation in the UV range (355 nm) is necessary. This method was successfully introduced in polymer chemistry.[214,215] However, the generated thioaldehyde is not just a good dienophile, but also reacts readily with nucleophiles.[216] Since nucleophilic moieties are omnipresent in chemistry, the ligation method is on the one hand very versatile yet on the other hand less specific.

Another light activated DA reaction is the photoenol technique. It is based on *ortho*-methyl benzaldehyde or *ortho*-methyl benzophenone derivates, which form orthoquino dimethanes (so-called photoenols) upon irradiation (see Scheme 2.14). The pho-

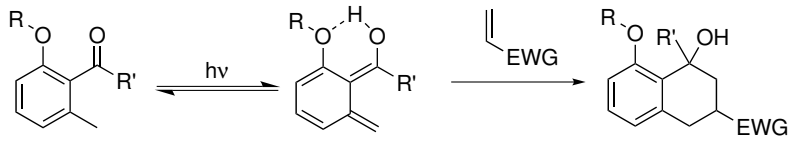

Scheme 2.14 General reaction scheme for a photoenol reaction.

toenol species is a highly reactive diene, undergoing rapid DA reactions with electron deficient alkenes, such as maleimide, fumarates or acrylates. If no suitable reaction partner is accessible, the diene species returns to the non-activated species (starting material) without forming any side products, making it a highly specific and versatile ligation method. Although the cycloaddition behavior of photoenols was investigated already in the early 70s,[217] the group of Barner-Kowollik just recently introduced their application in the realm of polymer science.[218] The successful utilization of photoenols includes the preparation of block copolymers,[219,220] single chain nanoparticles,[221] cyclic polymers[222,223] or spatially resolved surface modification.[224–226]

3

Preparation of Amphiphilic Block Copolymers Featuring a Reversible Hetero Diels-Alder Linkage

The modular synthesis of amphiphilic block copolymers with a reversible linkage is the key element of the presented concept of the new membrane preparation method. The following sections* describe the development and synthesis of the respective building blocks (Section 3.1 and Section 3.2), their ligation and the thermo-responsive behavior of the linkage (Section 3.3), as well as a method for the preparation of amphiphilic triblock terpolymers with a reversible linkage (Section 3.4).

* Parts of the current chapter are reproduced from M. Langer, J. Brandt, A. Lederer, A. S. Goldmann, F. H. Schacher, C. Barner-Kowollik, *Polym. Chem.* **2014**, *5*, 5330–5338. - Published by The Royal Society of Chemistry and permission granted: http://www.rsc.org/journals-books-databases/journal-authors-reviewers/licences-copyright-permissions/#reuse-permission-requests (13.05.2016-10:18). M. Langer designed and conducted all experiments unless otherwise stated, performed all NMR analysis, and wrote the manuscript. J. Brandt performed the DLS and high temperature SEC experiments, supervised by A. Lederer. A. S. Goldmann, F. H. Schacher, and C. Barner-Kowollik motivated and supervised the project and contributed to scientific discussions.

3.1 Matrix A: The Hydrophobic Building Block

For simplicity, the term "Matrix A" replaces the term "hydrophobic building block" in the rest of the thesis. As Matrix A, a copolymer constituted of styrene and isoprene was chosen. In radical polymerizations, isoprene is known to be incorporated into the polymer backbone as three different isomers (1,2; 1,4 and 3,4).[227] The residual vinyl groups of the 1,2 and 3,4 isomers of isoprene in the side chain can be used for subsequent crosslinking after membrane formation. Thus, the mechanical stability and the resistance against solvents of the generated membranes can be increased by crosslinking. To be able to introduce the Cp moiety at the end group of the prepared polymer, a bromine-functional RAFT agent (**CTA-1**) was designed and synthesized (see Scheme 3.1). The newly developed RAFT agent is based on the well-known CTA 2-(((dodecylthio)carbonothioyl)thio)-2-methyl- propanoic acid (DMP, **2**).[228,229] It is com-

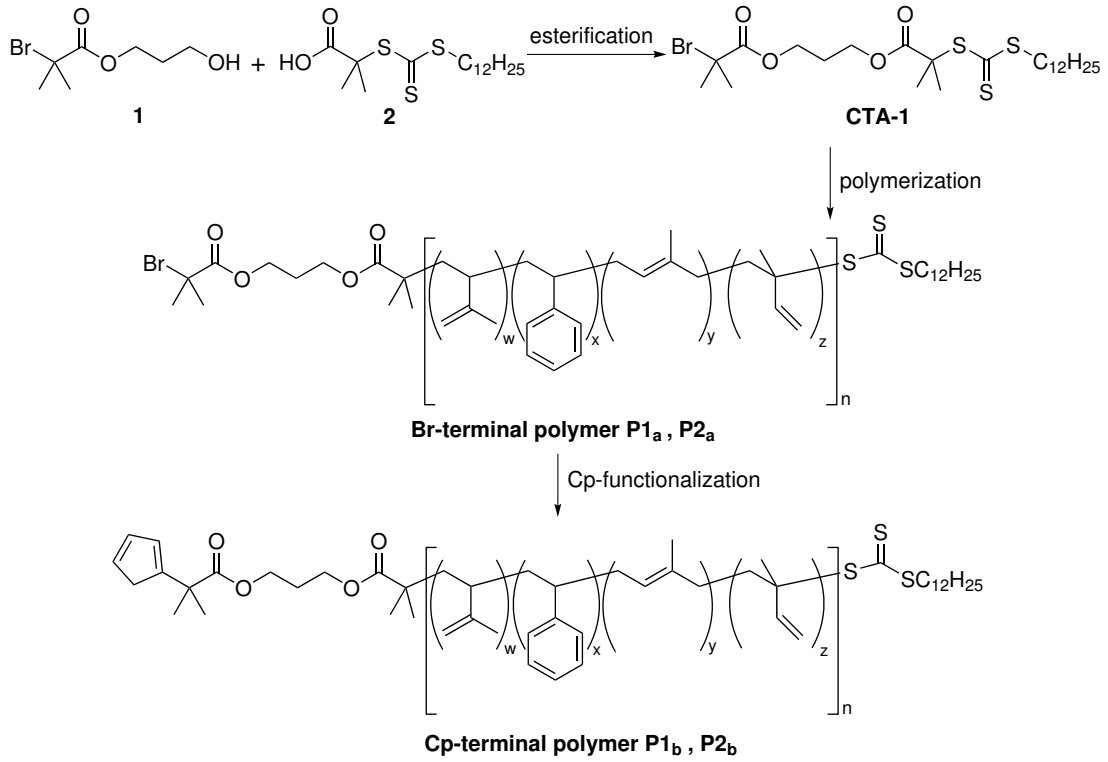

Scheme 3.1 Synthetic strategy for the preparation of Cp-functional Matrix A. Esterification: DMAP, DCC, DCM, 0 °C; polymerization: bulk, 20 mol% isoprene, 80 mol% styrene, VAm-110, 110 °C; Cp-functionalization: $NiCp_2$, NaI, $P(Ph)_3$, dry THF, ambient temperature.

posed of a trithiocarbonate with a tertiary R-group, able to control the polymerizations of styrene and isoprene.[227,230] The facile preparation *via* a Steglich esterification involves 3-hydroxypropyl-2-bromo-2-methyl- propanoate (**1**) to introduce a bromine functionality at the R-group. The successful synthesis of the CTA was confirmed by ^{1}H NMR spectroscopy (see Figure 3.1, for more characterization details refer to Chapter 6). To

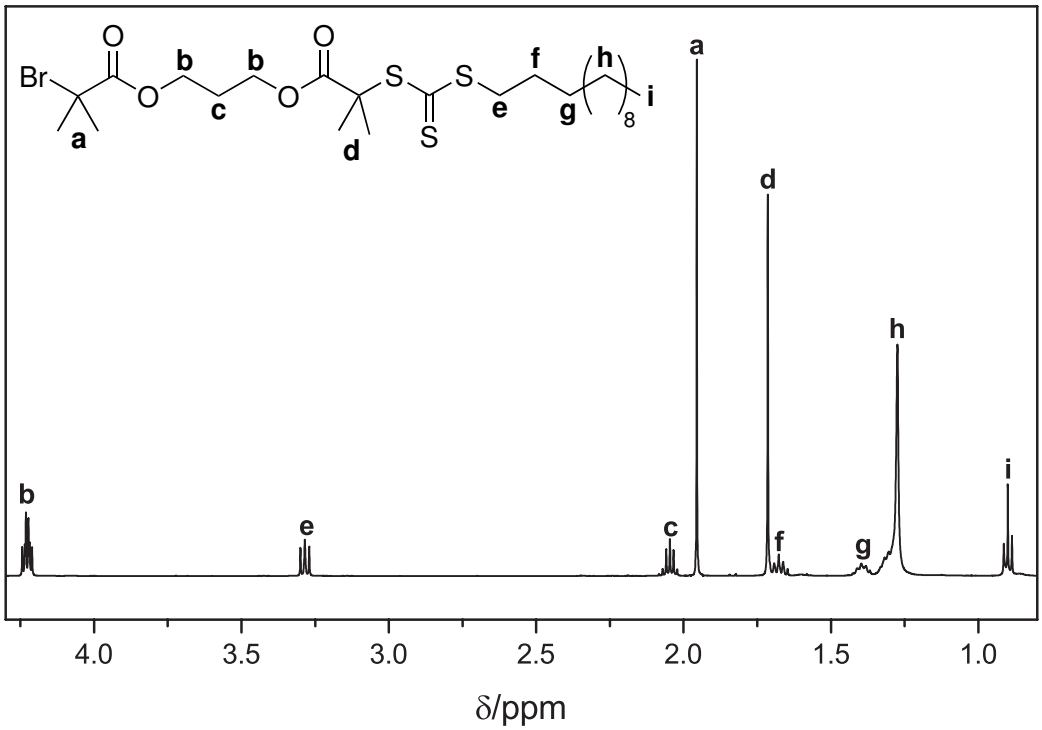

Figure 3.1 ^{1}H NMR spectrum (500 MHz) of the Br-functional RAFT agent **CTA-1** (DMP-Br) in $CDCl_3$ at ambient temperature.

verify the control afforded by the RAFT process leading to polymers with high end group fidelity, kinetic studies were carried out for the copolymerization of styrene and isoprene using **CTA-1** (see Figure 3.2 and Table 3.1).

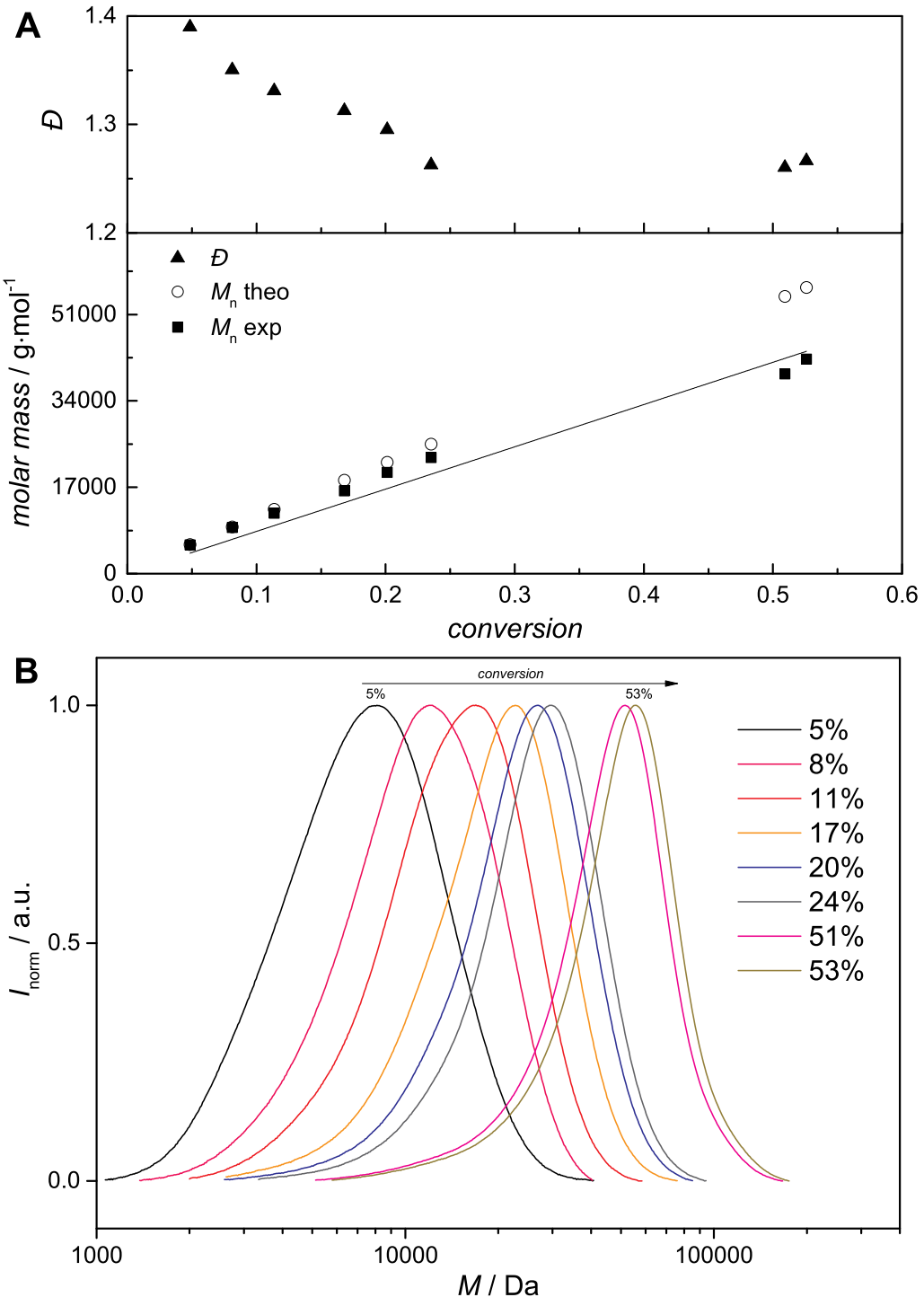

Figure 3.2 **A**: Evolution of the *molar mass* and *Đ* versus *conversion* during the copolymerization of styrene (80 mol%) and isoprene (20 mol%): $[\text{monomer}]_0 = 8.9\ \text{mol L}^{-1}$, $[\textbf{CTA-1}]_0 = 8.2\ \text{mmol L}^{-1}$, $[\text{VAm-110}]_0 = 1.7\ \text{mmol L}^{-1}$, 110 °C. The theoretical molecular weights and DPs were calculated from the CTA concentration and the conversion. **B**: SEC traces of the respective data points from **A**. The SEC was calibrated with narrow PS standards.

Table 3.1 The degree of polymerization (DP), the theoretical and the experimental *molar mass* and $Đ$ for several conversions during the copolymerization of styrene (80 mol%) and isoprene (20 mol%): $[\text{monomer}]_0 = 8.9\,\text{mol}\,\text{L}^{-1}$, $[\textbf{CTA-1}]_0 = 8.2\,\text{mmol}\,\text{L}^{-1}$, $[\text{VAm-110}]_0 = 1.7\,\text{mmol}\,\text{L}^{-1}$, 110 °C. The theoretical molecular weights and DPs were calculated from Equation 2.1.

conversion	DP	$M_{\text{n,theo}}$ [g mol^{-1}]	$M_{\text{n,exp}}$ [g mol^{-1}]	$Đ$
5 %	53	5700	5700	1.39
8 %	89	9000	9100	1.35
11 %	124	12600	12000	1.33
17 %	184	18000	16000	1.31
20 %	220	22000	20000	1.30
24 %	257	25500	23000	1.26
51 %	557	54500	39000	1.26
53 %	575	56000	42000	1.27

The SEC traces corresponding to all the data points are depicted in diagram **B** of Figure 3.2. With progressing conversion a linear increase of the experimental molecular weight can be observed. The black line in the diagram **A** (Figure 3.2) is inserted to guide the eye. For the calculation of the theoretical M_n Equation 2.1 is applied. As the molecular weight of two different monomers needs to be considered, an average monomer molecular weight (96.94 g mol^{-1}), corresponding to the employed ratio of isoprene/styrene (20/80), is used. Considering the inaccuracy of the SEC (about 10 %) and the PS calibration, theoretical M_n is in good agreement with the observed values. In contrast to the M_n, the $Đ$ is decreasing from 1.39 to 1.27 with progressing conversion, which constitutes further supporting evidence for a controlled polymerization. In combination, the linear increase of the molar mass, the good agreement of $M_{\text{n,theo}}$ and $M_{\text{n,exp}}$ and low $Đ$ values are proof of a controlled copolymerization of styrene and isoprene.

Subsequently, two poly(isoprene-*co*-styrene) (P(I-*co*-S)) copolymers, one with lower molecular weight (**P1**, $M_n = 9200\,\text{g mol}^{-1}$, $Đ = 1.22$, see Figure 3.3) and one with higher molecular weight (**P2**, $M_n = 50\,000\,\text{g mol}^{-1}$, $Đ = 1.36$, see Figure 3.3) were prepared. The molar fraction of isoprene in the generated copolymers was determined *via* NMR spectroscopy and resulted in 27 mol% for **P1** and 24 mol% for **P2**. The reactivity ratios found in literature for a copolymerization of isoprene and styrene vary between 1.3 and 2.02 for isoprene and between 0.42 and 0.53 for styrene.[231] Reactivity ratio values above

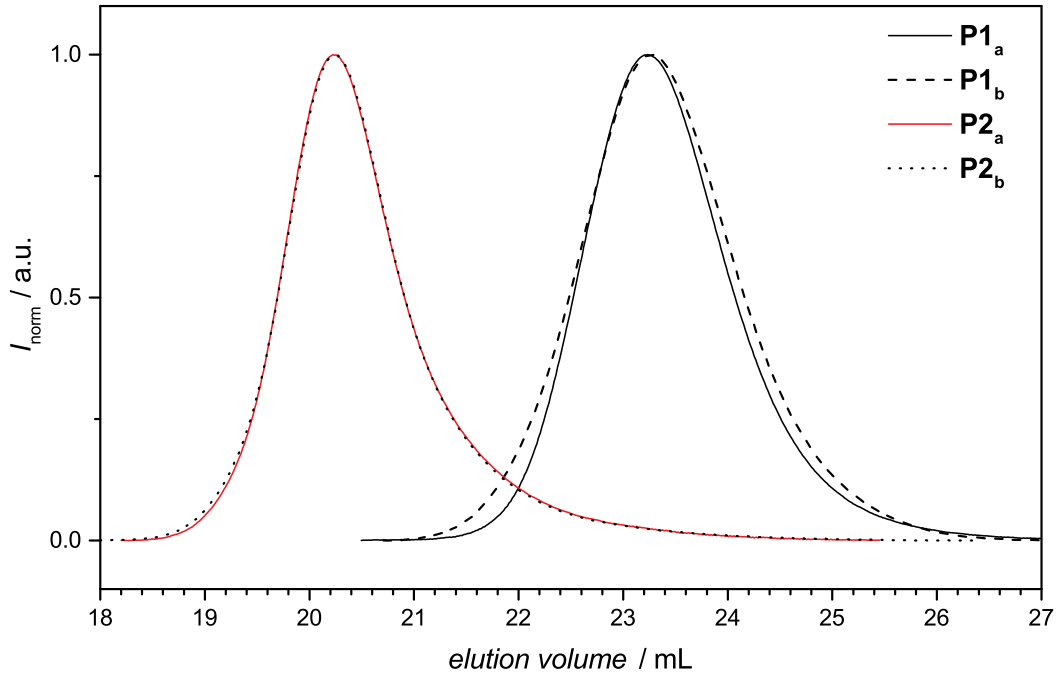

Figure 3.3 SEC traces of polymers **P1** and **P2** before ($\mathbf{P1_a}$ and $\mathbf{P2_a}$) and after ($\mathbf{P1_b}$ and $\mathbf{P2_b}$) Cp-transformation.

1.0 mean that the monomer radical prefers to react with a monomer of its own species rather than with a monomer from the other species (meaning that isoprene radicals prefer to react with isoprene monomer instead of styrene). For reactivity ratios below 1.0, the opposite is true (meaning that styrene radicals prefer to react with isoprene monomer instead of styrene). Hence, it is consistent with theory that the percentage of isoprene found in the polymer is higher than the percentage of the initial monomer feed. The difference between the two polymers (27 mol% for **P1** and 24 mol% for **P2**) derives from the different conversions (30 % for **P1** and 39 % for **P2**). Copolymerizations with reactivity ratios divergent from 1.0, change the actual monomer feed with conversion. At the beginning, isoprene is consumed faster than styrene. Hence, the fraction of isoprene in the monomer feed decreases and it becomes less available. Thus, the consumption rate of isoprene decreases with increasing conversion. As a result, the percentage of isoprene in the obtained polymer is highest for low conversions and decreases with progressing conversion. As an example, for a copolymerization with 100 % conversion

the ratio of monomers observed in the polymer needs to be equal to the ratio of the initial monomer mixture, regardless of the reactivity ratios.

Due to a smaller repeating unit to end group ratio and better solubility properties, **P1** was used for detailed NMR analysis and DLS experiments after ligation with a low molecular weight hydrophilic block (please refer to Section 3.3). **P2** was used for macroscopic separation experiments and membrane formation *via* SNIPS (please refer to Section 3.3 and Chapter 4).

The Cp-transformation of the Matrix A polymers was straightforward. In general, two approaches for the substitution of bromine with Cp exist. The use of sodium cyclopentadienyl (NaCp) as a source for nucleophilic Cp implicates a high reactivity of the Cp-anion towards functional groups such as ester moieties.[232,233] Since two ester moieties are present in the Matrix A polymers, the NaCp based approach for the Cp transformation is not suitable. Nickelocene ($NiCp_2$) as nucleophilic source, on the other hand, is a mild and effective transformation that tolerates a wide range of functional groups, including ester moieties.[234] Thus, it was the method of choice. Since it is known that Cp groups undergo dimerization,[235] the comparison of the SEC traces before and after the functionalization of the polymers **P1** and **P2** is essential (see Figure 3.3). The SEC traces of both polymers do not show any side products due to dimerization. The successful substitution of bromine with Cp can be verified by the proton signals appearing between 6.5 ppm and 6.1 ppm associated with the vinyl protons of the Cp moiety in the ^{1}H NMR spectra of polymer $\mathbf{P1}_b$ (see Figure 3.4). Full conversion – and therefore close to quantitative Cp transformation – was assessed by the successful conjugation of the building blocks **P1** and **P2** with respective hydrophilic polymer blocks, verified *via* SEC (please refer to Section 3.3).

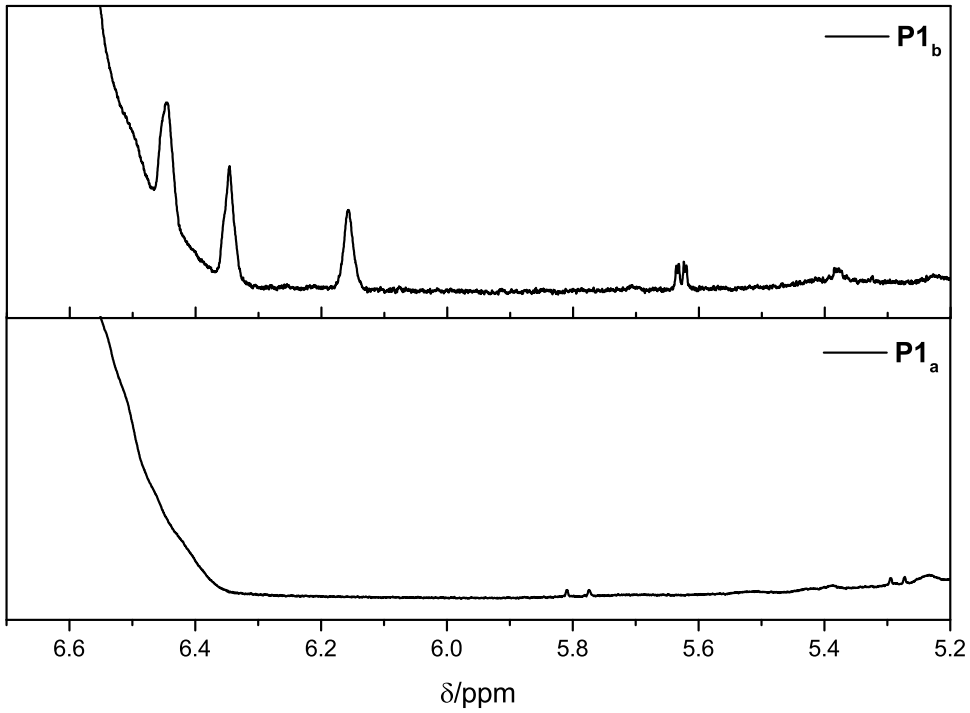

Figure 3.4 ^{1}H NMR spectra (500 MHz, $CDCl_3$, ambient temperature) of polymer **P1** before (**P1$_a$**) and after (**P1$_b$**) the Cp-transformation in the relevant region (6.7 ppm–5.2 ppm) for Cp protons.

3.2 Matrix B: The Hydrophilic Building Block

For simplicity the term "Matrix B" replaces the term "hydrophilic building block" in the rest of the thesis. As selection criteria for Matrix B polymers the solubility characteristics of the polymers are of major importance. In order to be suitable for the SNIPS process, the polymer needs to be soluble in water and in the employed casting solution. Additionally, in the process of the thesis other limitations emerged, caused by the choice of the RAFT-HDA-concept as ligation method. It was found that HDA capable CTAs are sensitive towards amide and amine moieties, as present in the monomers *N*,*N*-dimethylaminoethyl methacrylate (DMAEMA) and *N*-isopropyl acrylamide (NIPAM). Moreover, a polymer with an acrylate backbone is required, since it was found that HDA–RAFT agents are not able to undergo HDA conjugations when a methacrylate monomer is employed in the RAFT polymerization (however, the reverse functions by using a Cp-terminal poly(methacrylate) and a RAFT terminal poly(acrylate)). Thus, the three acrylates

(triethylene glycol methyl ether acrylate (TEGA), hydroxyethyl acrylate (HEA) and acrylic acid (AA)) shown in Scheme 3.2 were employed for the preparation of Matrix B polymers *via* CRP using the phosphoric HDA-RAFT agent **CTA-2**. To verify the control

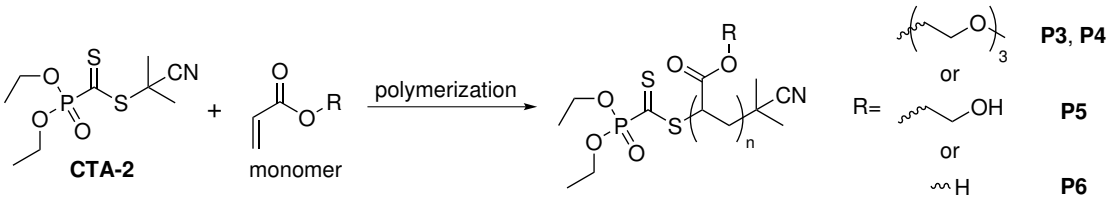

Scheme 3.2 Synthetic route for the preparation of Matrix B polymers. Polymerization: dioxane (ethanol for HEA), AIBN, 70 °C (60 °C for HEA).

afforded by the RAFT process, leading to polymers with high end group fidelity, kinetic studies were carried out exemplarily for the polymerization of triethylene glycol methyl ether acrylate (see Figure 3.5 and Table 3.2). The SEC traces corresponding to all the data points are depicted in diagram **B** of Figure 3.5. The multimodal distribution of the SEC traces with 2 % and 4 % conversion are due to the high resolution in the low molecular weight area of the employed SEC system. Each peak corresponds to a single polymer chain with a certain amount of monomer units. With progressing conversion a linear increase of the detected molecular weight can be observed. The black line in the diagram **A** (Figure 3.5) is inserted to guide the eye. For the calculation of the theoretical M_n Equation 2.1 is applied. Considering the inaccuracy of the SEC (about 10 %) and the PMMA calibration, the theoretical M_n is in good agreement with the observed values.

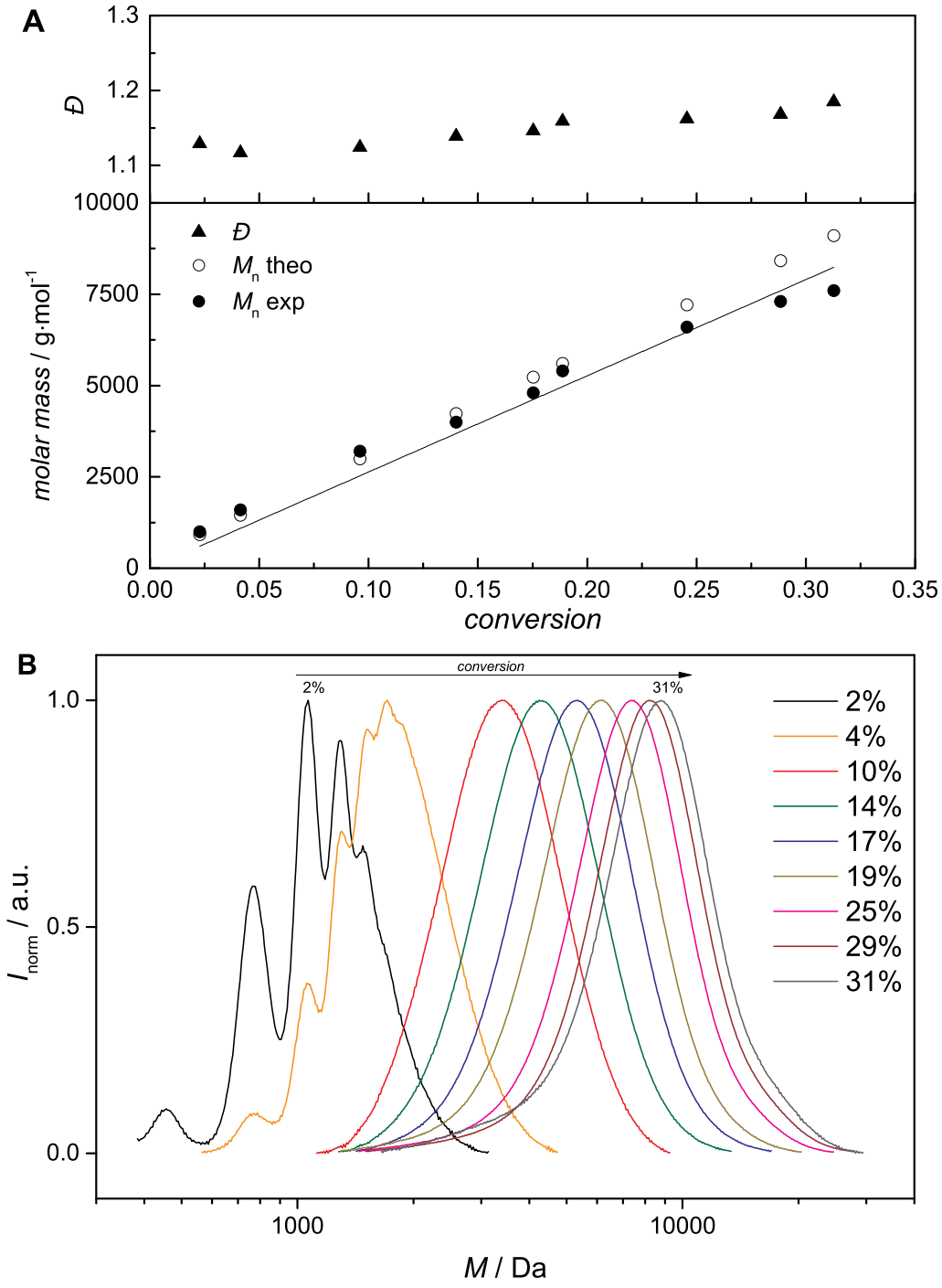

Figure 3.5 **A**: Evolution of the *molar mass* and *Đ* versus *conversion* during the polymerization of TEGA in dioxane: $[\text{monomer}]_0 = 3.9\,\text{mol}\,\text{L}^{-1}$, $[\textbf{CTA-2}]_0 = 30.2\,\text{mmol}\,\text{L}^{-1}$, $[\text{AIBN}]_0 = 5.2\,\text{mmol}\,\text{L}^{-1}$, 70 °C. The theoretical molecular weights and DPs were calculated from the CTA concentration and the conversion. **B**: SEC traces of the respective data points from **A**. The SEC was calibrated with narrow PMMA standards.

Table 3.2 The degree of polymerization (DP), the theoretical and the experimental *molar mass* and $Đ$ for several conversions during the polymerization of TEGA in dioxane: $[\text{monomer}]_0$ = 3.9 mol L^{-1}, $[\textbf{CTA-2}]_0$ = 30.2 mmol L^{-1}, $[\text{AIBN}]_0$ = 5.2 mmol L^{-1}, 70 °C. The theoretical molecular weights and DPs were calculated from the CTA concentration and the conversion.

conversion	DP	$M_{n,theo}$ [g mol^{-1}]	$M_{n,exp}$ [g mol^{-1}]	$Đ$
2 %	3	900	1000	1.13
4 %	5	1500	1600	1.12
10 %	12	3000	3200	1.12
14 %	18	4200	4000	1.14
18 %	23	5200	4800	1.15
19 %	24	5600	5400	1.16
25 %	32	7200	6600	1.16
29 %	37	8400	7300	1.17
31 %	40	9100	7600	1.19

In comparison with the copolymerization of isoprene and styrene, the $Đ$ is not decreasing with progression of the conversion. However, the very low values between 1.1 and 1.2 further support the evidence of a controlled polymerization. In combination, the linear increase of the molar mass, the good agreement of $M_{n,theo}$ and $M_{n,exp}$ and low $Đ$ values are proof for a controlled polymerization. Subsequently, a high and a low molecular weight poly(triethylene glycol methyl ether acrylate) (PTEGA, **P3**: M_n = 6600 g mol^{-1}, $Đ$ = 1.12 and **P4**: M_n = 35 000 g mol^{-1}, $Đ$ = 1.30), poly(hydroxyethyl acrylate) (PHEA, **P5**: M_n = 1500 g mol^{-1}, $Đ$ = 1.09) and poly(acrylic acid) (PAA, **P6**: M_n = 4000 g mol^{-1} (NMR calculation)) were prepared. The SEC traces of **P3** and **P4** can be found in Section 3.3. For the SEC traces and NMR spectra of **P5** and **P6** please refer to Chapter 6 Figure 6.4 - 6.7. SEC analysis for PAA is not straight forward because the polymer tends to interact with column material and is only soluble in very polar solvents. For **P6** an aqueous Na_2HPO_4 buffered system with a PSS Suprema column, with poly(hydroxymethacrylate) copolymer network as solid phase, was employed. Because no narrow molecular weight PAA standards were available at that time, the SEC analysis was conducted without calibration. In order to avoid the problems associated with SEC analysis of PAA, it possible to esterify the acid moieties of the polymer with methanol (yielding poly(methyl acrylate)) and perform the analysis on an organic solvent based SEC system.[236] However,

the combination of dRI and UV detector of the employed aqueous SEC system gives evidence about the $Đ$. The $Đ$ is defined as the mass average molar mass, divided by the number average molar mass ($Đ = M_w / M_n$).[237] Meaning, for a low $Đ$, number and mass average distributions need to have similar values. Since the only UV active moiety of **P6** is the RAFT end group, the UV signal trace is equivalent to the number distribution of the polymer. The dRI signal trace (mass distribution) is in good agreement with the UV trace (see Figure 6.6), implying a low $Đ$ and a high end group fidelity. The NMR calculation for the molecular weight determination was performed by comparison of the integral of the resonances from the RAFT end group with the integral of the resonances from the backbone.

P3 was used for detailed NMR analysis and DLS experiments after ligation with **P1** (please refer to Section 3.3). **P4** was used for macroscopic separation experiments and membrane formation *via* SNIPS (please refer to Section 3.3 and Chapter 4). The polymers **P5** and **P6** (and **P3**) were used for grafting experiments on Cp-functional surfaces (please refer to Section 4.3).

3.3 Ligation and Cleavage of the Building Blocks

Among the three prepared hydrophilic polymer types, PTEGA was chosen as Matrix B for the preparation of amphiphilic block terpolymers (see Scheme 3.3), because it is soluble in a wide range of organic solvents and water, thus most suitable for the SNIPS process. The conjugation reactions were performed in ethyl acetate in the presence of

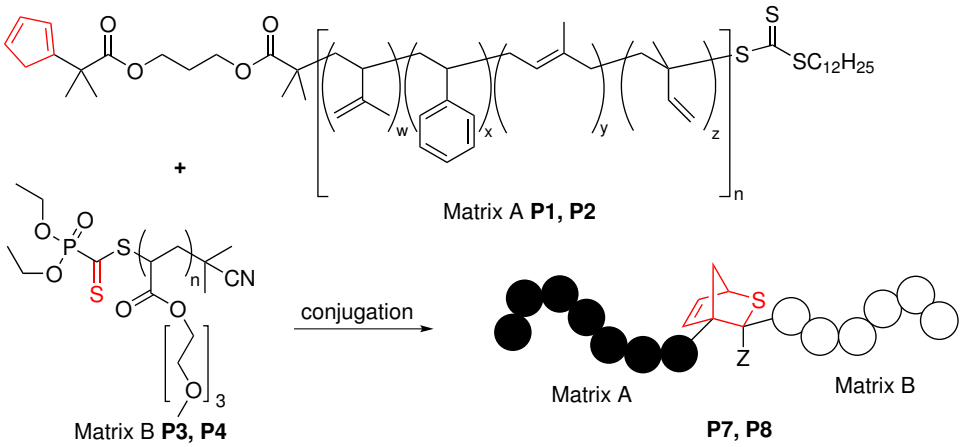

Scheme 3.3 Synthetic strategy for the preparation of amphiphilic block terpolymers. Conjugation: ethyl acetate, $ZnCl_2$, ambient temperature.

$ZnCl_2$ as catalyst at ambient temperature. The total concentration of polymers was kept at 50 g L^{-1}. The utilization of a catalyst is not mandatory for a successful ligation (please refer to the high temperature size exclusion (HT-SEC) experiments described later in this section). Nevertheless, it was found that the reaction rate, especially for the larger building blocks, is more than seven times higher in the presence of $ZnCl_2$. The SEC traces of the generated poly(isoprene-*co*-styrene)-*block*-poly(triethylene glycol methyl ether acrylate) (P(I-*co*-S)-*b*-PTEGA) terpolymers (**P7**: M_n = 16 000 g mol^{-1}, $Đ$ = 1.15; **P8**: M_n = 68 000 g mol^{-1}, $Đ$ = 1.32) and their respective building blocks (**P1** and **P3** respectively **P2** and **P4**) are depicted in Figure 3.6. As expected, the resulting block copolymer **P7** shows a significant shift to lower elution volume, compared to the building blocks **P1** and **P3**. Moreover, the $Đ$ value of **P7** ($Đ$ =1.15) is in between the values of the building blocks **P1** and **P3** (**P1**: $Đ$ = 1.22 and **P3**: $Đ$ = 1.12). The low $Đ$ value and the shift to a lower retention volume indicate the successful conjugation and thus, close to quantitative

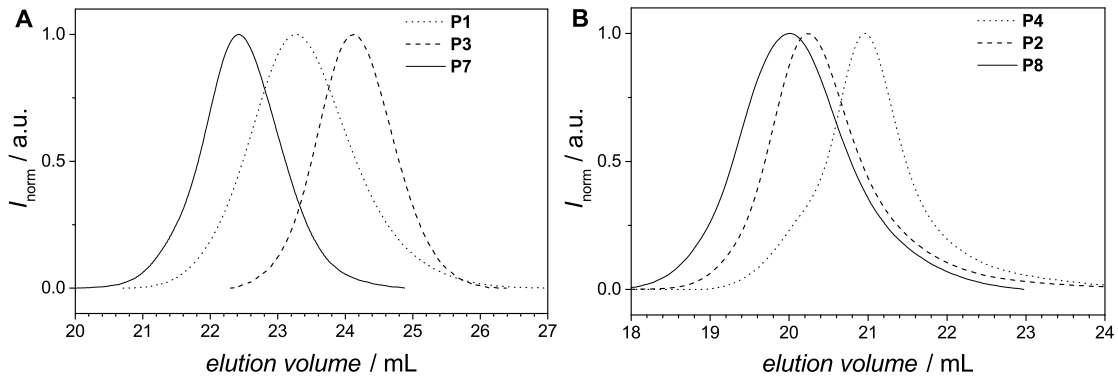

Figure 3.6 **A**: SEC traces of the polar building block PTEGA (**P3**, dashed line, M_n = 6600 g mol^{-1} (PMMA calibration), $Đ$ = 1.12), the non-polar building block P(I-*co*-S) (**P1**, dotted line, M_n = 9200 g mol^{-1} (PS calibration), $Đ$ = 1.22) and the resulting block terpolymer P(I-*co*-S)-*b*-PTEGA (**P7**, solid line, M_n = 16 000 g mol^{-1} (PS calibration), $Đ$ = 1.15). **B**: SEC traces of the polar building block PTEGA (**P4**, dotted line,M_n = 35 000 g mol^{-1} (PMMA calibration), $Đ$ = 1.30), the unpolar building block P(I-*co*-S) (**P2**, dashed line, M_n = 50 000 g mol^{-1} (PS calibration), $Đ$ = 1.36) and the resulting block terpolymer P(I-co-S)-*b*-PTEGA (**P8**, solid line, M_n = 68 000 g mol^{-1} (PS calibration), $Đ$ = 1.32).

Cp-transformation of the building block **P1**.[238,239] For the block terpolymer with higher molecular weight (**P8**), the shift to lower retention volumes, compared to its building blocks **P2** and **P4**, is less pronounced than for polymer **P7**. This observation is associated with the fact that high molecular weight polymers have a small elution volume and small shifts in this area have a larger effect on the resulting molecular weight, compared to the area of bigger elution volumes and low molecular weight polymers. Thus, the shift of the block terpolymer **P8** compared to its building blocks is in the expected range. Furthermore, the $Đ$ value of **P8** ($Đ$ = 1.32) is in between the values of the building blocks **P2** and **P4** (**P2**: $Đ$ = 1.36 and **P4**: $Đ$ = 1.30). Again, low $Đ$ values and the shift to lower elution volumes indicate a successful and quantitative conjugation. In addition, **P1**, **P3** and **P7** were analyzed *via* ^{1}H NMR spectroscopy (see Figure 3.7). The spectrum of the block terpolymer **P7** is composed of the sum of the resonances from the individual building block polymers **P1** and **P3**. Comparing the integrals from the resonances of the individual building blocks, the molar ratio of PTEGA and P(I-*co*-S) in the resulting block terpolymer can be determined. In Table 3.3 the calculated ratios from both block terpolymers and the content of isoprene is collated. For a determination of the amount

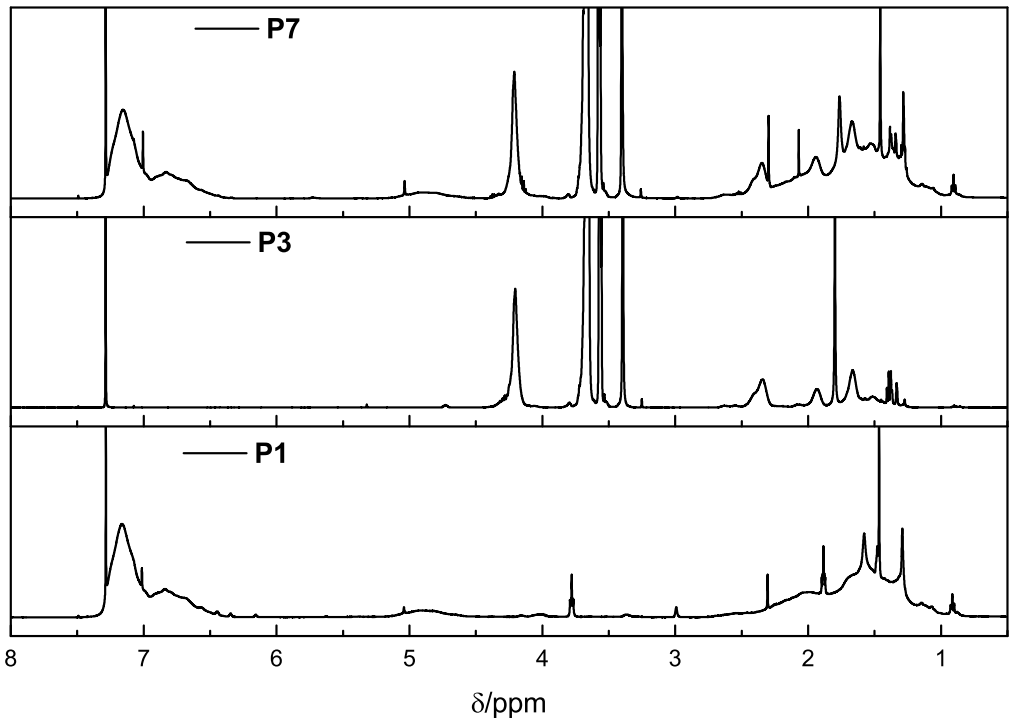

Figure 3.7 ^{1}H NMR spectra (500 MHz, $CDCl_3$, ambient temperature) of the non-polar building block **P1**, the polar building block **P3** and the resulting block terpolymer **P7**.

of vinyl groups in the side chains of the block terpolymer by calculating the ratio of 1,2 and 3,4 isomers, the signals of the respective resonances are of insufficient intensity. The ratio of 1,4, 1,2 and 3,4 isomers present in polyisoprene prepared by RAFT using DMP as CTA was published previously.[227] It can be expected that the control of the polymerization with DMP-Br is very similar to DMP. Thus, the amount of vinyl side chains has been calculated for both block terpolymers close to 2 mol%. This quantity

Table 3.3 Molar ratios of P(I-*co*-S)/PTEGA for the block terpolymers **P7** and **P8**, isoprene content of the building block P(I-*co*-S) and the respective block terpolymer. All values were determined by comparison of the integrals (from the ^{1}H NMR spectra of Figure 3.7) of the individual components.

polymer	molar ratio P(I-*co*-S)/PTEGA	fraction of isoprene in P(I-*co*-S) [mol%]	fraction of isoprene in the block terpolymer [mol%]
P7(**P1**)	72/28	27	19
P8(**P2**)	75/25	24	18

is expected to be sufficient for potential cross linking after the eventual membrane formation.

Further inspection of the ^{1}H NMR spectra of the polymers **P1** and **P7** in the region of the vinyl moiety (6.7 ppm–5.2 ppm, see Figure 3.8) clearly indicates a strong decrease of the resonances of the Cp moiety from polymer **P1** after the HDA reaction. Consequently,

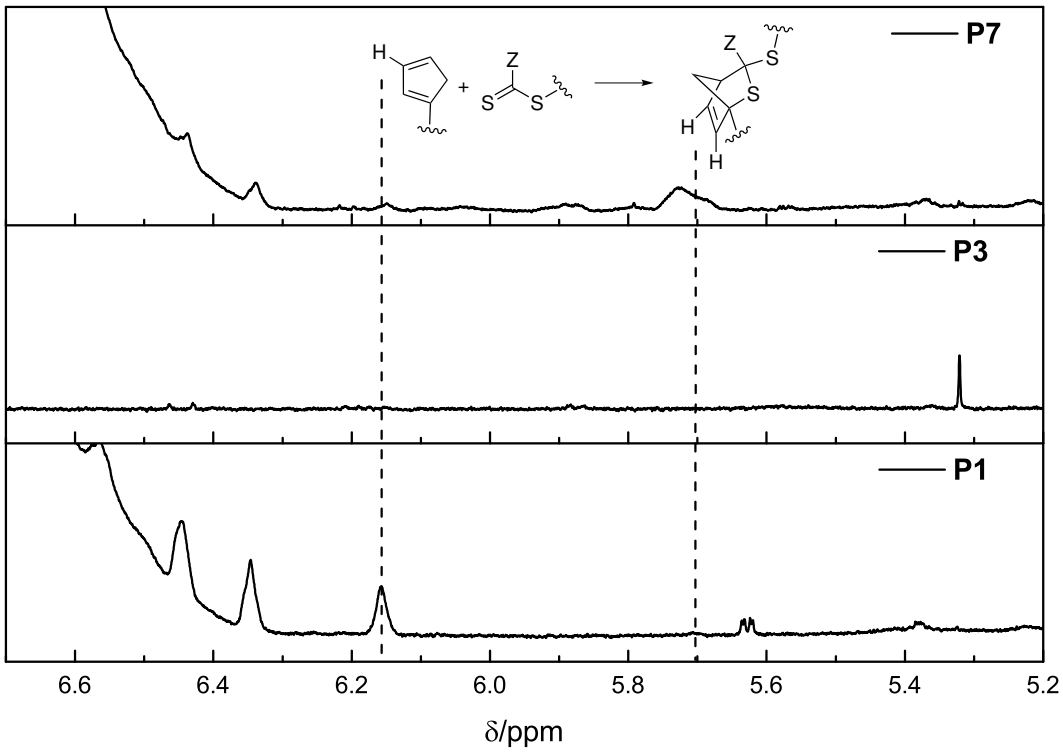

Figure 3.8 Enlarged section of the ^{1}H NMR spectra (500 MHz, $CDCl_3$, ambient temperature) of the non-polar building block **P1**, the polar building block **P3** and the resulting block terpolymer **P7** in the relevant region (6.7 ppm–5.2 ppm) for the HDA reaction. The dashed lines mark the position of the resonances corresponding to the proton of the Cp moiety (left) and the resonance of the protons of the HDA reaction product (right).

the block terpolymer **P7** reveals a new resonance, corresponding to protons of the HDA reaction product. The spectrum of **P3** is added as well to prove that the new signal is not associated with a resonance thereof.

In the following, the low molecular weight block terpolymer **P7** was subjected to detailed HT-NMR, HT-DLS and HT-SEC analysis, to examine the thermo responsiveness of the HDA linkage.[240] The conclusions thereof can also be assigned to the high molecular weight block terpolymer **P8**, which is later on employed in the SNIPS pro-

cess for membrane preparation (please refer to Chapter 4). The two resonances at 6.16 ppm and 5.72 ppm of the Cp moiety and the HDA reaction product are essential for following the bonding and debonding of the hetero Diels-Alder linkage by HT-NMR analysis. At ambient temperature, the equilibrium of the HDA reaction of **P1** with **P3** is completely shifted towards the HDA reaction product, *i.e.* the block copolymer **P7**. However, by increasing the temperature the retro HDA reaction becomes favored and the equilibrium shifts towards the reactants **P1** and **P3**. To determine the temperature when the equilibrium is completely shifted towards the initial building blocks, ^{1}H NMR spectra of the block terpolymer **P7** were recorded while increasing the temperature from 25 °C to 85 °C (see Figure 3.9). Information of the position of the equilibrium

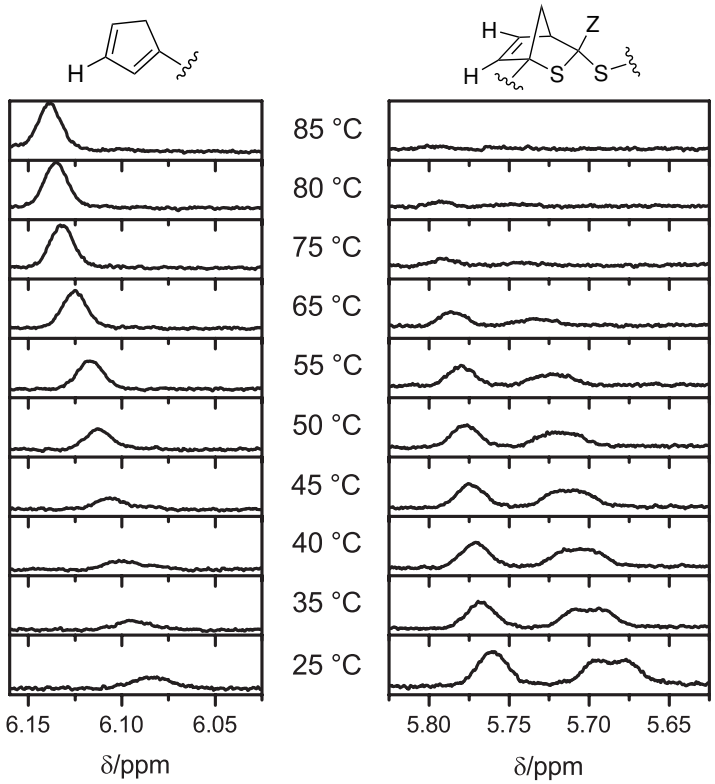

Figure 3.9 ^{1}H NMR spectra (400 MHz, toluene-d_8–DMSO-d_6, 1 : 1) of the block terpolymer **P7** at variable temperatures. The resonances of the Cp moiety are depicted on the left hand side (6.2–6.0 ppm) and the resonances associated with the HDA reaction product are depicted on the right hand side (5.85–5.6 ppm).

between the block terpolymer **P7** and the reactants **P1** and **P3** is obtained by comparing the intensities of the resonance of the Cp proton (6.2–6.0 ppm) and the resonance of

the protons from the HDA reaction product (5.85–5.6 ppm). To ensure equilibrium conditions for each temperature step, successive NMR spectra have been recorded until the intensity arrangement of the current spectrum was identical with the one recorded before. From 45 °C to 85 °C, the intensity of the resonance of the Cp moiety is increasing continuously. Simultaneously, the intensity of the resonance corresponding to the HDA reaction product is decreasing. The complete disappearance of the peaks at 5.85–5.6 ppm at 85 °C and concurrent appearance of the resonance peak at 6.2–6.0 ppm indicate that the equilibrium is completely shifted towards the building blocks **P1** and **P3**. The drift of the signals towards a lower field is due to the increasing temperature. The NMR experiment was performed in a mixture of toluene-d_8 and DMSO-d_6 (1 : 1). This mixture was used to ensure a moderate polarity to keep both building blocks in solution after debonding. In addition, a high boiling point was preferred because the cleavage temperature is relatively high.

Having determined the cleavage temperature, further HT-NMR experiments have been performed in $CDCl_3$ in the presence of $ZnCl_2$ as catalyst, using a NMR pressure tube. Note that the different solvents employed slightly affect the resonances appearance and position. In order to evidence that the bonding and debonding of the building blocks **P1** and **P3** is reversible with temperature, ^{1}H NMR spectra of the block terpolymer **P7** were performed and cycled 4 times between 25 °C and 90 °C (see Figure 3.10). Again, the regions of the resonance from the Cp proton (6.1–6.0 ppm) and of the protons of the HDA reaction product (5.85–5.6 ppm) were investigated. The bonding/debonding behavior can be observed over all 4 succeeding repetitions. For every cycle, in the region of the HDA reaction product only the baseline can be detected at 90 °C, whereas the resonance of the Cp moiety has full intensity, revealing complete transformation into the two separate building blocks. Concomitantly, at 25 °C the resonance of the Cp moiety disappears for each cycle, whilst the highest intensity of the resonance of the HDA reaction product can be observed. It takes approximately 30 min until the equilibrium state is established for the cleavage of the block terpolymer at 90 °C. Complete rebonding was achieved after 24 h at 25 °C. The difference in reaction time, compared to the synthesis of **P7** (16 h), can be explained by the absence of stirring of the reaction mixture in the NMR tube

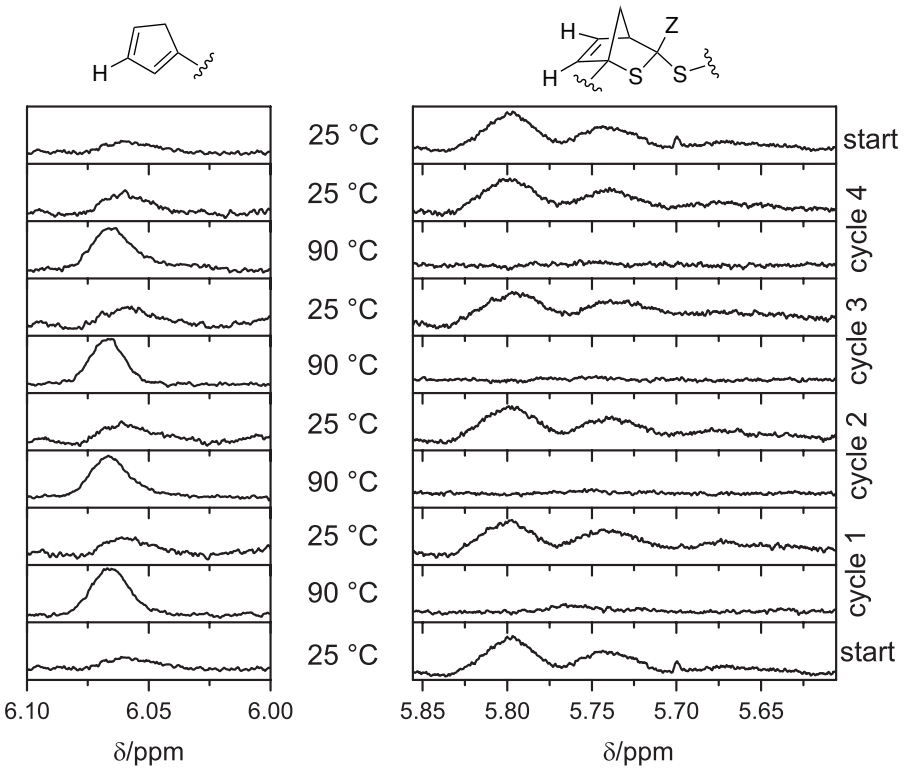

Figure 3.10 ^{1}H NMR spectra (400 MHz, $CDCl_3$) of the block terpolymer **P7** at alternating temperatures in four heating/cooling cycles between 25 °C and 90 °C. The resonances of the Cp moiety are depicted on the left side (6.1–6.0 ppm) and the resonances associated with the HDA reaction product are shown on the right side (5.85–5.6 ppm). For better comparison, the starting spectrum is depicted at the bottom and on top of the figure.

and thus the bonding reaction is diffusion controlled, leading to a longer reaction time for the block terpolymer formation. In $CDCl_3$ no drift of the signals towards lower field at elevated temperatures was observed.

To further underpin the results of the HT-NMR experiments, HT-DLS analysis of the block terpolymer **P7** have been conducted. Since no pressure stable DLS cuvettes were available, the choice of solvents was limited by their boiling points and their ability to dissolve both individual building blocks as well as scattering properties. **P7** was dissolved in a mixture of *N,N*-dimethylacetamide (DMAc, 80 vol%) and toluene (20 vol%) in the presence of $ZnCl_2$ as catalyst revealing the best possible conditions for the HT-DLS measurements. For the block terpolymer **P8** no suitable conditions were found due to solubility issues. Representative examples of autocorrelation functions and the resulting size distributions can be found in Section 6.5 (Figure 6.8 and 6.9,

respectively). Unimers with a hydrodynamic radius (R_h) of close to 2.5 nm are detected at 30 °C for the block terpolymer (please refer to Figure 3.11). When the sample is

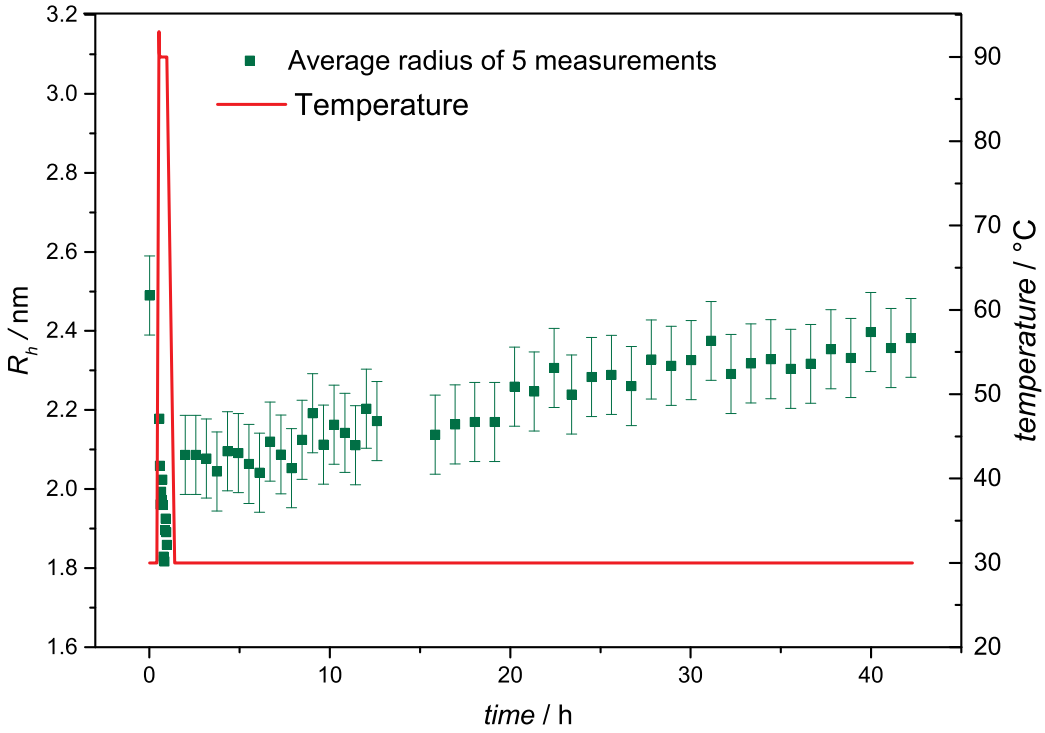

Figure 3.11 HT-DLS experiment of block terpolymer **P7** in a mixture of DMAc (80 vol%) and toluene (20 vol%) in the presence of $ZnCl_2$ as catalyst. The green squares depict the average radius of 5 subsequently measured values in the specified time interval. The experimental standard deviation is close to 0.1 nm. Due to the fast and large change of the actual radius when the sample is heated at 90 °C, no average radius is calculated for that temperature. The red solid line displays the temperature evolution.

heated to 90 °C, the detected radius decreases to values below 2.0 nm, indicating that the block terpolymer is cleaved into the individual building blocks, which form significantly smaller unimers. As soon as the temperature is decreased again to 30 °C, the block terpolymer – and hence the corresponding unimers – start to reform and the radius increases again continuously with time up to the initially recorded average size (2.4 nm). To examine the reversible bonding and debonding behavior of the HDA linkage, 4 temperature cycles between 30 °C and 90 °C were performed (refer to Figure 3.12). At 90 °C, the system was allowed to equilibrate for 30 min until no further changes in R_h were observed. Equally, at 30 °C, the depicted radius was measured after the equilibrium

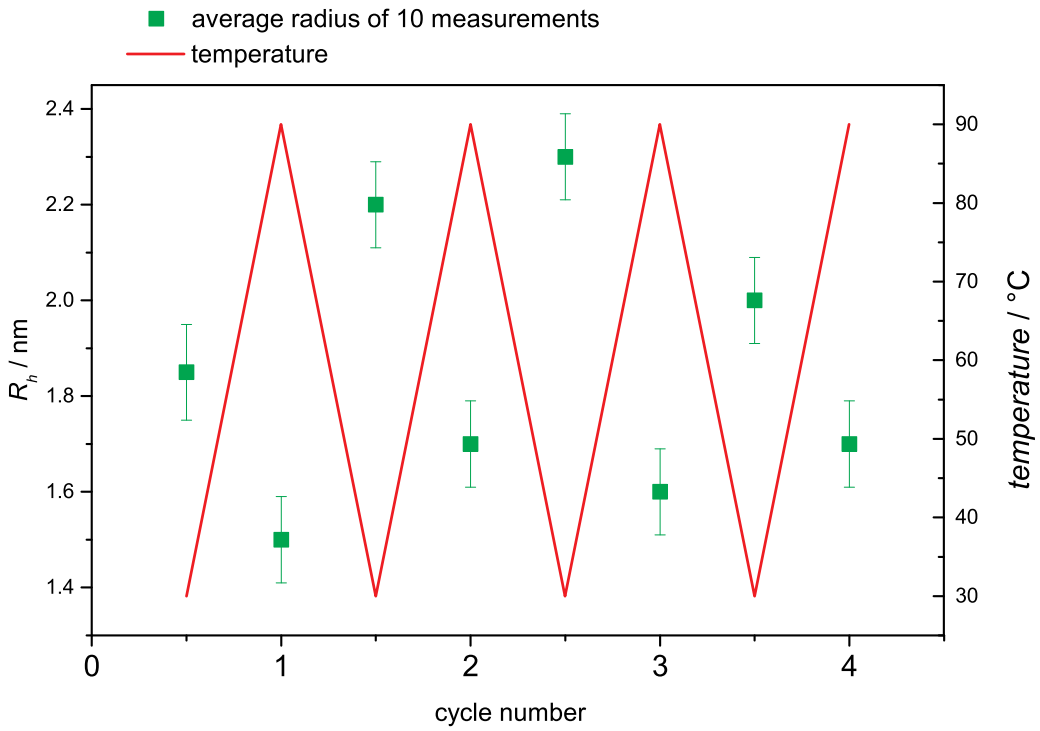

Figure 3.12 HT-DLS cycles of block terpolymer **P7** in a mixture of DMAc (80 vol%) and toluene (20 vol%) in the presence of $ZnCl_2$ as catalyst. The green squares represent the average radius of 10 subsequently measured values with an experimental standard deviation of 0.1 nm. The red solid line displays the temperature evolution.

was established. For every temperature switch the expected change of the detected radius can be observed. In contrast, the building block (**P1**) as reference exhibits a R_h of approximately 1.6 nm and no significant change with varying temperature could be observed. However, the respective radii for each cycle at 90 °C and at 30 °C vary more than expected (90 °C: 1.5–1.7 nm; 30 °C: 1.9–2.3 nm). A possible explanation for this observation is associated with the change of the actual ratio of the employed solvent mixture during the measurement. Since sealed DLS cuvettes are not commercially available and thus could not be used, a certain amount of solvent evaporates constantly during the experiment (boiling point DMAc: 165 °C, boiling point toluene: 110 °C). Therefore solvent had to be added continually, which possibly affected the experiment and the data evaluation. The composition of the solvent mixture is influencing the solubility of the polymers. A change in the ratio of toluene to DMAc can possibly lead to small aggregates that affect the measured R_h averages. Additionally, the calculated

R_h is indirectly proportional to the solution viscosity, consequently the data evaluation depends on the solvent composition. In summary, the results of the HT-DLS experiments clearly underpin the results of the HT-NMR analysis.

To further support the results of the HT-NMR and HT-DLS analysis, cycled HT-SEC experiments were performed. The block terpolymer **P7** was dissolved in 1,2,4-trichlorobenzene (TCB; 5 g L^{-1}) and the SEC-vial placed into the preheated autosampler (90 °C). The sample was measured immediately in order to monitor the conjugated state (see Figure 3.13, solid black line, 0 min). However, it must be noted that at this point the

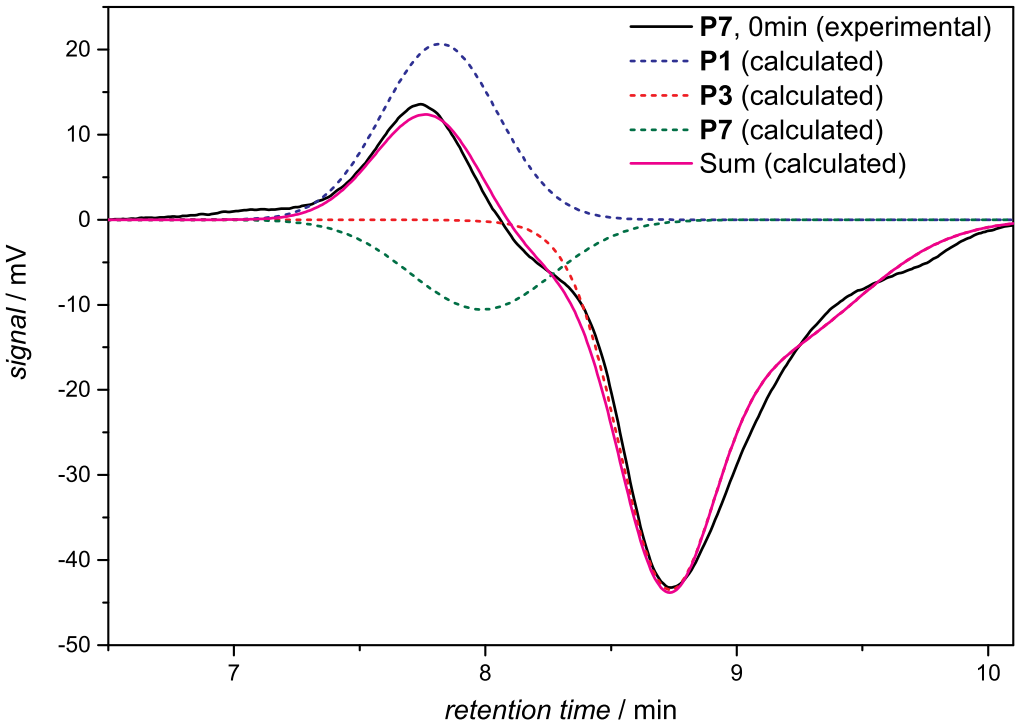

Figure 3.13 HT-SEC trace of **P7** in TCB at 90 °C. The black solid line represents the measurement immediately after the sample was placed into the autosampler (0 min), the dashed lines indicate the mathematically fitted fractions of the polar block (**P3**), the non-polar block (**P1**) and the block terpolymer (**P7**). The pink solid line represents the sum of all theoretical peaks.

completely bonded state cannot be monitored because the sample is subjected to 90 °C for approximately 7–10 minutes during the analysis and before the differential refractive index (dRI) detector is reached. Hence, debonding of the hetero Diels-Alder linkage partially takes place. Consequently, three distinct distributions can be observed, *i.e.* the block terpolymer and its two building blocks. The unpolar building block **P1** shows a

positive dRI signal at a retention time of close to 7.8 min (peak maximum), whereas the polar block **P3** shows a large negative dRI signal at approximately 8.6 min retention time (peak maximum). The block terpolymer reveals a small negative signal at a retention time of close to 8.1 min, overlapping with the building block signals. Calculated distributions of the individual species are depicted as dashed lines. The assignments are based on HT-SEC measurements of the particular building blocks. For validation, the sum of the three calculated distributions is compared with the experimental data, showing a good compliance. Next, the retro HDA reaction was allowed to proceed completely within 30 min at 90 °C in the autosampler. Subsequently, a new chromatogram of the same sample was recorded, representing the debonded state (refer to Figure 3.14, black solid line, 30 min) with maximum intensity (respectively in positive and negative direction) of the building blocks. Again, calculated distributions are depicted as dashed lines.

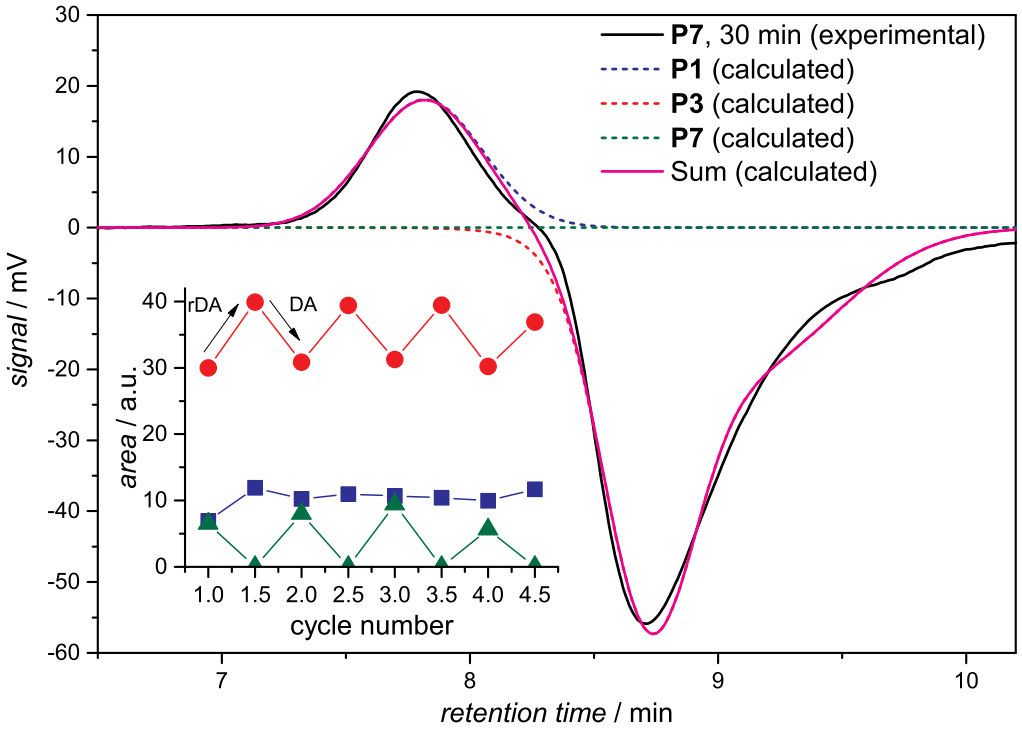

Figure 3.14 HT-SEC trace of **P7** in TCB at 90 °C. The black solid line represents the measurement 30 min after the sample was placed into the autosampler, the dashed lines indicate the mathematically fitted fractions of the polar block (**P3**), the non-polar block (**P1**) and the block terpolymer (**P7**). The pink solid line represents the sum of all theoretical peaks. The inset diagram shows the evolution of the peak areas of the three calculated distributions, alternating for every bonding/debonding cycle (**P1** blue squares, **P3** red dots, **P7** green triangles).

The distribution of the block terpolymer disappears completely. Next, the sample was removed from the autosampler and kept at ambient temperature, whereas the HDA conjugation of the building blocks proceeds within 5 days (without the presence of any catalyst). This procedure was repeated 4 times, a collection of all HT-SEC traces can be found in Figure 3.15. The signal intensities have been evaluated in detail by

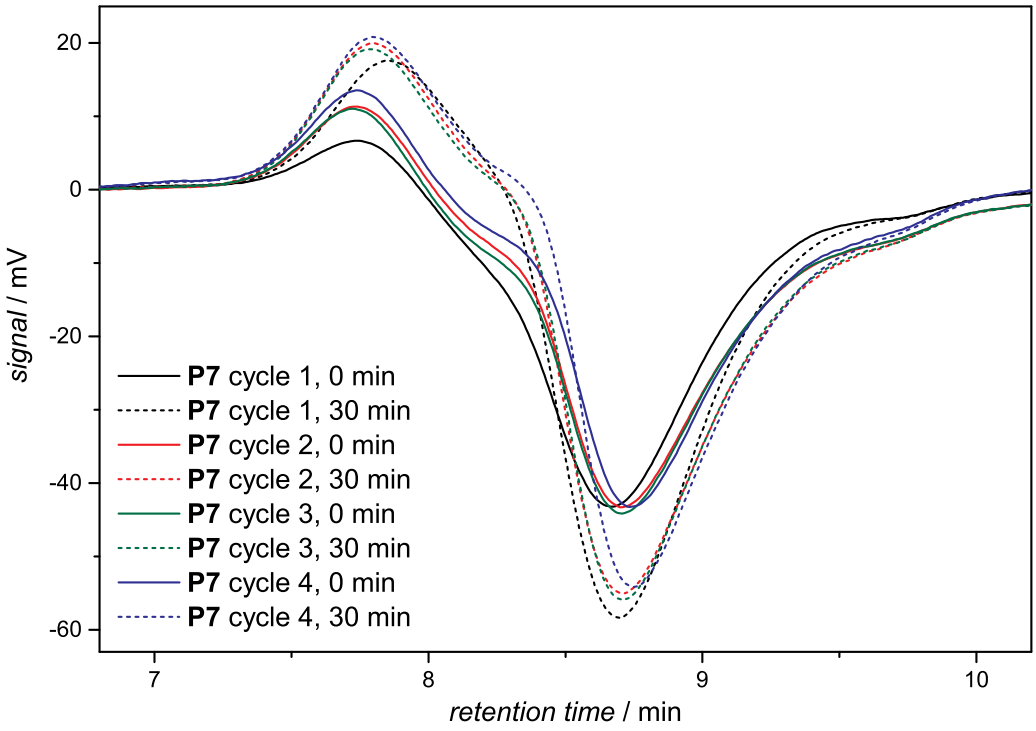

Figure 3.15 HT-SEC traces of **P7** in TCB at 90 °C. The solid lines represent the measurements immediately after the sample was placed into the autosampler. The dashed lines represent the measurements 30 min after the previous measurement. The individual cycles have been measured at intervals of 5 days.

deconvolution of the chromatograms to determine the peak areas. The results are displayed in the inset diagram in Figure 3.14. The trend of the data clearly demonstrates the expected effects: the peak area and thus the concentration of both building blocks (**P1** blue squares, **P3** red dots) increases during the retro HDA reaction and it decreases during the HDA reaction (the intensity of **P1** is minor because of the low dn/dc value and thus the changes in peak area are less pronounced). As expected, the observation for the block terpolymer (green triangles) is inverse. The separation of the specific polymers on the HT-SEC column is not purely entropically driven but also caused by

enthalpic interactions (adsorption of polar polymers on the column material at high temperatures with TCB as eluent was already observed in other experiments). Thus, the observed retention time of the amphiphilic block terpolymer is in between the constituting building blocks. In conclusion, the constant difference of the dRI signal intensities of the building blocks between the measurements after 0 min and 30 min delay in the autosampler at 90 °C for the respective cycles confirms again the temperature dependent cleavage of the HDA linkage, here without the presence of any catalyst.

For the larger block terpolymer **P8** HT-SEC measurements have been performed as well. However, even when the sample was measured immediately after insertion, only the distributions of the building blocks could be observed. This finding can be explained by an entropy driven effect of reversible conjugated polymer systems.[210] The larger chain length of **P8** compared to **P7** lowers the retro HDA reaction temperature. Hence, the reaction proceeds faster in the 90 °C heated HT-SEC environment. Besides this distinction, the linkage of both block terpolymers should behave alike. In order to simulate the cleavage of Matrix B from a membrane, generated from **P8**, a macroscopic separation study was performed. First, an aqueous dispersion of **P8** was prepared. On that account the block terpolymer was dissolved in THF and subsequently added to water. Next, the THF was removed under reduced pressure. Then the dispersion was heated for 30 min at 90 °C and subsequently cooled to ambient temperature (see Figure 3.16). At 90 °C the amphiphilic block copolymer **P8** is cleaved, yielding its building blocks **P2*** and **P4***. **P2*** is not soluble in water and thus remains precipitated. **P4*** is in principal soluble in water, yet has a lower critical solution temperature (LCST) at 70 °C. Above this temperature, **P4** precipitates as a viscid liquid. Hence, the polymers **P2*** and **P4*** aggregate and form a large macroscopic agglomerate (red arrow in Figure 3.16 **B**) at 90 °C. Cooling the mixture to ambient temperature dissolves **P4*** in water. In contrary, **P2*** remains insoluble and forms again an aqueous dispersion. Finally, **P2*** and **P4*** were separated *via* centrifugation. The obtained polymers were analyzed *via* SEC and compared with the SEC traces of the original building blocks **P2** and **P4** and the block terpolymer **P8** (see Figure 3.17). The SEC traces of **P2*** and **P2** are in good agreement. However, for **P4*** the SEC trace shows a shoulder in the elution volume

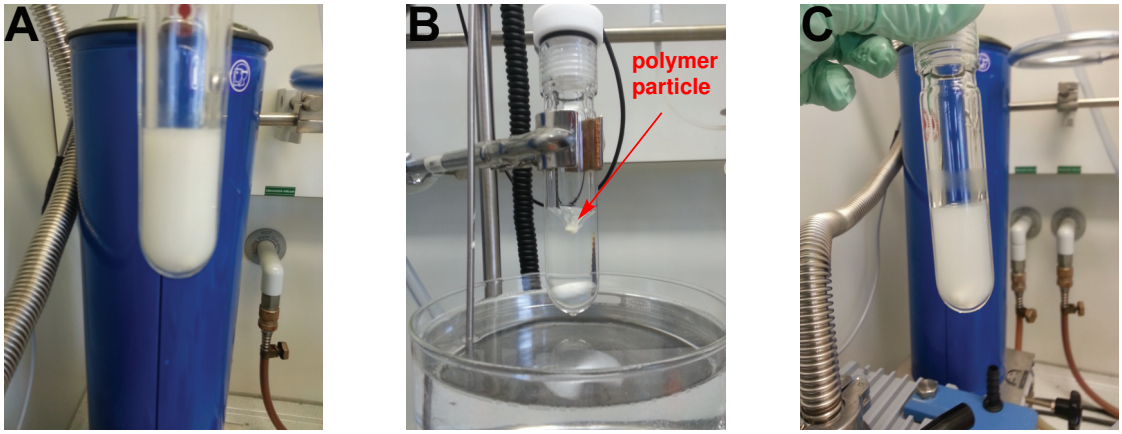

Figure 3.16 Images of the macroscopic cleavage of the block terpolymer **P8**, into the building block polymers **P2*** and **P4***. **A** block terpolymer dispersion in water at ambient temperature. **B** at 90 °C the building blocks are separated. Due to the LCST of **P4**, the building block polymers **P4*** and **P2*** aggregate and form a macroscopic agglomerate (red arrow). **C** cooled to ambient temperature, **P4*** dissolves in water, whereas **P2*** forms an aqueous dispersion.

region of **P2**. Most probably a small amount of **P2*** particles was not entirely separated from the solution of P4*.

This in-depth study of the behavior of the temperature responsive HDA linkage, employed for the synthesis of the amphiphilic block terpolymers P(I-*co*-S)-*b*-PTEGA, indicates that it is suitable for the reversible membrane encoding concept. HT-NMR showed that for temperatures above 45 °C the equilibrium starts to shift towards initial building blocks. In case of surface ligation a small shift towards open linkage is enough

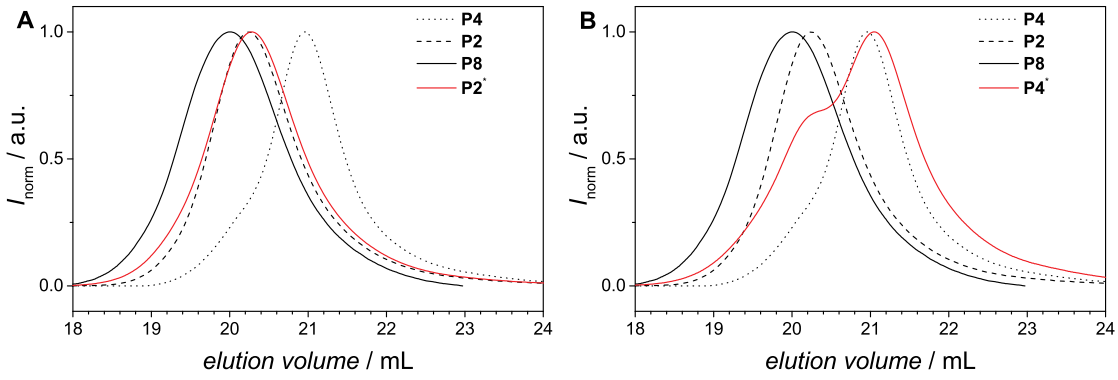

Figure 3.17 SEC traces of the building blocks after macroscopic separation (**A** non-polar block P(I-*co*-S), **P2***, solid red line; **B** polar block PTEGA, **P4***, solid red line), in comparison to the original building blocks (**P2** and **P4**) and the block terpolymer (**P8**).

to detach reactants and exclude them from the reaction equilibrium. Hence, for following membrane experiments mild conditions of only 50 °C can be employed to remove the Matrix B polymers of the pore surface with percolation of water. The cycled HT-NMR, HT-DLS and HT-SEC experiments proved that the Cp moieties are still reactive after cleavage. Thus, it should be feasible to graft dienophiles onto the pore surface after the initial Matrix B was removed from the membrane.

3.4 An Amphiphilic Triblock Quaterpolymer with a Reversible Linkage

In order to further increase the variety of possible membrane modifications, a dual functional CTA capable of highly efficient sequential thermal and photoinduced ligation, generating α,ω-functional polymers, was developed.[†] The novel CTA enables the possibility to graft diblock copolymer on a Cp functional membrane by a later explained strategy, increasing the options to tailor the surface chemistry. To exemplarily demonstrate the versatility, an amphiphilic triblock quaterpolymer poly(isoprene-*co*-styrene)-*block*-poly(ethyl acrylate)-*block*-poly(ethylene oxide) (P(I-*co*-S)-*b*-PEA-*b*-PEO) was prepared.

The novel CTA combines the HDA capable **CTA-2** with a photoenol moiety at its R-group, able to undergo efficient light-induced ligation. Consequently, the polymers obtained from this RAFT agent contain two orthogonally addressable end groups. The resulting molecular structure thereof as well as the key steps of the synthetic route are shown in Scheme 3.4. The first step of the CTA synthesis is the preparation of the precursor molecule **4** by a Markovnikov addition of HBr to a vinyl benzyl photoenol (**3**), which was previously prepared according to a literature protocol.[241] Since it provides a

[†] Parts of the current section are adapted with permission from M. Langer, J. O. Mueller, A. S. Goldmann, F. H. Schacher, C. Barner-Kowollik, *ACS Macro Lett.* **2016**, *5*, 597–601. Copyright ©2016 American Chemical Society. M. Langer designed and conducted all experiments unless otherwise stated and wrote the manuscript. J. O. Mueller provided fumarate fuctionalized PEO and helped with synthetic discussions. A. S. Goldmann, F. H. Schacher, and C. Barner-Kowollik motivated and supervised the project and contributed to scientific discussions.

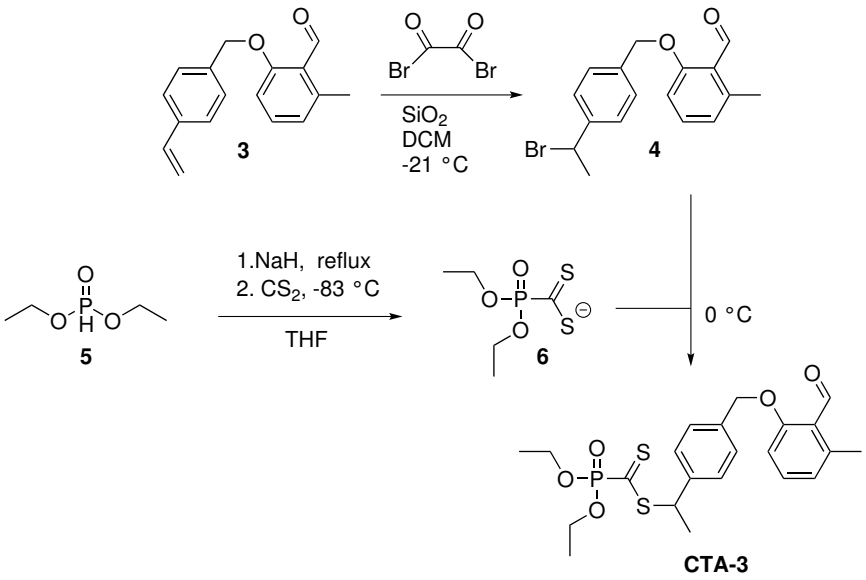

Scheme 3.4 Synthetic strategy for the preparation of the dual functional **CTA-3**.

constantly low, yet sufficient, amount of HBr by reaction with ambient moisture, oxalyl bromide was chosen as a source of HBr. Supplemental addition of water is not required. In order to favor the formation of the desired Markovnikov product, SiO_2 is added to the mixture as surface catalyst.[242] Subsequent reaction of diethylphosphite (**5**) with NaH and CS_2 generates the phosphoric thiocarbonyl thio anion (**6**). Next, a substitution of the bromine, from the previously synthesized precursor **4**, with the thiocarbonyl thio anion **6** yields the dual functional **CTA-3** (yield 33%, ^{1}H NMR see Figure 3.18, for more characterization details refer to Chapter 6).

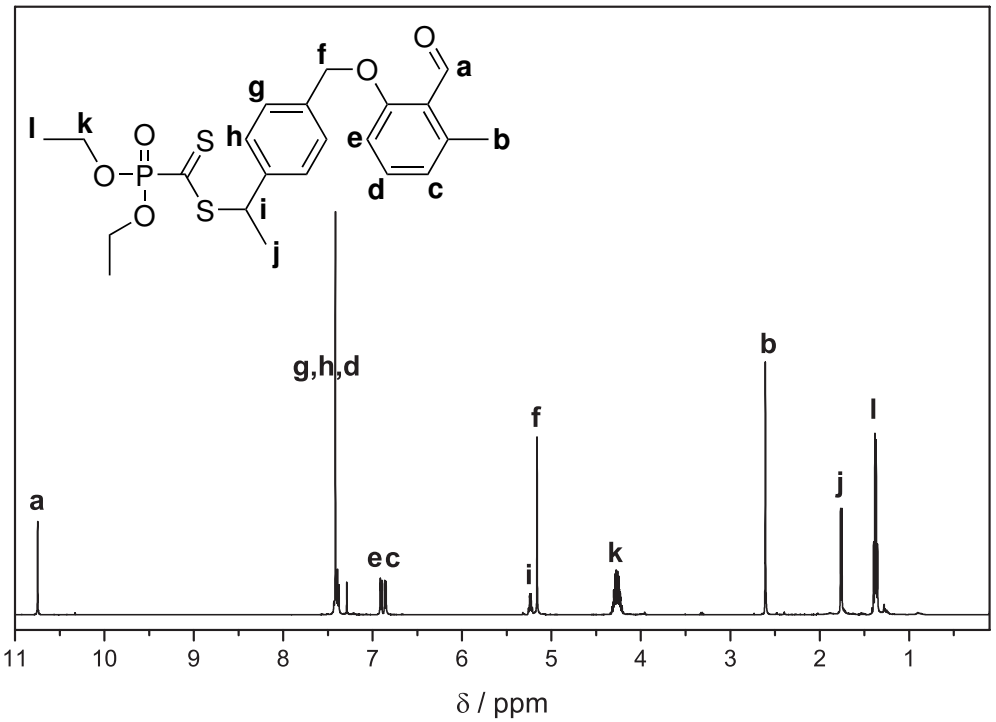

Figure 3.18 ^{1}H NMR spectrum (500 MHz, $CDCl_3$, ambient temperature) of the dual functional **CTA-3**.

Subsequently, preparation of the (P(I-*co*-S)-*b*-PEA-*b*-PEO) triblock quaterpolymer was targeted, utilizing the developed **CTA-3** (see Scheme 3.5). First, the α,ω-functional building block **P9** is prepared *via* RAFT polymerization of ethyl acrylate. In a second step, the phosphorus dithionyl ester end group is employed for the thermally triggered HDA conjugation with the Cp terminated **P1**, affording the diblock terpolymer **P10**. Finally, the third polymer block, fumarate functionalized poly(ethylene oxide), is attached *via* the UV-light triggered photoenol reaction at λ_{max} = 370 nm, affording the triblock quaterpolymer **P11**.

For the preparation of the α,ω-functional polymer **P9**, ethyl acrylate was chosen because it has a moderate polarity (compared to the polymers employed for Matrix A and Matrix B in the previous sections) and is well suited for the analysis *via* ESI-MS. The polymerization of **P9** was conducted within 7 h in bulk at 70 °C, using AIBN as initiator (M_n = 1200 g mol^{-1}, $Đ$ = 1.24; for the SEC trace of **P9** refer to Figure 3.21). A noteworthy fact is the observation of strong inhibition and retardation effects for this polymerization. Within the 7 h of polymerization only 4 % conversion were achieved, which is unusual

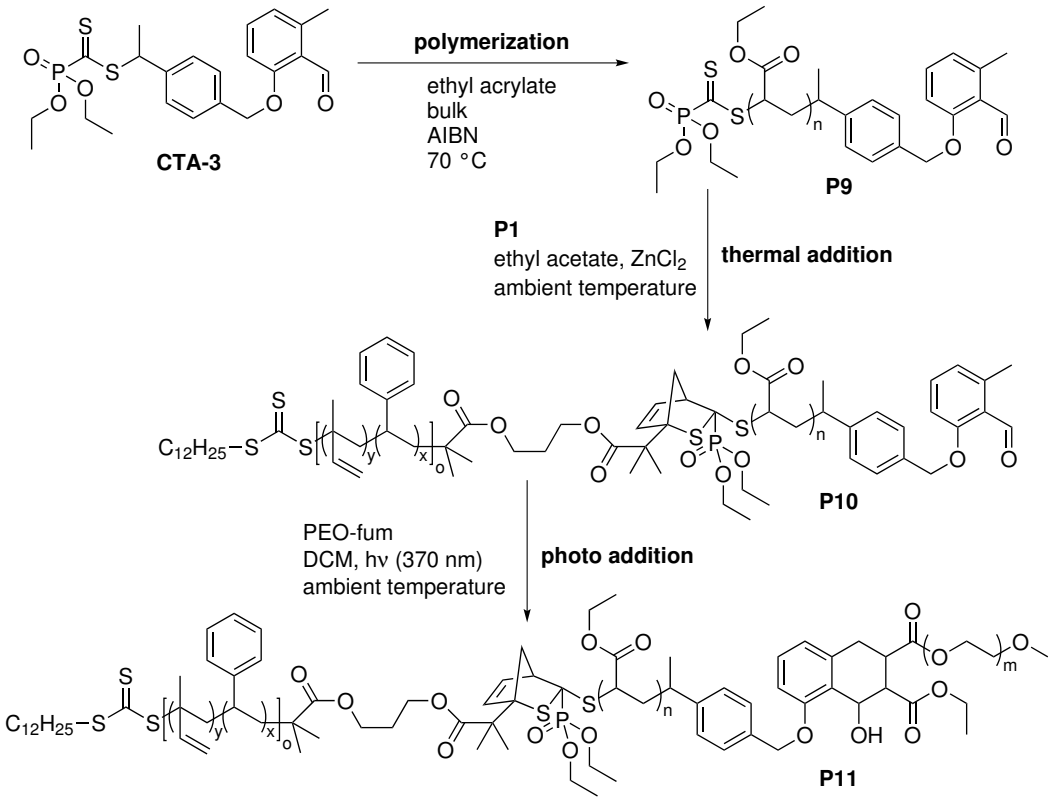

Scheme 3.5 Synthetic strategy for the preparation of the triblock quaterpolymer poly(isoprene-*co*-styrene)-*block*-poly(ethyl acrylate)-*block*-poly(ethylene oxide) *via* modular ligation.

for acrylates. NMR spectroscopy was used to follow the monomer conversion during the reaction. An inhibition time of approximately 4 h was observed. Possible reasons for this observations were already discussed in Section 2.1.3. The long inhibition time may be assigned to the secondary R-group of the employed **CTA-3**. All other polymerizations of acrylates, where **CTA-2** (same Z-group, but tertiary R-group) was employed as RAFT agent, did not show such a behavior. As an example, the preparation of **P3** (triethylene glycol methyl ether acrylate) was conducted within 3 h and achieved a conversion of 19 %. Since both RAFT agents (**CTA-2** and **CTA-3**) feature the same Z-goup, the observed retardation (4 % conversion in 3 h) is due to the comparative high concentration of CTA in the reaction mixture. However, neither inhibition, nor retardation had a negative effect on the end group fidelity of the obtained polymer **P9** and small molecular weight for efficient NMR and ESI-MS analysis was pursued in any case.

In order to evidence the orthogonally addressable reactivity of the thiocarbonyl thio and photoenol group, reactions with small organic compounds were carried out. For the HDA reaction of the thiocarbonyl thio moiety of the RAFT end group, Cp was used as small molecule, resulting in polymer **P9**$_a$ (M_n = 1200 g mol^{-1}, $Đ$ = 1.30). The reaction was conducted at ambient temperature in dichloromethane over night and the polymer was recovered *via* precipitation in a mixture of acetonitrile/water (1/1, v/v). Subsequently, a solution of polymer **P9**$_a$ and diethyl fumarate in acetonitrile was exposed to UV-light (λ_{max} = 370 nm) at ambient temperature for 2.5 h. Precipitation in a mixture of acetonitrile/water (1/1, v/v) yielded the polymer **P9**$_b$ (M_n = 1500 g mol^{-1}, $Đ$ = 1.27). **P9**, **P9**$_a$ and **P9**$_b$ were analyzed via ^{1}H NMR spectroscopy (for the complete NMR spectra please refer to Figures 6.13, 6.14, and 6.15 in Section 6.5). The proton resonances associated with the corresponding end groups of the polymers are depicted in the magnified areas in Figure 3.19. For species **P9** (top), the characteristic resonance appears

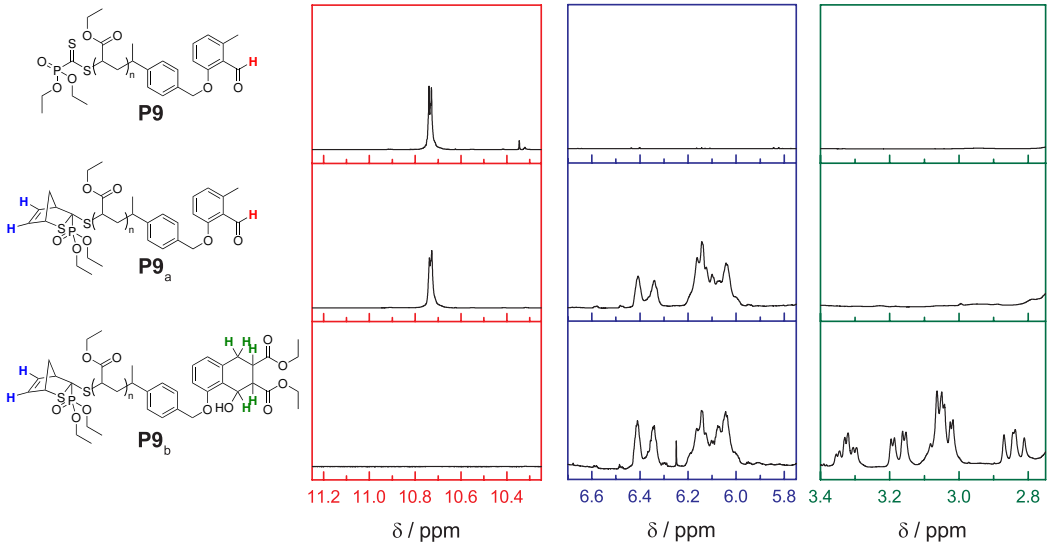

Figure 3.19 Expanded ^{1}H NMR spectra of the polymers **P9** (top), **P9**$_a$ (middle), and **P9**$_b$ (bottom) showing the respective characteristic proton resonances as shown on the left-hand side. For a better overview, the color of the frame of each segment matches the color of the relevant protons in the molecular structures, assigned to the corresponding resonances. The full NMR spectra can be found in Figures 6.13, 6.14, and 6.15 in Section 6.5.

at 10.7 ppm, referring to the proton of the aldehyde group of the photoenol moiety. Species **P9**$_a$ (middle) exhibits the same aldehyde resonance at 10.7 ppm, and in addition, new resonances in the region between 6.5 and 6.0 ppm are present, corresponding to

the protons of the formed HDA product with Cp. It should be mentioned that the distinction between endo and exo-products of the Diels–Alder reactions is not critical for polymer conjugations. Hence, only the structure of the endo isomer is shown. For polymer **P9**$_b$ (bottom) the proton signal of the aldehyde moiety at 10.7 ppm disappears, as expected after the quantitative photoinduced Diels–Alder reaction with diethyl fumarate. Simultaneously, the resonances corresponding to the protons of the Diels–Alder adduct with diethyl fumarate appear, having a chemical shift ranging from 3.4 to 2.8 ppm.

To corroborate the results of NMR spectroscopy, detailed ESI-MS analyses were performed (see Figure 3.20). The ESI-MS spectra of **P9**, **P9**$_a$, and **P9**$_b$ are shown from top to bottom in the diagram. For both reactions the m/z ratios of the resulting material are shifted quantitatively (66.0470 for the Cp addition and 172.0736 for the diethyl fumarate addition). No residual signals at the m/z values of the respective starting materials are evident, implying full conversion of the reactants. The exact values for the theoretical and experimental m/z ratios of the polymers **P9**, **P9**$_a$, and **P9**$_b$ having four monomer units are collated in Table 3.4.

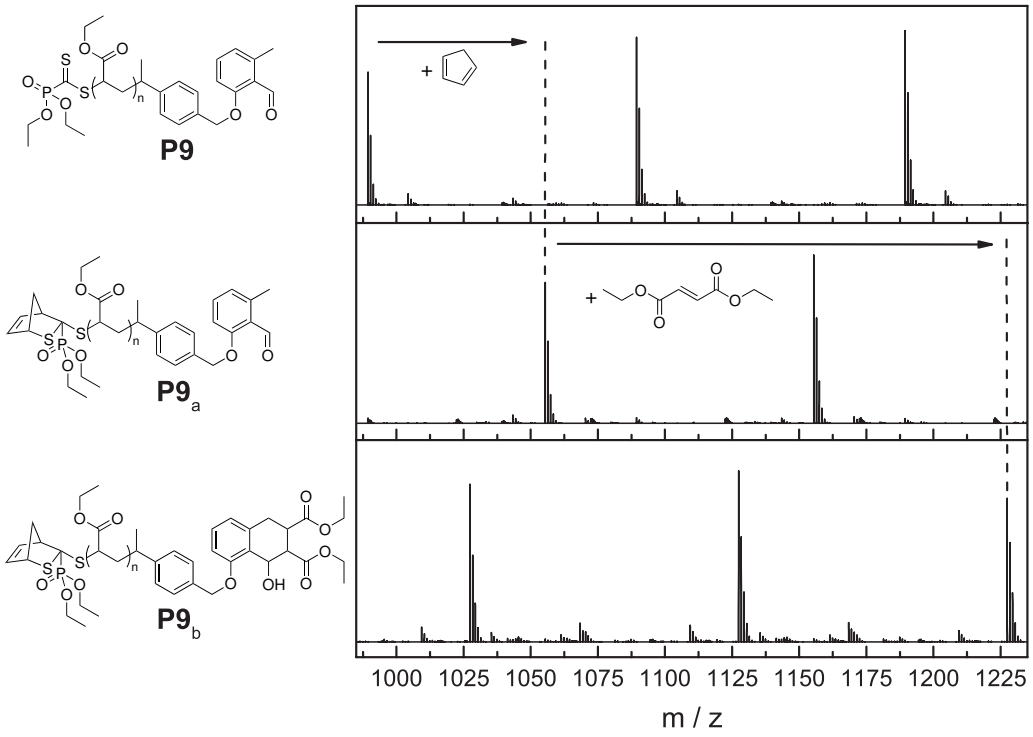

Figure 3.20 ESI-MS of polymer **P9** (top), **P9**$_a$ (middle), and **P9**$_b$ (bottom) between m/z = 985–1235.

Table 3.4 Theoretical and experimental m/z values for the building blocks **P9**, **P9**$_a$, and **P9**$_b$ having four monomer units, respectively.

polymer	m/z_{theo}	m/z_{exp}	$\Delta m/z$
P9	889.3032	889.3025	0.0007
P9$_a$	955.3502	955.3507	0.0005
P9$_b$	1127.4238	1127.4242	0.0004

Although orthogonally adressable, it is important to perform the HDA reaction prior to the photoaddition. The reverse order could lead to side reactions with the RAFT end group, like step growth polymerization or single-chain folding. However, it was already proven that the HDA reaction is reversible (please refer to Section 3.3). So the HDA reaction with Cp could be used as protection of the C=S-double bond. After photo ligation the Cp could be removed at elevated temperatures and the HDA capable RAFT end group is accessible again. Thus, a reverse order of ligation steps is still possible or the generated block copolymers could be grafted onto a Cp-functionalized (membrane) surface.

Having successfully proven the orthogonal addressability of both end groups of **P9**, the conjugation with polymers was investigated as noted above (see Scheme 3.5). The conjugation with Cp terminal **P1** proceeds within 24 h in ethyl acetate at ambient temperature with $ZnCl_2$ as catalyst, yielding the diblock terpolymer P(I-*co*-S)-*b*-PEA (**P10**). As the third block, fumarate-functionalized poly(ethylene oxide) (PEO-fum) was employed as a suitable counterpart for the subsequent photoenol ligation. The reaction was conducted within 2.5 h of UV-light irradiation (λ_{max} = 370 nm) at ambient temperature in dichloromethane, resulting in the amphiphilic triblock quaterpolymer P(I-*co*-S)-*b*-PEA-*b*-PEO (**P11**). For NMR spectra of **P10** and **P11** please refere to the Figures 6.16 and 6.17 respectively. The SEC traces of the generated polymers **P9** (M_n = 1200 g mol^{-1}, $Đ$ = 1.24), **P10** (M_n = 10 500 g mol^{-1}, $Đ$ = 1.26), and **P11** (M_n = 12 500 g mol^{-1}, $Đ$ = 1.37) as well as the SEC traces of the building blocks **P1** (M_n = 9400 g mol^{-1}, $Đ$ = 1.24) and PEO-fum (M_n = 3000 g mol^{-1}, $Đ$ = 1.04) are depicted in Figure 3.21. For both polymer conjugations (**P10** and **P11**), the elution volume of the products is shifted to lower values compared to the corresponding precursor polymers (**P1**/**P9** and **P10**/PEO-fum, respectively), in-

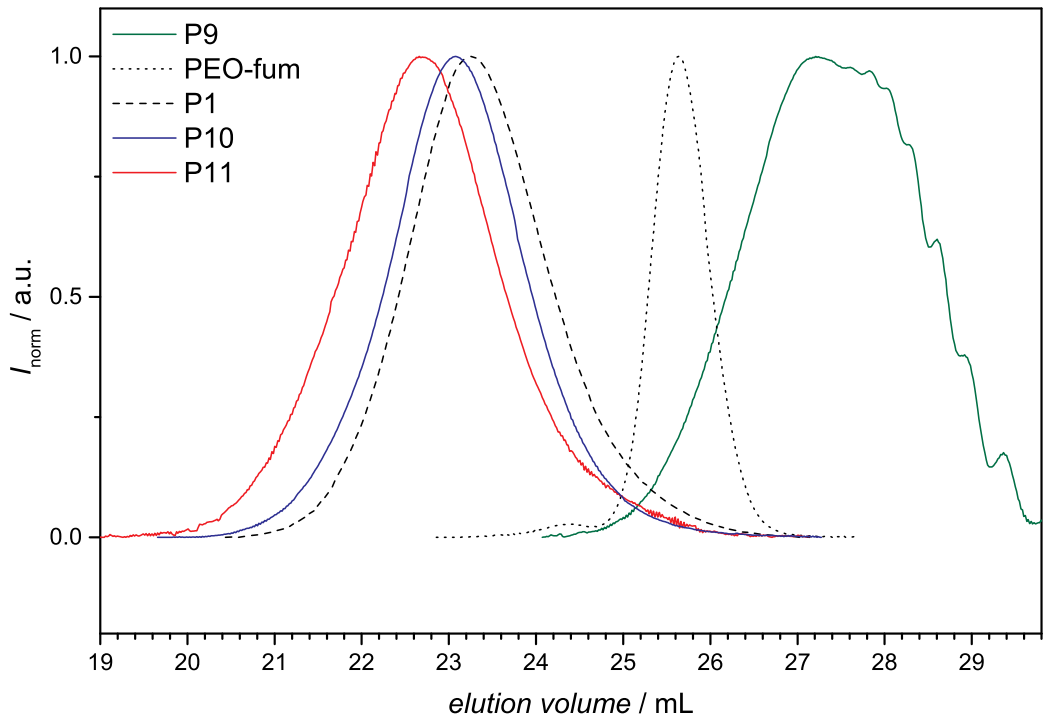

Figure 3.21 SEC traces of building block **P9** (M_n = 1200 g mol^{-1}, $Đ$ = 1.24, solid green line), **P10** (M_n = 10 500 g mol^{-1}, $Đ$ = 1.26, solid blue line), and **P11** (M_n = 12 500 g mol^{-1}, $Đ$ = 1.37, solid red line) as well as the traces of the building blocks **P1** (M_n = 9400 g mol^{-1}, $Đ$ = 1.24, dashed line) and PEO-fum (M_n = 3000 g mol^{-1}, $Đ$ = 1.04, dotted line).

dicating an increase of the respective molecular weight and thus a successful ligation. Moreover, in the area of the low molecular weight polymers (for **P9** close to 27.2 mL and for PEO-fum approximately 25.8 mL elution volume) no significant residual signal is observed. Although the molecular weight values obtained from the PS calibration of the SEC is not accurate, it confirms that the sum of the relative molecular weights of the starting polymers equals approximately that of the formed block copolymer. The ligation of **P1** (9400 g mol^{-1}) with **P9** (1200 g mol^{-1}) results in **P10** with a molecular weight of 10 500 g mol^{-1}; the modular ligation of **P10** (10 500 g mol^{-1}) with PEO-fum (3000 g mol^{-1}) results in **P11** with a molecular weight of 12 500 g mol^{-1}. However, for both polymer conjugation reactions an increase of dispersity was observed. In theory, the conjugation of two narrowly dispersed polymers results in a decrease of $Đ$.[238] This discrepancy can be explained by the fact that the theory assumes 100 % end group fidelity. Nevertheless, as discussed in Section 2.1.3, termination is not completely suppressed in the RAFT

process, and a small amount of chains carry the 2-cyanopropyl end group of the initiator AIBN.

The newly developed **CTA-3** increases the possibilities to tailor the surface chemistry of generated filter membranes. Either amphiphilic triblock quaterpolymers could be directly employed in the SNIPS process or a diblock copolymer could be grafted onto a Cp-functional pore surface *via* the protection and re-generation concept of the HDA RAFT end group with molecular Cp.

4

Membranes Generated *via* Reversible HDA Chemistry

Due to the collaboration with the group of Prof. Dr. Felix Schacher (University Jena) and the availability of the required instruments, all membranes, as well as the SEM images, were prepared by Christoph Hörenz or Dr. Christian Pietsch. However, the author stayed one month in Jena to investigate conditions for the SNIPS process himself.

4.1 Preparation of Membranes *via* SNIPS

Establishing suitable SNIPS process conditions for a new polymer system is not straight forward. Many parameters such as the choice of the solvents for the casting solution, the ratio of the used solvents, the concentration of polymer in the casting solution, the temperature, the relative humidity and the self assemble time have pronounced influence in the film formation behavior and membrane morphology. By trial and error, conditions for a successful film formation, employing diblock terpolymer **P8** in the

SNIPS process, were found (see Table 4.1). The polymer (15 wt%) was dissolved in a

Table 4.1 Found SNIPS process conditions for the diblock terpolymer **P8** generating the membrane **M1**.

parameter	conditions
solvent mixture	THF/dioxane
solvent ratio	50/50 (wt%)
concentration of polymer	15 wt%
temperature	22 °C
rel. humidity	50 %
film casting gap	200 µm
precipitation bath	water
self assembly time	360 s

mixture of THF (42.5 wt%) and dioxane (42.5 wt%). The solution was cast on a polished sheet of glass using a 200 µm gap doctor blade and a Coatmaster 510 (Erichsen GmbH, Germany). During the process the temperature was kept at 22 °C and the rel. humidity at 50 %. After a self assemble time of 360 s, the glass sheet (with the cast film on top of it) was immersed into a precipitation bath of deionized water, yielding the membrane **M1**. The often used solvent mixture of DMF and THF did not lead to any film formation with every applied solvent ratio and self assemble time. Instead, only the formation of micelles was observed after the immersion of the glass sheet (with the cast film on top of it) into the precipitation bath. A reason could be the high hydrophlilicity of PTEGA. Only with the THF and dioxane mixture and an unusual long open time a successful film formation was achieved.

Characterization *via* scanning electron microscopy (SEM) revealed an isotropic cross section and a thickness of approximately 18 µm (see Figure 4.1-4.3). Although the membrane appears very dense in the cross section, it was possible to purge water through it.

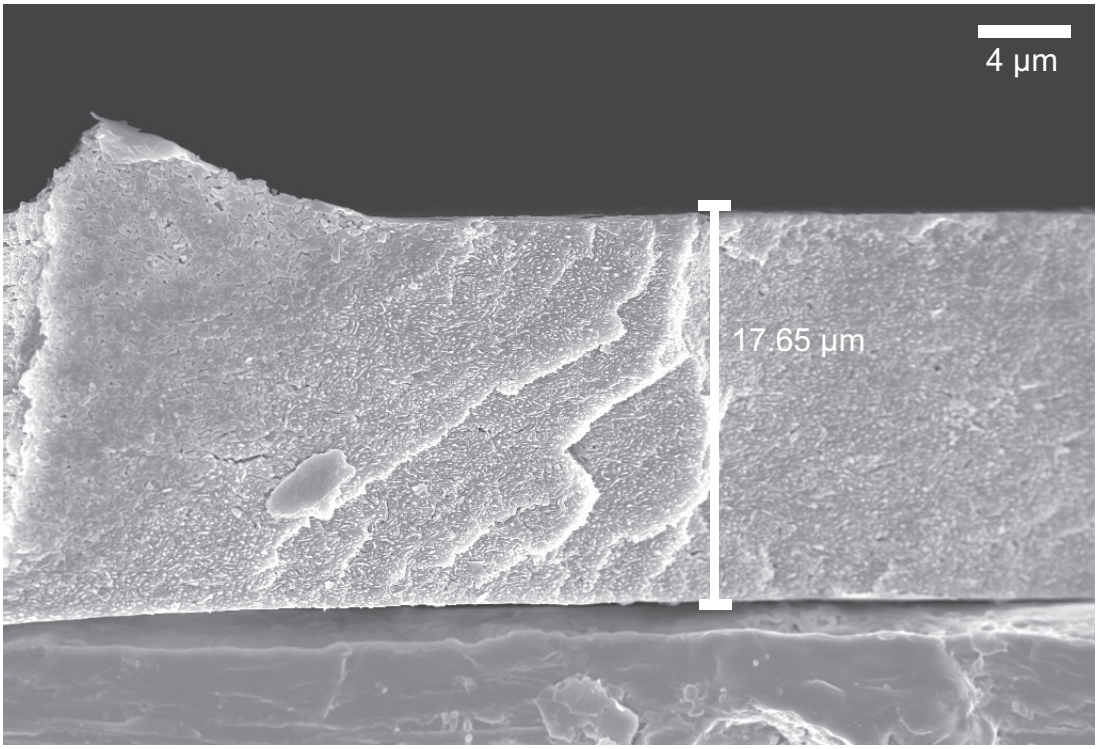

Figure 4.1 SEM image from the cross section of membrane **M1** (magnification: 2.33 kX).

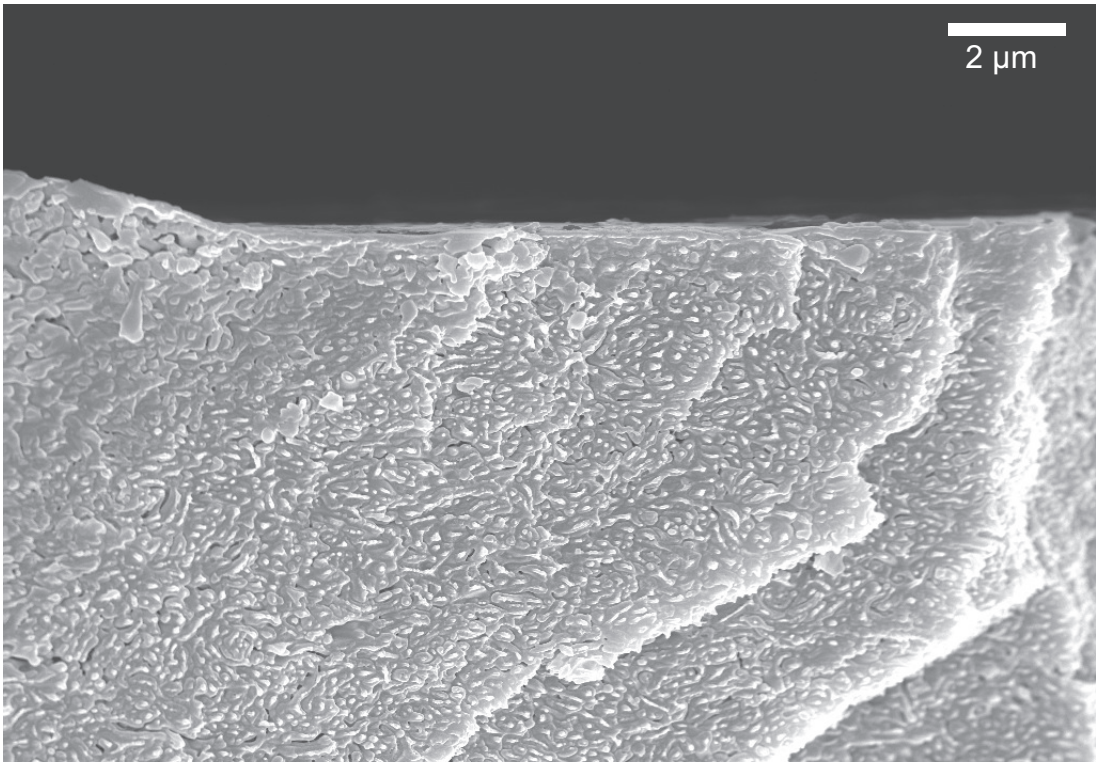

Figure 4.2 SEM image from the cross section of membrane **M1** (magnification: 6 kX).

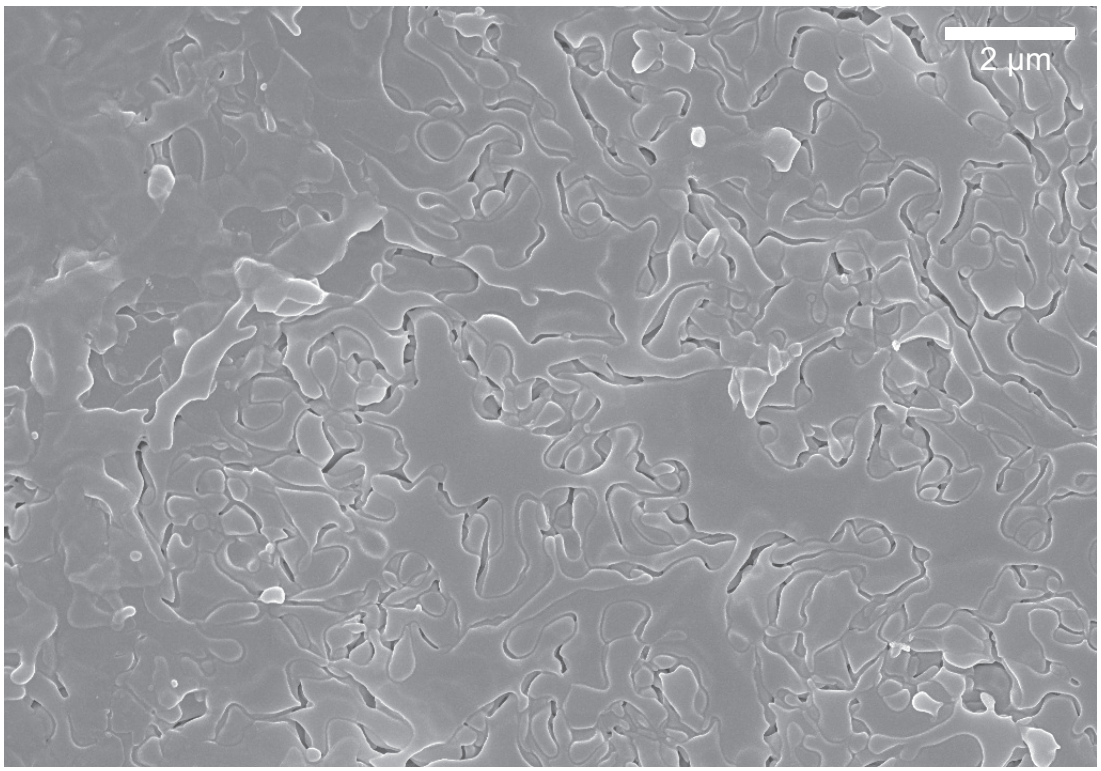

Figure 4.3 SEM image from the top view of membrane **M1** (magnification: 7 kX).

However, due to the small thickness of **M1** the mechanical stability is very low, exacerbating handling of the membrane without damaging it. Moreover, the small pores and high density could prevent efficient cleavage of Matrix B from the surface of the membrane. In order to improve the generated morphology, an additional diblock terpolymer with a smaller PTEGA block composition was prepared. Therefore, a PTEGA polymer (**P12**: M_n = 18 000 g mol^{-1}, $Đ$ = 1.16) with lower molecular weight, compared to **P4**, was synthesized and subsequently conjugated with **P2** to yield the diblock terpolymer **P13** (**P13**: M_n = 60 000 g mol^{-1}, $Đ$ = 1.33). For the corresponding SEC traces please refer to Section 6.5, Figure 6.18. Thus, the fraction of PTEGA is reduced from 25 wt% (**P8**) to 17 wt% (**P13**). Again, suitable conditions for a successful film formation, now employing diblock terpolymer **P13** in the SNIPS process, were investigated (see Table 4.2). For the preparation of membrane **M2** the ratio of THF/dioxane was changed to 70/30 (wt%) and the polymer concentration was increased to 20 wt%. Moreover, the self assembly

Table 4.2 Found SNIPS process conditions for the diblock terpolymer **P13** generating the membrane **M2**.

parameter	conditions
solvent mixture	THF/dioxane
solvent ratio	70/30 (wt%)
concentration of polymer	20 wt%
temperature	22 °C
rel. humidity	50 %
film casting gap	200 µm
precipitation bath	water
self assembly time	40 s

time could be reduced to 40 s. All other parameter were kept identical to the employed conditions for membrane **M1**.

Characterization of **M2** *via* SEM showed that the morphology was successfully improved (see Figure 4.4-4.6). The thickness increased to approximately 28 µm and significantly larger pores were generated, the structure is less dense. Moreover, the morphology from the top layer differs from the supporting substrate. The rather smooth surface is punctuated with small (20-100 nm) holes (see Figure 4.6).

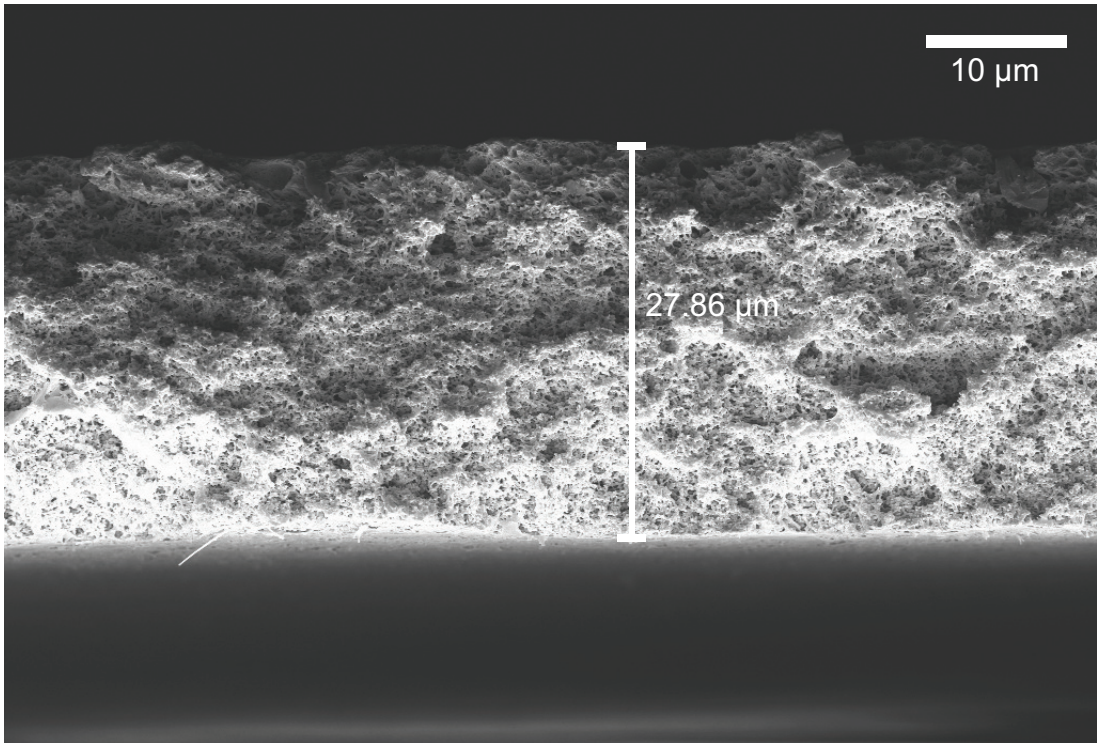

Figure 4.4 SEM image from the cross section of membrane **M2** (magnification: 1.47 kX).

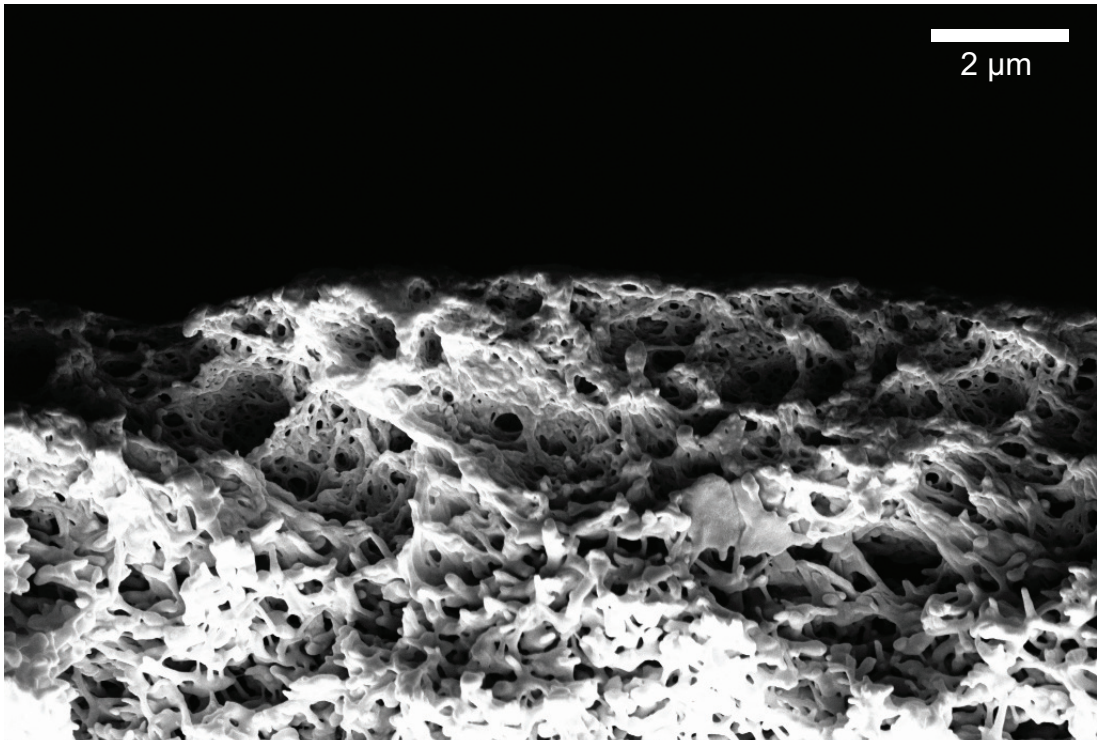

Figure 4.5 SEM image from the cross section of membrane **M2** (magnification: 7.5 kX).

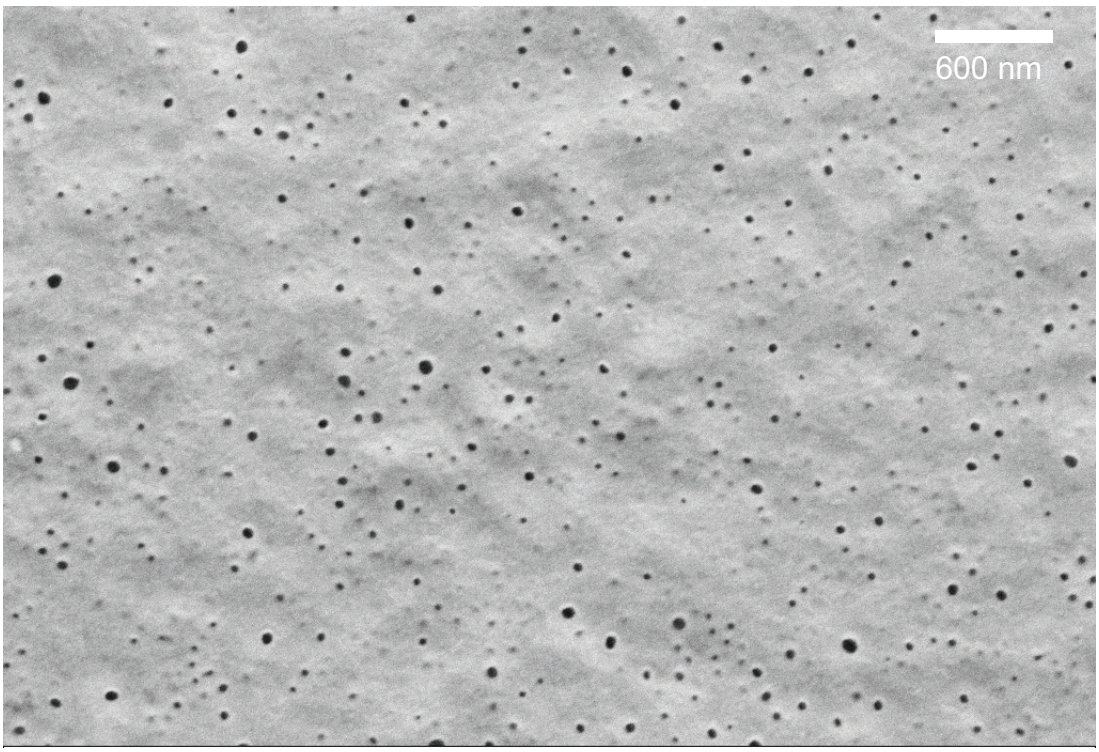

Figure 4.6 SEM image from the top view of membrane **M2** (magnification: 20 kX).

4.2 Cleavage of Matrix B from the Surface

To initiate the cleavage of Matrix B from the surface of the membranes, the membranes were immersed in hot water. The applied temperature is of key importance for the cleavage kinetics and the preservation of the membrane morphology. It was found that above 60 °C the membrane morphology is not stable (see Figure 4.7). Pores merge and

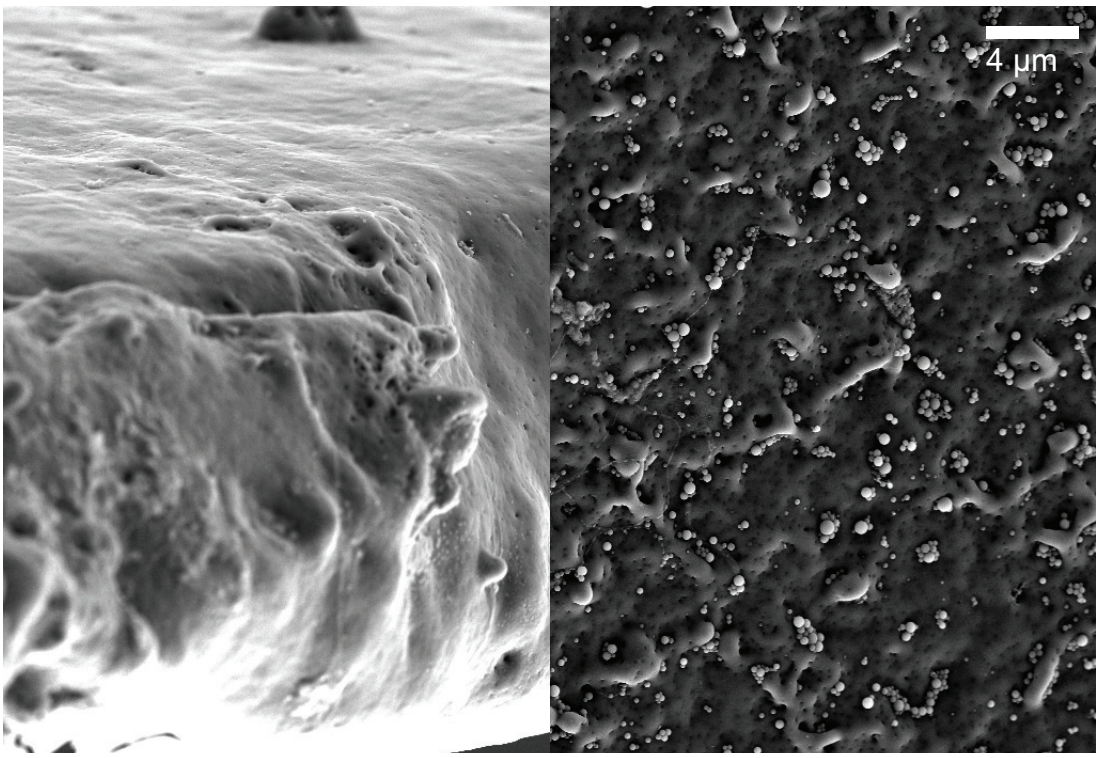

Figure 4.7 SEM image from cross section (left side) and the top view (right side) of membrane **M1** after immersion in water above 60 °C (magnification: 2 kX).

round particles form at the surface. Moreover, the diameter of the immersed membrane pieces is shrinking in a macroscopic scale (a disk with 10 mm diameter to approximately 7 mm diameter).

Hence, the cleavage was performed at 50 °C. At this temperature the membrane morphology proved to be stable. Comparison *via* SEM showed similar structures before and after the cleavage of Matrix B from the surface (see Figure 4.8-4.10).

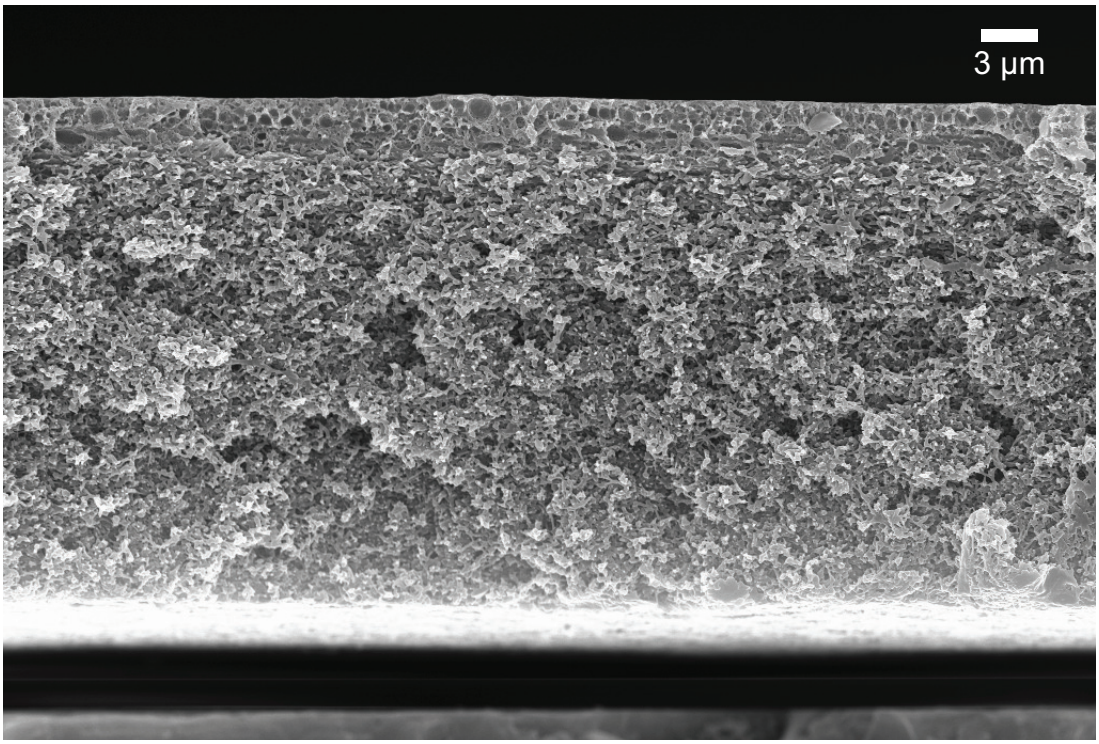

Figure 4.8 SEM image from the cross section of membrane **M2** after cleavage process at 50 °C (magnification: 2 kX).

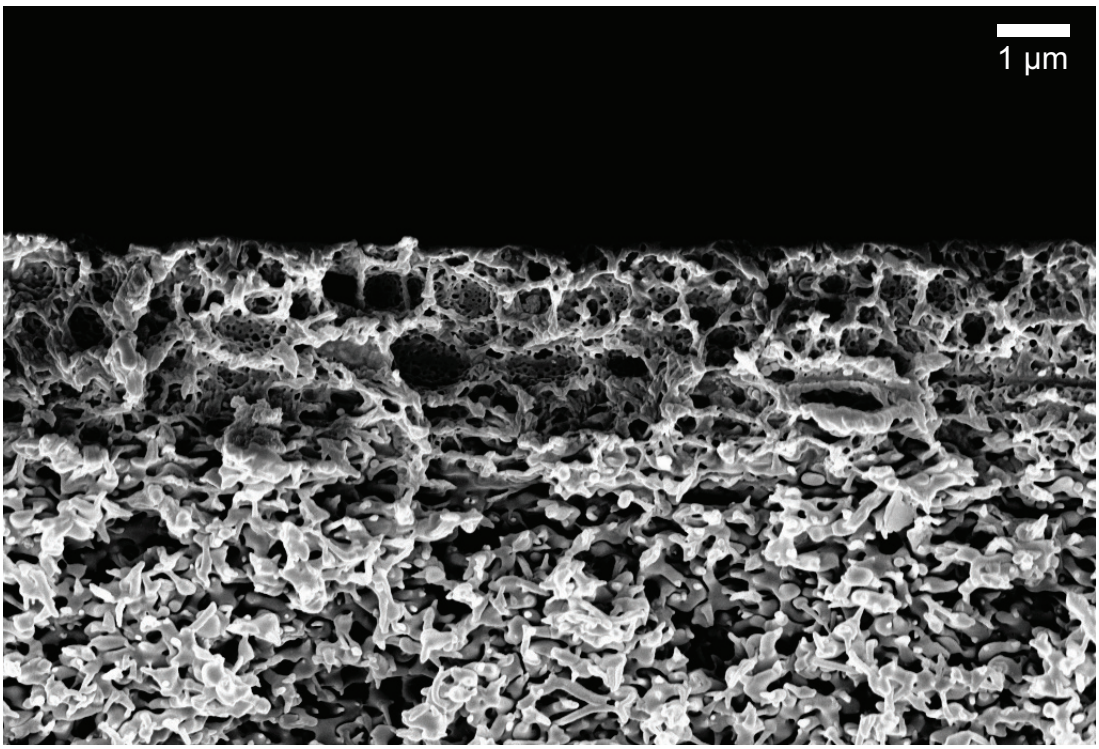

Figure 4.9 SEM image from the cross section of membrane **M2** after cleavage process at 50 °C (magnification: 7.5 kX).

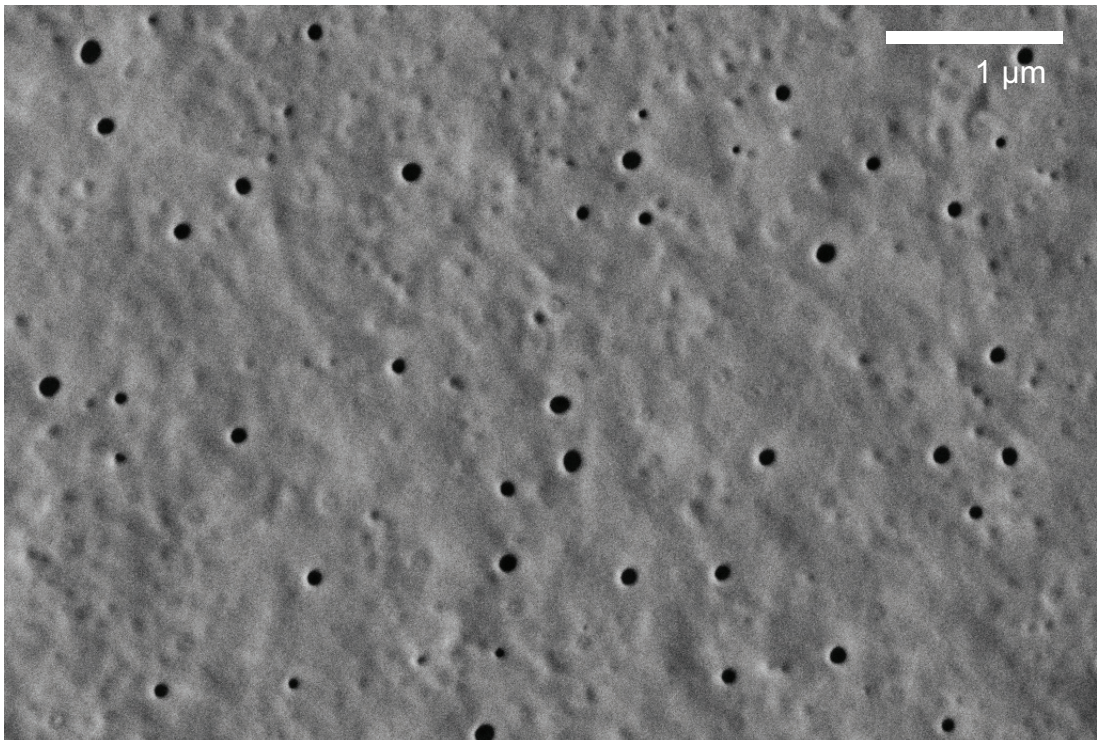

Figure 4.10 SEM image from the top view of membrane **M2** after cleavage process at 50 °C (magnification: 18.15 kX).

To evidence the cleavage of Matrix B from the surface and follow the reaction kinetics, parts of the membrane were dried, dissolved in $CDCl_3$ and subsequently analyzed *via* NMR spectroscopy. The integral of the PTEGA block signal around 3.31 ppm is monitored in reference to the integral of the resonances of PS in the aromatic area, which are not affected by the cleaving procedure. Figure 4.11 exemplarily shows the evolution of the PTEGA resonance from the diblock terpolymer **P8**, over the membrane formation of **M1**, to the kinetic data points of the cleaving conditions within 14 days. An interesting circumstance is the fact that after the SNIPS process the fraction of PTEGA is already decreased to 71 %, implying that polymer chains with a high fraction of Matrix B stay in solution and do not participate in the membrane formation. The difference in ppm between polymer and membrane resonances in the diagram appears to be significant, yet is negligible in absolute numbers (0.0006 ppm) and probably due to the temporal distance of the measurements. Under cleaving conditions the integral of the PTEGA resonance continuously decreases with time.

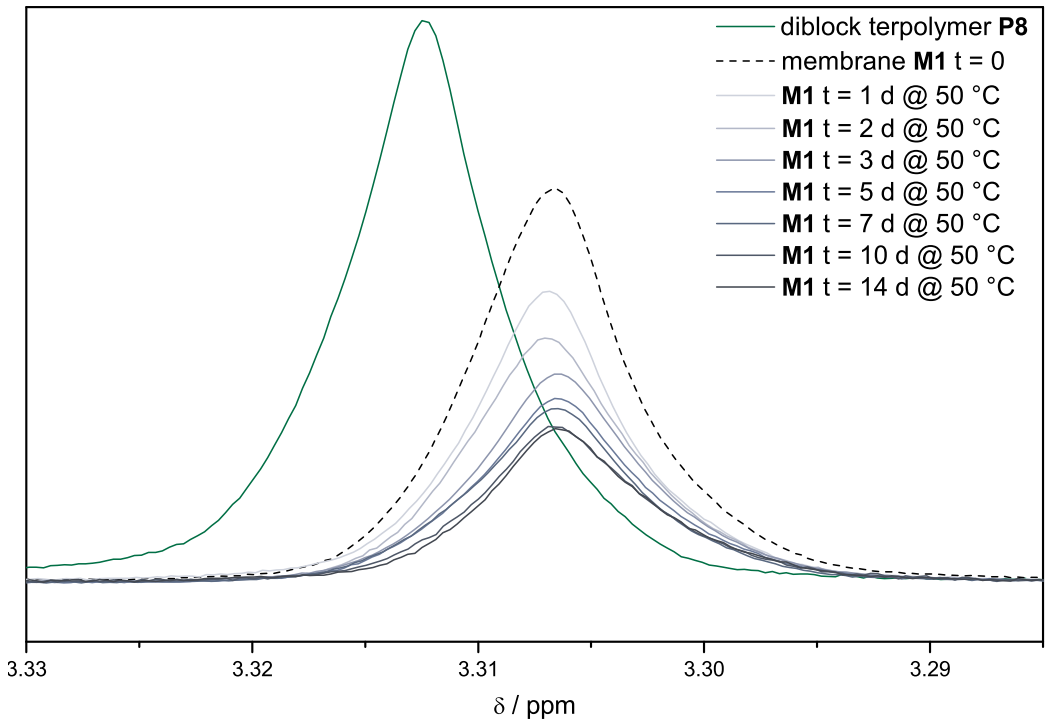

Figure 4.11 Enlarged section of the ^{1}H NMR spectra (500 MHz, $CDCl_3$) of polymer **P8** (green line), the membrane **M1** (dashed line) and the kinetic samples from the cleavage process of **M1** (from light to dark blue) in the region for the relevant PTEGA resonance around 3.31 ppm.

A kinetic plot of the PTEGA fraction for both membranes (**M1** and **M2**) is depicted in Figure 4.12. The 100 % starting point represents the corresponding integral of the PTEGA resonance after membrane formation. For both membranes (**M1** and **M2**) under cleavage conditions, the fraction of PTEGA decreases with time until a minimum level is reached. However, membrane **M2** reaches a lower minimum (27 %) in half the time (7 days) compared to membrane **M1** (41 % in 14 days). This phenomenon can be explained by the different morphology of the membranes. The larger pores of **M2** facilitate the removal of free PTEGA polymer chains, contrarily the dense structure and small pores of **M1** support re-attachment reactions, thus slowing down the cleaving process. In both cases the PTEGA fraction does not approximate 0 %. This can be explained by the fact that with the SNIPS process a certain amount of diblock terpolymer chains are completely incorporated into the membrane framework. Otherwise the thickness of the framework structures would be limited by the chain length of the employed Matrix A

polymers, which is not the case. Only the Matrix B polymers directly on the pore surface of the membranes can be removed. Thus, the minimum fraction of PTEGA, reached under cleavage conditions, is dependent upon the incorporated amount of Matrix B polymers. Again, the difference between **M1** and **M2** is due to the different morphology.

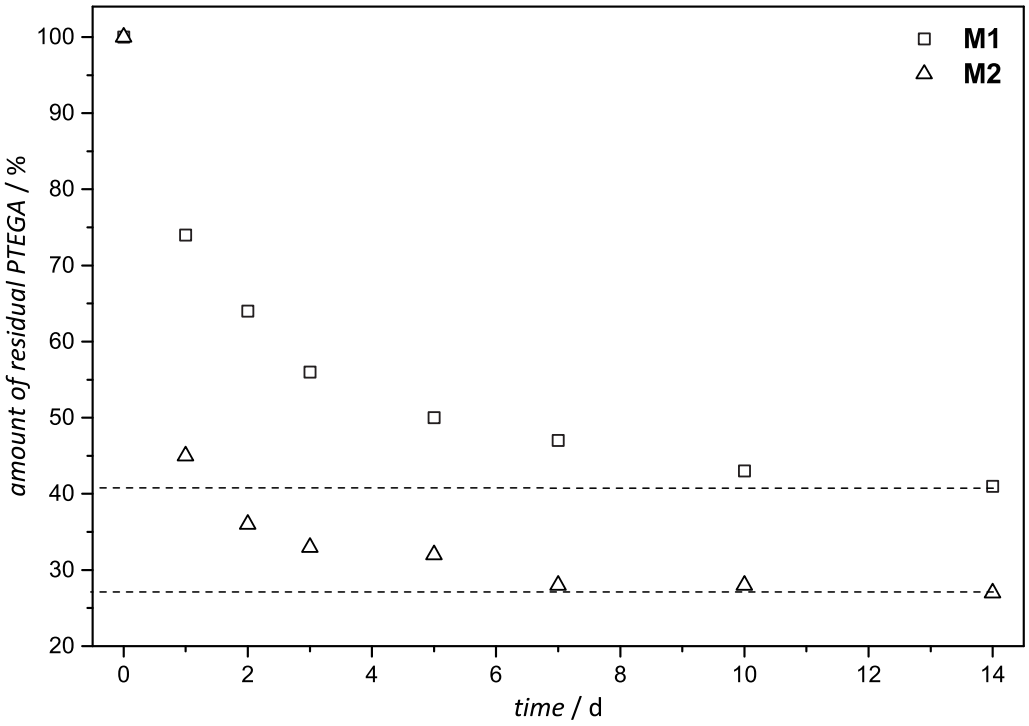

Figure 4.12 Evolution of the fraction of PTEGA for the membranes **M1** (squares) and **M2** (triangles) during the cleavage procedure. The dashed lines represent the individually achieved minimum at 41 % (**M1**) and 27 % (**M2**).

In summary, the cleavage of Matrix B from the surface of the membranes is achieved by immersion of the membranes in 50 °C hot water. It was observed that at higher temperatures the morphology is not stable. The pores were closed and round particles were found all over the surface. In addition, it was found that the rate of the cleavage depends strongly on the morphology of the employed membrane. In a dense framework with only little pores the removal of the hydrophilic polymer blocks after cleavage is hampered, whereby the entire process is slowed down.

4.3 Grafting Hydrophilic Blocks onto Cp-Functional Surfaces by Micromolding in Capillaries

In order to test the ability of the Matrix B polymers **P3**, **P5** and **P6** to attach on a Cp functional pore surface, the polymers were employed to generate polymer patterns onto Cp functional silicon wafers by micromolding in capillaries (MIMIC).* The capillaries mimic the pores of a membrane.

The general concept of the preparation of surfaces patterned with Matrix B polymer brushes is depicted in Scheme 4.1. Silicon wafers activated with piranha solution were coated with 11-bromoundecyl trichlorosilane. Subsequently, the bromine was substituted with Cp. MIMIC was employed to pattern the surfaces with three different polymers (**P3**, **P5** and **P6**). The bromine functionalization of activated silicon wafers with 11-bromoundecyl trichlorosilane proceeded within 45 min in toluene at ambient temperature. Cp functional surfaces were prepared with NaCp from the bromine terminated surfaces by substitution with Cp in THF at ambient temperature overnight. The successful surface functionalizations were evidenced by water contact angle measurements (see Figure 4.13). The contact angle increases from <10° for the activated silicon wafer to 88°

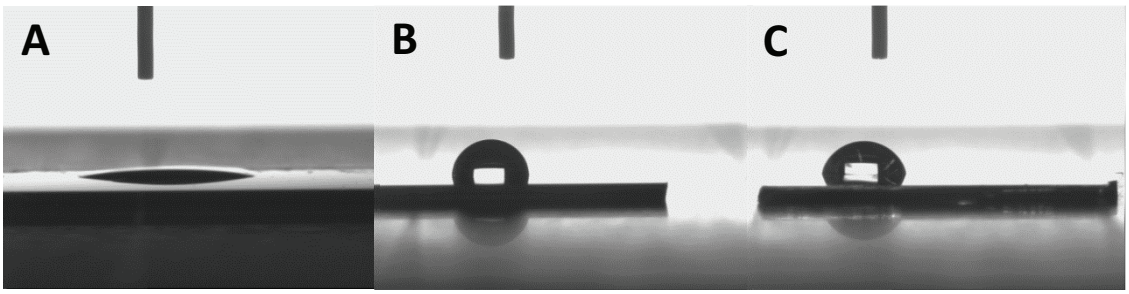

Figure 4.13 Pictures of the water contact angle measuremts for **A** the activated silicon wafers (<10°), **B** the Br functional surfaces (88°) and **C** the Cp functional surface (71°).

for the Br functional surface. After Cp substitution the surface becomes slightly more

* Parts of the current section are adapted with permission from B. Vonhören, M. Langer, D. Abt, C. Barner-Kowollik, B. J. Ravoo, *Langmuir* **2015**, *31*, 13625–13631. Copyright ©2015 American Chemical Society. B. Vonhören and M. Langer wrote the manuscript. M. Langer synthesized and characterized the polymers, B. Vonhören conducted the experiments and characterizations on the silicon wafers. D. Abt performed the Tof-SIMS measurements. C. Barner-Kowollik and B. J. Ravoo motivated and supervised the project and contributed to scientific discussions.

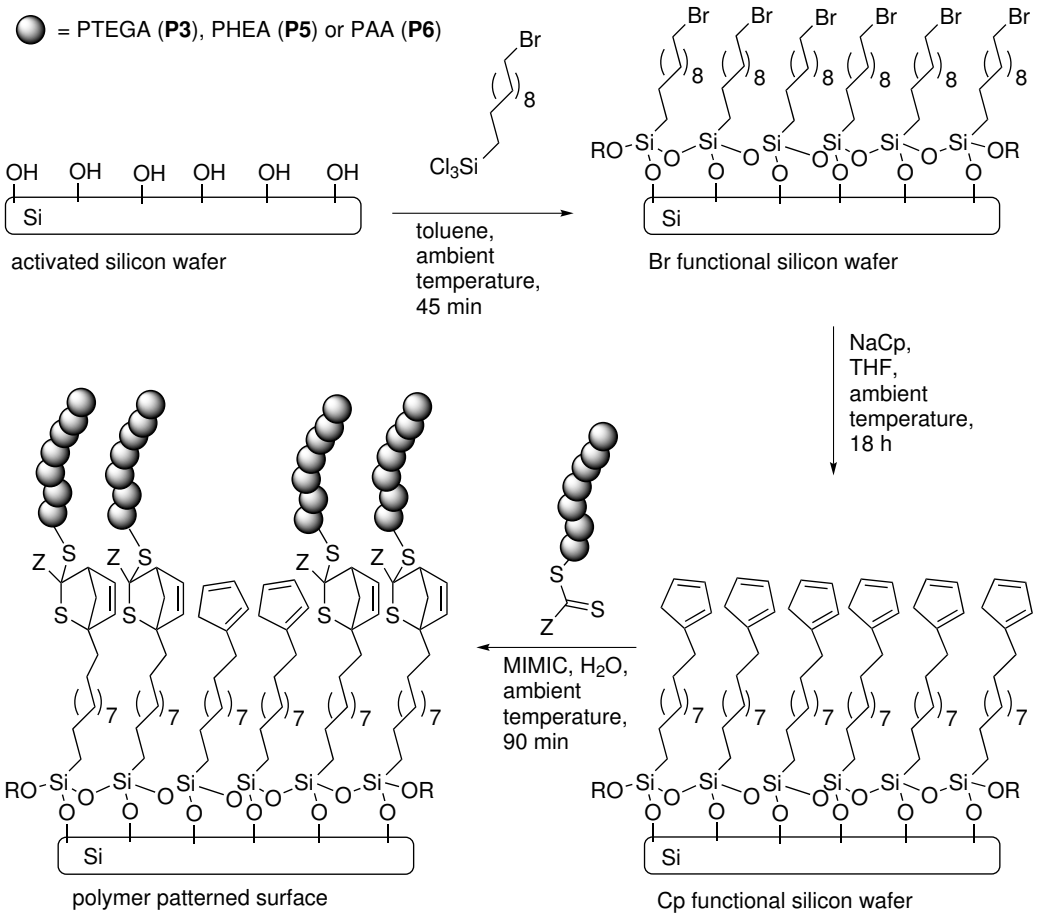

Scheme 4.1 General concept for the preparation of polymer patterned surfaces *via* MIMIC.

hydrophilic, which leads to a small decrease in the contact angle to 71°. The change in hydrophobicity is a good indication for the successful substitution. XPS analysis were performed to further support the results of the water contact angle measurements. The appearance of a bromine signal (Br 3d, 71 eV) in the XP spectrum provides further evidence of the successful attachment of the bromosilane to the activated silicon wafer (please refer to Figure 6.19 in Section 6.5). Furthermore, the bromine signal vanishes after the substitution with Cp (Figure 6.19).

Finally, the three polymers **P3**, **P5** and **P6** were grafted onto the Cp surfaces in a patterned fashion by MIMIC. To this end, aqueous solutions with low polymer concentrations ($30\,g\,L^{-1}$) were prepared, each of them containing one of the polymers. Subsequently, poly(dimethylsiloxane) PDMS stamps with different line patterns were placed on the Cp SAMs, and a small drop of polymer solution (5 µL) was placed at the open end of the capillaries (Figure 4.14).

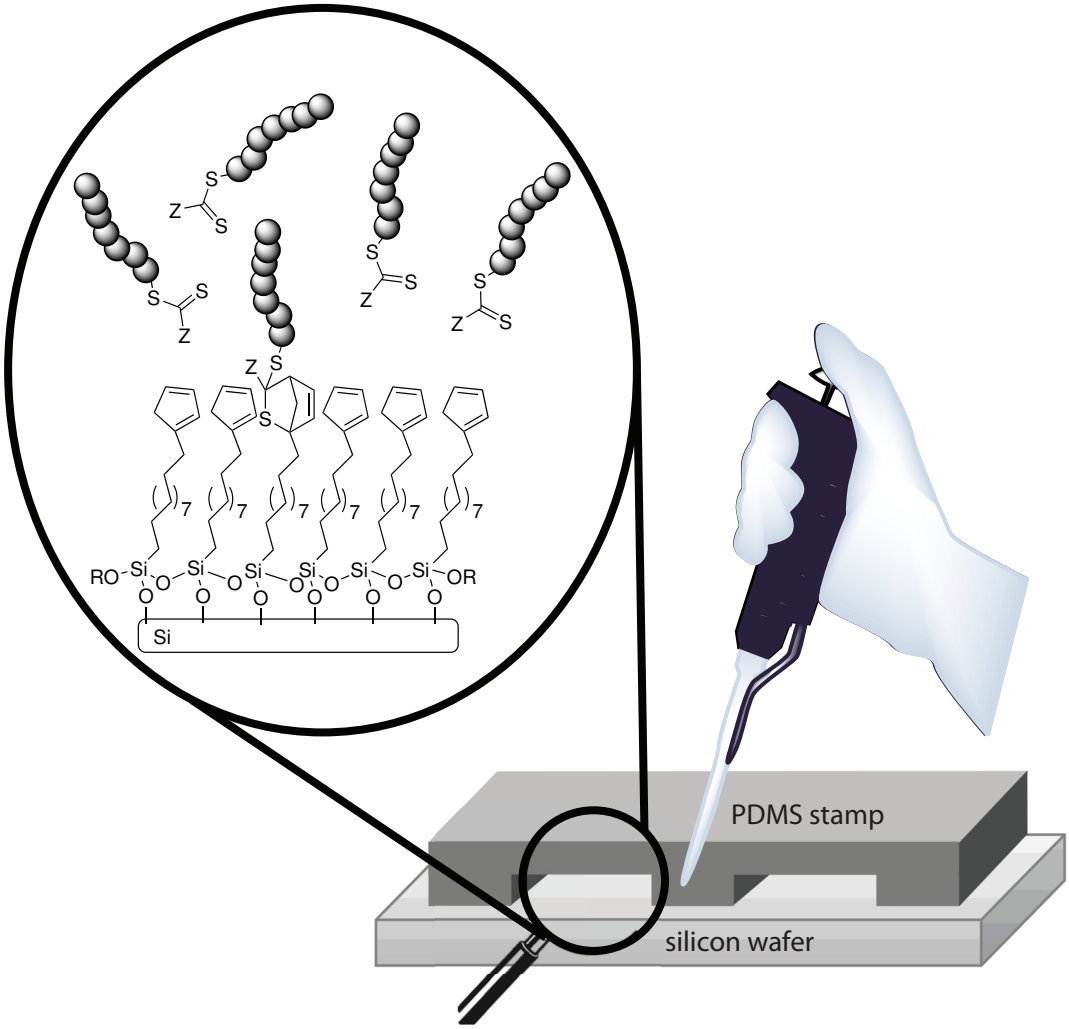

Figure 4.14 Illustration of the MIMIC procedure. 5 µL aqueous polymer solution are placed at the open end of the PDMS stamp capillaries.

In the MIMIC process, the filling of the capillaries is not always straightforward. Depending on the viscosity of the solvent and the interfacial free energies of the stamp and the surface, the rate of filling can be low.[243] Certain combinations of stamp, surface and solvent completely hamper the filling process. It is especially difficult if water is the solvent of choice. In the present study, oxidized PDMS stamps were used to increase the fill rate. Oxidizing the stamps with ozone leads to an increase in the density of silanol groups on the surface of the stamp. Hence, the stamps become significantly more hydrophilic. Although the Cp functional surface is quite hydrophobic (static contact angle of 71°), the capillaries were filled within a few seconds with the aqueous solutions, when oxidized PDMS stamps were employed. In case of the planned membrane functionalization, the hydrophobic pores can be purged by application of pressure. In aqueous media the HDA reaction proceeds very fast without the need of any catalyst.[19] After a reaction time of 90 min the PDMS stamp was removed from the surface and the silicon wafer was cleaned by rinsing with water, ethanol, and acetone and sonication in water. The patterned areas were approximately 1.0 cm × 0.5 cm in size.

The polymer patterned surfaces were comprehensively analyzed by a set of surface analytical methods. Due to the hydrophilic character of the three polymers, the water contact angles of the modified surfaces decrease after the polymer deposition (52° for **P3** (PTEGA), 56° for **P5** (PHEA) and 40° for **P6** (PAA) ; see Figure 4.15, inset). Since

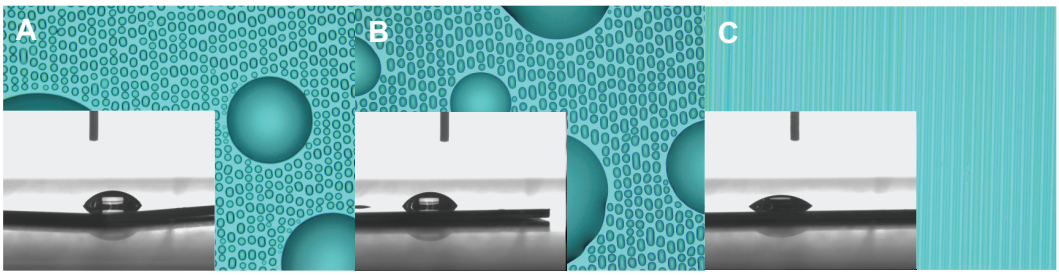

Figure 4.15 Microscopy pictures of the water condensation experiment and pictures of the water contact angle measurement. **A**: **P3**, PTEGA, 52°; **B**: **P5**, PHEA, 56°; **C**: **P6**, PAA, 40°.

the contact angles (and thus the hydrophobicity) of the Cp functional surface and the polymer coated surfaces differ by 15–31°, water should preferably condense on the polymer brushes. The optical microscopy images in Figure 4.15 display the expected

phenomenon and are a first strong indication that patterned polymer surfaces were obtained. For **P3** and **P5** the result is similar, single water drops are aligned in rows. In case of **P6**, the most hydrophilic polymer, the water forms a continuous film where the polymer brushes are grafted onto the surface.

Further characterization of the samples by AFM was challenging. Contamination (such as dust particles) and measurement artifacts disturbed most experiments. High-quality AFM images were obtained only for **P6** (see Figure 4.16). The observed average height of the brushes was close to 1 nm, which corresponds to a grafting density close to 0.14 chains nm^{-2}.[244] The pattern of the brushes exhibits a high spatial resolution in accordance with the applied stamp pattern and only a small number of defects could be observed, which derive from unfilled capillaries.

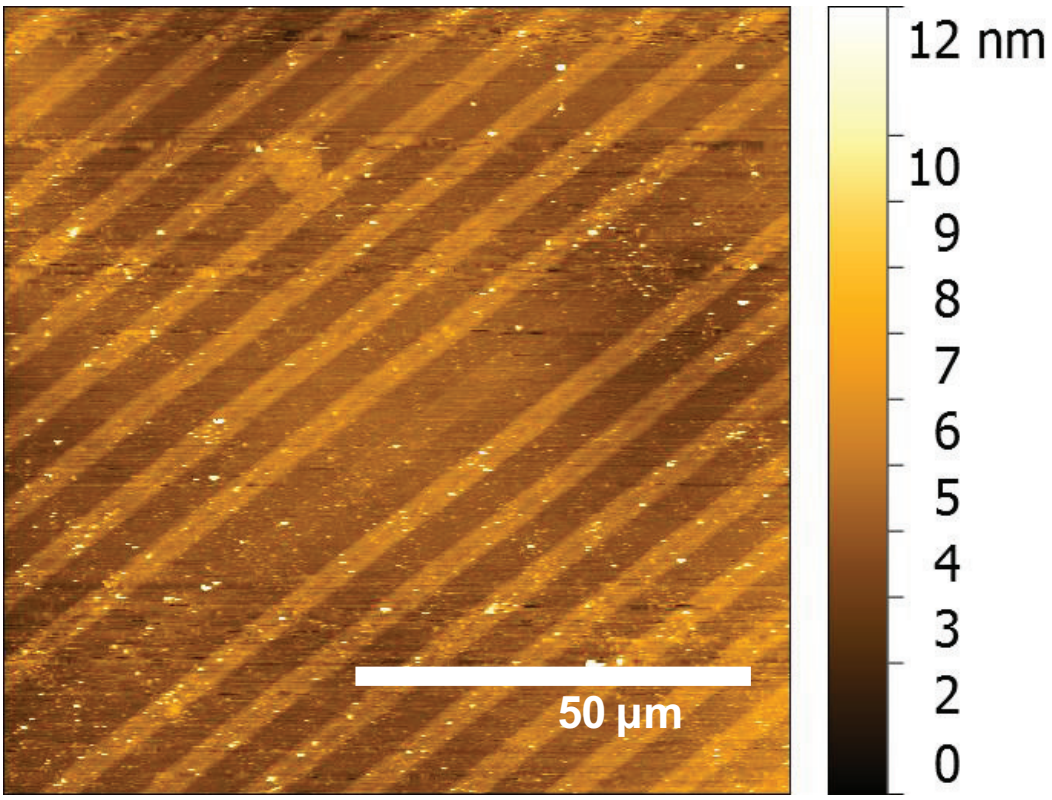

Figure 4.16 AFM height image (10 mm^2) of **P6** (stamp pattern, 5 µm contact area spaced by 3 µm).

The atomic composition of the samples was investigated by XPS. The carbon signal spectra of the Cp functional surface exhibits a single peak at 285 eV, which is characteristic for aliphatic and aromatic bound carbon (see Figure 4.17, **A**). Carbon signals with higher

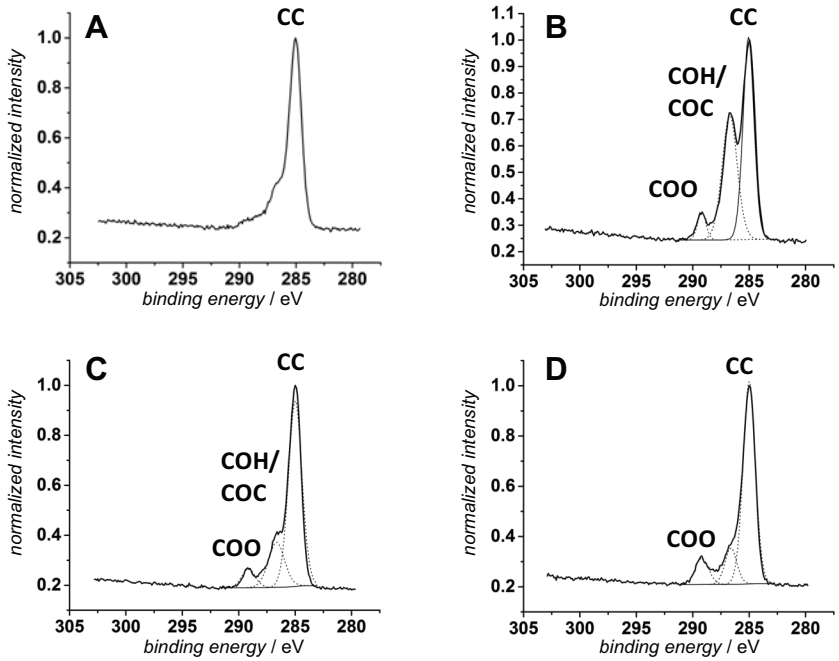

Figure 4.17 C 1s high-resolution scans of XPS measurements of the Cp functionalized silicon wafer (**A**) and of the three different polymers (**B**: **P3**, PTEGA; **C**: **P5**, PHEA; **D**: **P6**, PAA) patterned *via* MIMIC on Cp functionalized silicon wafers.

binding energies, which would indicate the presence of oxidized carbon species, were not observed. In contrast, all samples with polymer brushes exhibit pronounced additional peaks for oxidized carbons at binding energies of >285 eV (see Figure 4.17, **B**-**D**).[245] The additional signals of the sample covered with **P5** (PHEA, **C**) are characteristic for ester moieties (286.6 and 289 eV) and alcohols (286.6 eV). The sample with **P6** (PAA, **D**) brushes shows a signal at 289 eV corresponding to the carbon atoms of the acid group. The surfaces patterned with **P3** (PTEGA, **B**) brushes reveal the same signals as the PHEA brushes at 286.6 and 289 eV. However, the carbon signal at 286.6 eV is more pronounced, since PTEGA contains more C–O single-bond carbon atoms than PHEA. For all three polymers, the signals of the oxidized carbon species, compared to the C–C signal at 285 eV, are lower than what would be expected from the molecular structure.

The discrepancy is associated with the low thickness of the polymer layer. The observed carbon signal originates not only from the polymer brushes but also from the underlying Cp-alkyl layer, which contains only aromatic and aliphatic carbon moieties.

Time-of-flight secondary ion mass spectrometry (ToF-SIMS) imaging of the generated surfaces further supports the results described above. Signals detected at 26.0 u for all three different samples with **P3**, **P5** and **P6** brushes could be assigned to the secondary ion CN^-, which results from the R end group of the RAFT polymers. The observed fragment patterns generated with ToF-SIMS imaging correspond well to the negative patterns of the applied stamps, polymer stripes with a width of 15 µm spaced by 5 µm (see Figure 4.18). In addition, further characteristic fragments (PO_2^-, PO_3^-, CO_2^-, S^-, SH^-, and $OHCH_2CH_2^+$) for the respective RAFT polymers could be detected in a micropattern that corresponds to the stamp used for MIMIC (please refer to Section 6.5 Figures 6.20–6.24).

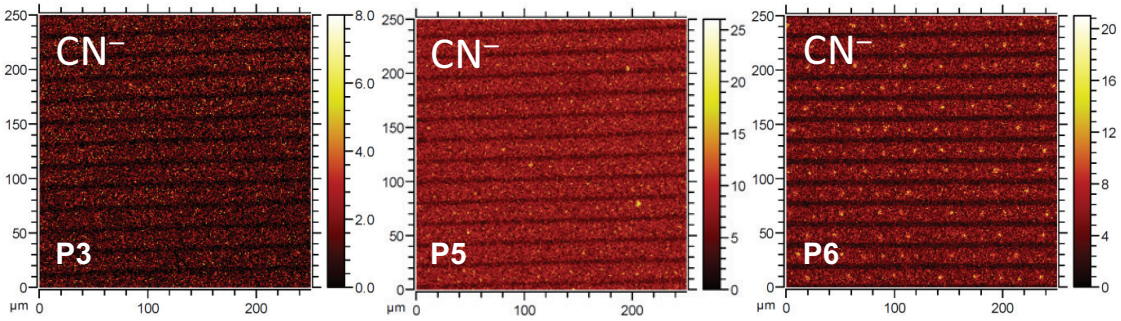

Figure 4.18 ToF-SIMS images of the three polymers **P3**, **P5** and **P6** patterned *via* MIMIC on Cp functional silicon wafers (stamp pattern, 5 µm contact area spaced by 15 µm).

In order to rule out that the polymers are only physically adsorbed, a negative control experiment was performed. A solution of **P6** was applied *via* MIMIC on a bromine-terminated surface. No patterned water condensation could be observed (please refer to Figure 4.19), confirming that the polymers are indeed covalently bound to the Cp functional surface and do not simply adsorb in an unspecific manner.

In an additional side project, the different protein repellent character of the generated surfaces were investigated. Thus, the patterned surfaces were submerged in a solution of rhodamine-labeled peanut agglutinin (PNA; 50 µg mL^{-1}) in 4-(2-hydroxyethyl)-1-

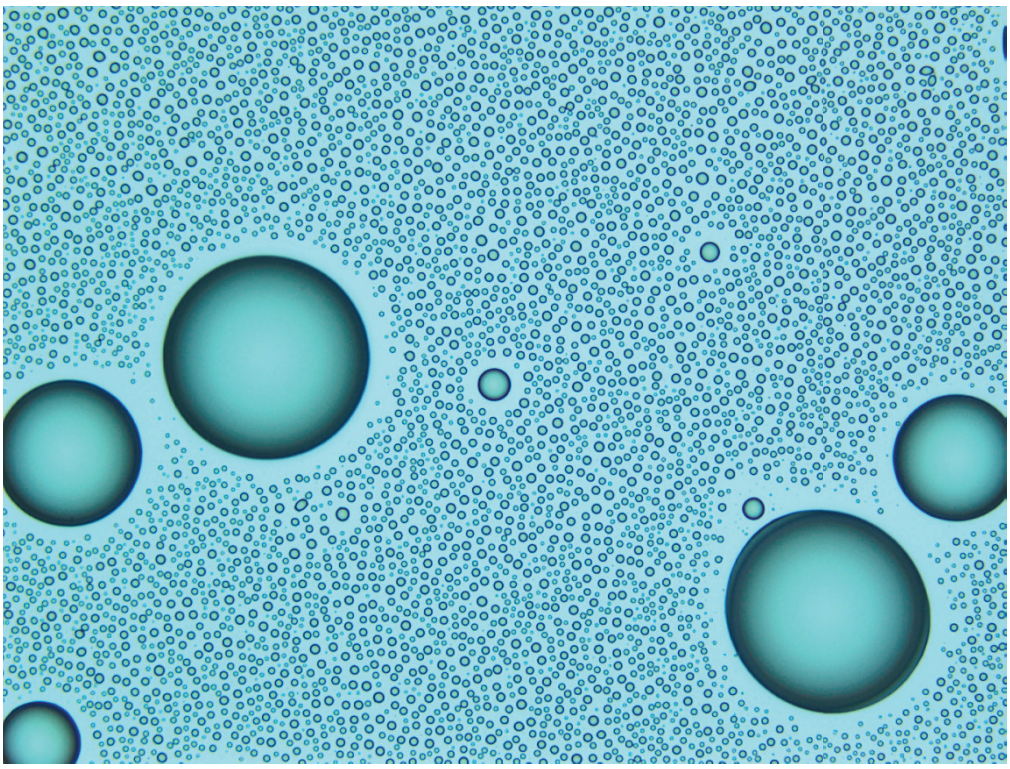

Figure 4.19 Microscopy picture of the water condensation from the negative control experiment.

piperazineethanesulfonic acid (HEPES) buffer (20 mM HEPES, 150 mM NaCl, 1 mM $CaCl_2$, 1 mM $MnCl_2$, pH 7.5) for 20 min and subsequently washed with HEPES buffer and distilled water. PNA was chosen because it was already available in the laboratory. The analysis of the generated samples by fluorescence microscopy provided clear evidence that the fluorescent protein preferably adheres to the areas without polymer coating (see Figure 4.20, the bright stripes). This experiment with rhodamine-labeled PNA is not only supporting the evidence of the generation of patterned polymer surfaces, but also shows that the surface chemistry is modified, by the grafting of the polymers onto the surface, in a way that fouling of PNA could be strongly reduced.

After demonstrating by a variety of analytical methods that patterned polymer surfaces can be prepared by MIMIC, it can be stated that the employed polymers can likely be used to be grafted onto the Cp functional pore surface from the membranes generated in Section 4.2.

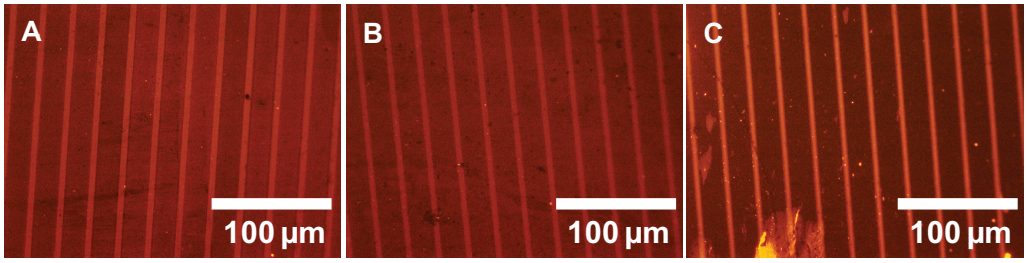

Figure 4.20 Fluorescence microscopy images of the polymer patterned (**A**: **P3**, **B**: **P5**, **C**: **P6**) sufaces after exposure to a solution with rhodamine-labeled PNA. Fluorescence of rhodamine-labeled PNA (bright lines) occurs only between the stripes of the polymer brushes (stamp pattern, 5 µm contact area spaced by 20 µm).

5

Summary and Outlook

Nanoporous block copolymer membranes become increasingly important for various applications such as waste water treatment, pharmaceutical separations or in biomedical engineering devices, to mention only a few. Besides the morphology (pore size, pore distribution and thickness) of the membrane, and its stability against mechanical stress and organic solvents, the surface chemistry (e.g. the polarity or the presence of certain functional groups) is key factor for every application.

Tailoring the surface chemistry of a given membrane is not straight forward. Thus, the current thesis describes the development and realization of a concept for the preparation of nanoporous block copolymer membranes with adjustable surface chemistry. An essential element of the concept is the modular synthesis of amphiphilic block copolymers with a switchable linkage between the individual blocks. After membrane formation, employing these kind of block copolymers, the polar block on the surface can be cleaved off and new components with the appropriate functional group can then be grafted onto the surface.

For the generation of the desired amphiphilic block copolymers with switchable linkage, the employed building block polymers were prepared *via* the RAFT technique. For the unpolar building block, a bromine functional RAFT agent was used to copolymerize styrene and isoprene. Subsequently, the bromine was replaced with cyclopentadiene to introduce a highly reactive diene at one end group of the polymer. For the preparation of the polar building blocks, a HDA capable RAFT agent was employed. As a result, the generated polymers can be used in conjugation reactions without the need of any post polymerization modification. Utilized monomers were triethylene glycol methyl ether acrylate, hydroxyethyl acrylate and acrylic acid.

In order to examine the thermal behavior of the HDA linkage, a low molecular weight poly(isoprene-*co*-styrene)-*block*-poly(triethylene glycol methyl ether acrylate) (P(I-*co*-S)-*b*-PTEGA) diblock terpolymer was prepared and subjected to detailed HT-NMR, HT-SEC and HT-DLS analysis. Moreover, a high molecular weight analogue of the P(I-*co*-S)-*b*-PTEGA diblock terpolymer was prepared and subsequently employed in a macroscopic cleavage experiment.

A dual functional CTA capable of highly efficient sequential thermal and photo induced ligation, generating α,ω-functional polymers, was developed in order to further increase the variety of possible membrane modifications. A HDA reaction with cyclopentadiene can be used as protection of the C=S-double bond. After photo ligation of the α,ω-functional polymer with a second block, the cyclopentadiene can be removed at elevated temperatures and the HDA capable RAFT end group is accessible again. Thus, the so generated block copolymers can be grafted onto a Cp-functionalized (membrane) surface. To exemplarily demonstrate the versatility of the dual functional CTA, an amphiphilic triblock quaterpolymer poly(isoprene-*co*-styrene)-*block*-poly(ethyl acrylate)-*block*-poly(ethylene oxide) (P(I-*co*-S)-*b*-PEA-*b*-PEO) was prepared.

For the preparation of nanoporous block copolymer membranes the high molecular weight analogue of the P(I-*co*-S)-*b*-PTEGA diblock terpolymer was employed in the SNIPS process. The resulting membranes were very fragile and had only small pores. Thus, another diblock terpolymer with a smaller PTEGA block was synthesized and

subjected to membrane formation. In this way, thicker membranes with bigger pores could be generated.

Cleaving off the polar polymer from the surface of both generated membranes was achieved by immersion in 50 °C hot water. This way, the morphology of the membranes was not affected by the cleaving procedure. The kinetics of the reaction was followed by NMR spectroscopy. It was found that the removal of the polar block from the surface of the membranes proceeds faster and to a larger extend for the second membrane, with the larger pores.

The ability of the generated polar polymer blocks (PTEGA, PHEA and PAA) to attach to a cyclopentadienyl functional surface in aqueous media in a pore like environment was tested by micromolding in capillaries on silicon wafers. The successful covalent functionalzation in the patterns of the applied stamps was confirmed *via* water contact angle measurements, vapor deposition pictures, XPS, AFM and ToF-SIMS.

In summary, the current thesis indicates that the developed concept for the preparation of nanoporous block copolymer membranes with feed stream specific pore surfaces *via* modular ligation chemistry should work in principle. However, until now it was not possible to graft any polymer or molecule onto the surface of the membranes with cleaved off hydrophilic block. The reason for this circumstance is not clear. A possible explanation could be that by simple immersion in the reaction mixture, the employed reactants in aqueous solution cannot migrate into the membrane because of its hydrophobic nature. Inserting the membranes in a flow cell, in order to purge the reaction mixture through it, was not possible since the membranes became very brittle after the cleaving of the hydrophilic block. Already during the insertion, damages such as fractures or large holes could not be avoided. A solution to that problem could be to increase the amount of isoprene in the hydrophobic block, to reduce the brittleness, and additionally increase the thickness of the membranes, to make them mechanically more stable. Therefore it may be necessary to exchange PTEGA with another hydrophilic block. An alternative explanation could be that after the cleavage procedure, the cyclopentadiene moieties are not accessible anymore. This would imply that the moieties migrate into the inner, hydrophobic framework of the membranes. In

this case, a possible solution could be the use of an amphiphilic triblock terpolymere for the membrane formation, consisting of one hydrophobic block, a small hydrophilic block in the middle and a large hydrophilic block. Then, the switchable HDA conjungation should be placed between the two polar blocks. Thus, after cleavage of the large polar block the reactive moieties would stay accessible on the surface of the membrane within a small hydrophilic layer of the middle block. A proposal for such a polymer is depicted in Figure 5.1. The hydrophobic block is generated *via* copolymerization of isoprene and styrene, employing a photoenol functionalized trithiocarbonate as CTA.[246] The hydrophilic middle block is prepared by ATRP with a furan protected maleimide containing ATRP initiator.[247] Subsequently the meleimide is deprotected and used for the conjugation with the hydrophobic block *via* photoenol reaction. Afterward, the residual bromine from the hydrophilic block is substituted with Cp. Now, the second hydrophilic block can be attached with the familiar RAFT-HDA chemistry.

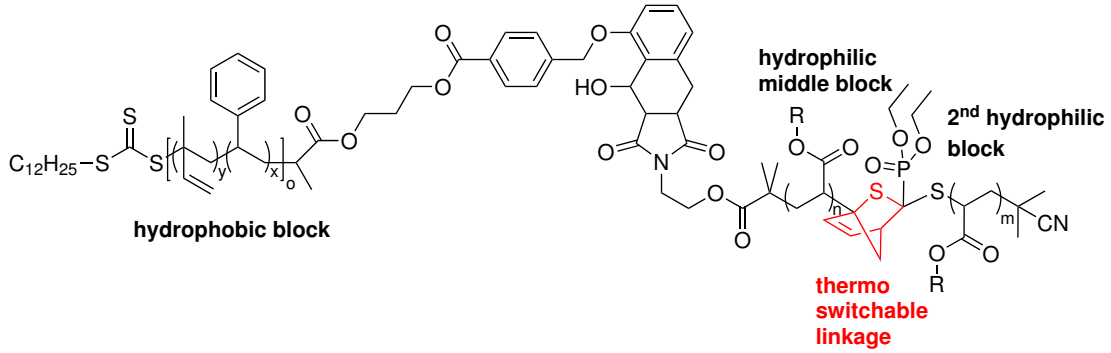

Figure 5.1 Structure of the proposed amphiphilic triblock terpolymer with a switchable linkage between two hydrophilic blocks.

6

Experimental Section

6.1 Materials

3-hydroxypropyl 2-bromo-2-methylpropanoate,[248] 2-(((dodecylthio)carbonothioyl)thio)-2-methyl propanoic acid (DMP),[249] triethylene glycol methyl ether acrylate (TEGA)[250] vinyl benzyl photoenol (2-methyl-6-((4-vinylbenzyl)oxy)benzaldehyde),[241] fumarate end-capped poly(ethylene glycol),[251] 2-cyanopropan-2-yl(diethoxyphosphoryl)methanedithioate (**CTA-2**)[252] and sodium cyclopentadiene (NaCp)[253] were synthesized according to literature protocols. TEGA was stored in the freezer, NaCp in a glove box. 2,2′-Azobis(2-methylpropionitrile) (AIBN) was recrystallized in methanol and stored in the freezer (-21℃). Isoprene (99 %, Abcr), styrene (99 %, Merck), ethyl acrylate (99 %, Merck), hydroxyethyl acrylate (99 %, Abcr) and dioxane (99 %, Abcr) were passed through a column of basic alumina (aluminum oxide 90 active basic, 0.063-0.2 mm, Merck) to remove the inhibitor and used immediately afterwards. Acrylic acid was distilled and stored in the freezer. Cyclopentadiene was cracked and distilled (169 ℃) from dicyclopentadiene and used immediately. Diethylphosphite (98 %, Acros), 4-(dimethylamino)pyridine

(DMAP) (99 %, Aldrich), *N,N′*-dicyclohexylcarbodiimide (DCC) (99 %, Abcr), HCl (32 %, Acros), $NaHCO_3$ (99 %, VWR), NaH (60 % with petrol ether, Aldrich), $MgSO_4$ (99 %, Carl Roth GmbH and Co. KG), 2,2'-Azobis(*N*-butyl-2-methylpropionamide) (VAm-110) (Wako), carbon disulfide (99.9 %, Acros), triphenylphosphine (99 %, Abcr), nickelocene (99 %, Abcr), NaI (99 %, Acros), oxalylbromide (98 %, Acros), silica gel (Geduran Si 60, 40-63 µm, for column chromatography, Merck), diethyl fumarate (97 %, Alfa Aesar), zinc chloride (98 %, Fluka), triethylamine (99 %, Acros) and dry THF (99 %, Acros) were used as received from the supplier. Dichloromethane (DCM), ethyl acetate, acetonitrile, *n*-hexane, methanol and tetrahydrofuran (THF) were all analytical grade and purchased from VWR.

6.2 Characterization Methods

Size Exclusion Chromatography (SEC)

SEC measurements were performed on a TOSOH Eco-SEC HLC-8320 GPC System, comprising an autosampler, a SDV 5 µm beadsize guard column (50 × 8 mm, PSS) followed by three SDV 5 µm columns (300 × 7.5 mm, subsequently 100 Å, 1000 Å and 10^5 Å pore size, PSS), and a differential refractive index (dRI) detector using tetrahydrofuran (THF) as the eluent at 30 °C with a flow rate of 1 mL min^{-1}. The SEC system was calibrated using narrow poly(styrene) standards ranging from 266 to 2.52 10^6 g mol^{-1}, respectively with narrow poly(methyl methacrylate) (PMMA) standards ranging from 800 to 1.82 10^6 g mol^{-1}. Calculation of the molecular weight proceeded *via* the Mark-Houwink-Sakurada (MHS) parameters for poly(styrene) in THF at 30 °C, *i.e.*, K = 13.63 10^{-3} mL g^{-1}, α = 0.714. For PMMA the corresponding MHS parameters were employed: K = 129.8 10^{-3} mL g^{-1}, α = 0.688.

SEC measurements of PAA were performed on a SECcurity GPC System - Polymer Standards Service (PSS) GmbH, Mainz - Agilent Technologies 1260 Infinity, comprising an autosampler, a Suprema 5 µm bead-size guard column (8 × 50 mm, PSS) followed by a mixed bed PSS Suprema linear S 5 µm column(8 x 300 mm), and a dRI and UV detector using $Na_2HPO_4 \cdot 2H_2O$ buffer (11.88 g L^{-1}) as eluent at ambient temperature with a flow rate of 1 mL min^{-1}.

Nuclear Magnetic Resonance (NMR) Spectroscopy

NMR measurements were conducted on a Bruker AM500 or a Bruker Ascend 400 (for the high temperature measurements) spectrometer at 500 or 400 MHz, respectively, for hydrogen nuclei. Samples were dissolved in $CDCl_3$, DMSO-d_6 or toluene-d_8 using residual solvent peaks for shift correction. Abbreviations used in the description of the materials' syntheses include singlet (s), doublet (d), triplet (t), quartet (q), and unresolved multiplet (m).

Electrospray Ionization-Mass Spectrometry (ESI-MS)

Mass spectra were recorded on a Q Exactive (Orbitrap) mass spectrometer (Thermo Fisher Scientific, San Jose, CA, USA) equipped with an HESI II probe. The instrument was calibrated in the m/z range 74-1822 using premixed calibration solutions (Thermo Scientific). A constant spray voltage of 4.7 kV and a dimensionless sheath gas of 5 were applied. The capillary temperature and the S-lens RF level were set to 320 °C and 62.0, respectively. The samples were dissolved with a concentration of 0.05 g L^{-1} in a mixture of THF and MeOH (3:2) containing 100 µmol of sodium triflate and infused with a flow of 5 µL min^{-1}.

High Temperature Dynamic Light Scattering (HT-DLS)

The HT-DLS experiments were carried out with a DynaPro Nanostar (WYATT Technology Corporation, USA) operating at a laser wavelength of 658 nm and observing the fluctuations of the scattered light at an angle of 90 °. For the analysis of the retro HDA and HDA reactions a solvent mixture of 80 vol% DMAc (with 2.75 $g\,L^{-1}$ $ZnCl_2$ as catalyst) and 20 vol% toluene was used and the concentration of the polymers (HDA-terpolymer and building block as reference) was 25 $g\,L^{-1}$. The hydrodynamic radius was determined at 30 °C and 90 °C taking into account the solution viscosities at the respective temperatures (measured with a rolling ball viscometer (Anton Paar, Austria)). Good experimental accuracy could be achieved by averaging 5 to 10 measurements – of each 10 to 25 single acquisitions – for each data point.

High Temperature Size Exclusion Chromatography (HT-SEC)

The HT-SEC experiments were conducted employing a PL-GPC 220 high temperature chromatograph (Agilent Technologies, USA) comprising an autosampler, a ResiPore column (Agilent Technologies, USA) and a built-in dRI detector, using 1,2,4-trichlorobenzene (TCB) as eluent at a flow rate of 0.9 $mL\,min^{-1}$. All components were set to the temperature of 90 °C. A calibration with polymer standards has not been performed since the analysis was only used to derive molecular weight independent data. The chromatograms were deconvoluted in Microsoft Excel®. First a chromatogram of the block terpolymer **P7** after the retro HDA reaction (*i.e.* complete debonding) was recorded. Gauss functions were fitted to both peaks in order to describe them mathematically. The functions can be used for simulating chromatograms of mixtures of **P1** and **P3** in any desired ratio (an overlay of two Gauss functions was used for **P3** to take into account the asymmetrical peak shape). The peaks were subsequently fitted to chromatograms of **P7** after a partial retro HDA reaction (not complete debonding) by varying the parameters that control the area of the peaks, yet keeping the parameters for peak position and width constant. To obtain an optimum mathematical fit, a further Gauss peak was added for describing the distribution between the peaks of **P1** and **P3**, which results from the presence of

the block copolymer **P7**. Due to the concentration sensitivity of the dRI detector the peak area of the simulated peaks can be correlated to the (weight) concentration of the corresponding polymers in the mixture. Hence, it is possible to track the change of the concentration of the individual components **P1**, **P3**, and **P7** over multiple cycles of the HDA/retro HDA experiment.

Scanning Electron Microscopy (SEM)

Samples for SEM were prepared as follows: Top view: Membrane slices were cut, placed on a glass surface and dried in vacuum for 6 h. Cross-sectional view: Membrane slices were deep-frozen in liquid nitrogen, broken, placed on a glass surface and also dried in vacuum for 6 h. Finally, the samples were coated with gold (≈8 nm) using a BAL-TEC SCD005 sputtering device (Balzers, Liechtenstein). SEM measurements were performed on a Zeiss (LEO) 1530 Gemini FESEM operating at 8 to 10 kV using an InLens detector.

Water Contact Angle

Water contact angles were measured by the sessile drop method on a DSA 100 goniometer (Krüss GmbH Wissenschaftliche Laborgeräte, Germany).

X-ray Photoelectron Spectroscopy (XPS)

XPS measurements were performed with an Axis Ultra DLD (Kratos Analytical Ltd, UK). A monochromatic Al Kα source (hν = 1486.6 eV) at 10 mA filament current and 12 kV filament voltage source energies was used. The pass energy was set to 20 eV for high resolution scans and to 160 eV for survey scans. The charge neutralizer was used to compensate for sample charging. All measurements were carried out in the “hybrid mode”. The data was evaluated with CasaXPS (version 2.3.15, Casa Software Ltd, UK) and the spectra were calibrated to aliphatic carbon (C1s = 285 eV).

Time of Flight Secondary Ion Mass Spectrometry (ToF-SIMS)

ToF-SIMS was conducted with a TOF.SIMS^5 instrument (IONTOF GmbH, Münster, Germany), equipped with a Bi cluster liquid metal primary ion source and a non-linear time-of-flight analyzer. For best spectral resolution, the Bi source was operated in the "bunched" mode providing 0.7 ns Bi_3^+ ion pulses at 25 keV energy and a lateral resolution of approximately 4 µm. The short pulse length allowed high mass resolution to provide chemical assignments of the complex mass spectra of the immobilized organic layers. Images larger than the maximum deflection range of the primary ion gun of 500 × 500 µm^2 were obtained using the manipulator stage scan mode. Primary ion doses were kept below 10^{11} ions·cm^{-2} (static SIMS limit). Spectra were calibrated on C^+, CH^+, CH_2^+, and CH_3^+; or on C^-, CH^-, and CH_2^-, respectively.

Lateral refinement was obtained conducting either the "burst alignment mode" or "delayed extraction" mode of the primary ion source. The "burst alignment mode" with 100 ns pulse width provides a highly focused ion beam to allow sub-µm resolution due to avoiding chromatic aberration of the Bi primary ion beam due to pulse bunching. "Burst aligment" mode provides nominal mass resolution only. The "delayed extraction" mode is also based on 100 ns primary ion pulses, but here the secondary ion extraction is not quasi-static but instead pulsed with a time delay relative to the impact of the primary ions. Therefore, the lateral resolution is comparable to the "burst alignment" mode but the spectral resolution is no longer dependent on the primary ion pulse width. Mass resolution, (expressed in m/дm) is for "bunched" mode in the order of 8000, and for delayed extraction in the order of 4000.

Atomic Force Microscopy (AFM)

AFM imaging was performed using a Nanowizard 3 from JPK Instruments operated in tapping mode with Veeco RTESP-Tapping Mode Etched Silicon Probes. The AFM was typically operated with a setpoint of 0.900 V and a scan rate of 1.00 Hz with a resolution of 512 x 512 pixels. The data was analyzed with Gwyddion (version 2.22).

Optical and Fluorescence Microscopy

For fluorescence microscopy imaging an Olympus BX 53 microscope was operated with an Olympus XC 10 camera and a X-Cite® Series 120Q by Lumen Dynamics as the irradiation source. Data processing was carried out with the software OLYMPUS Stream Start 1.8. Images were taken at 50-fold magnification with an exposure time of 50 ms.

6.3 Employed Devices and Methods

Employed UV-Lamp for the Photoenol Reaction

The employed UV-lamp is a compact low-pressure fluorescent lamp (Cleo PL-L, Philips Deutschland GmbH) emitting at 370 nm ± 50 nm, 36 W). The emission spectrum is depicted in Figure 6.1. The measured radiation energy at the distance (d = 60 mm) of the samples is 11.99 mW cm^{-2}.

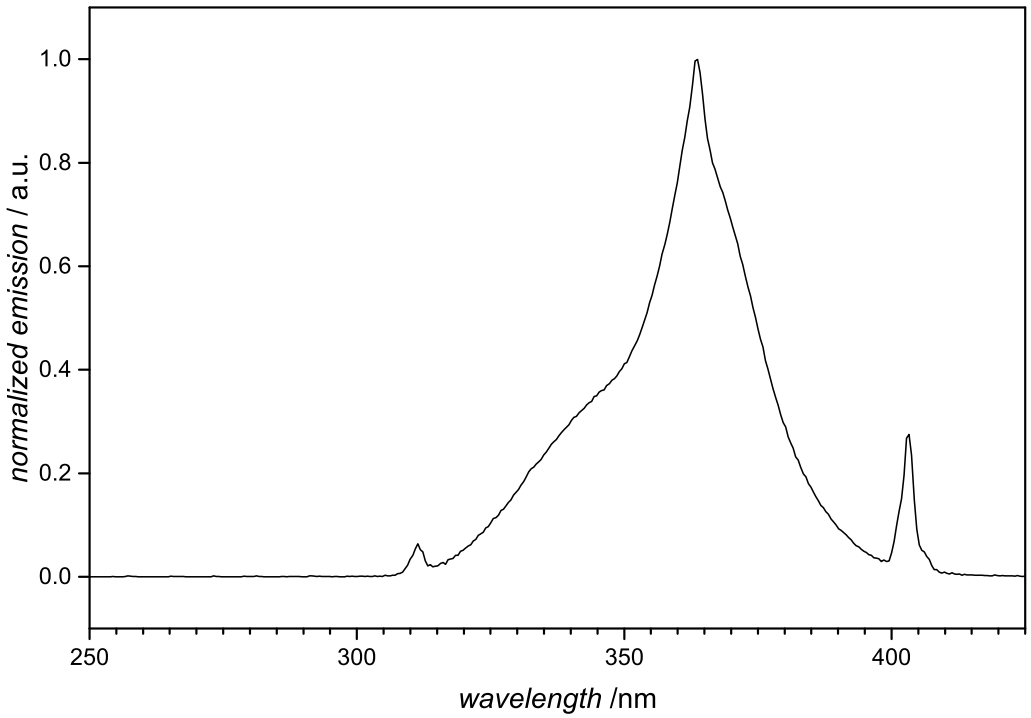

Figure 6.1 Emission spectrum of the employed UV-lamp.

Membrane Preparation

Membranes were prepared *via* the SNIPS process. A 20 wt% solution of **P13**, in a mixture of dioxane (24 wt%) and THF (56 wt%), was cast with a 200 µm doctor blade onto polished (with chloroform and iso -propanol) glass sheets using a Coatmaster 510 (Erichsen GmbH, Germany). A picture of the setup is shown in Figure 6.2. The film casting was performed in a climate chamber from PlasLabs to control both relative humidity (50 %) and temperature (22 ℃) during the process. After a self-assemble time of 40 s, the glass sheet (with the cast film on top of it) was immersed into a precipitation bath of deionized water, yielding the filter membranes. If not used immediately, the membranes were stored in deionized water at ambient temperature until further usage.

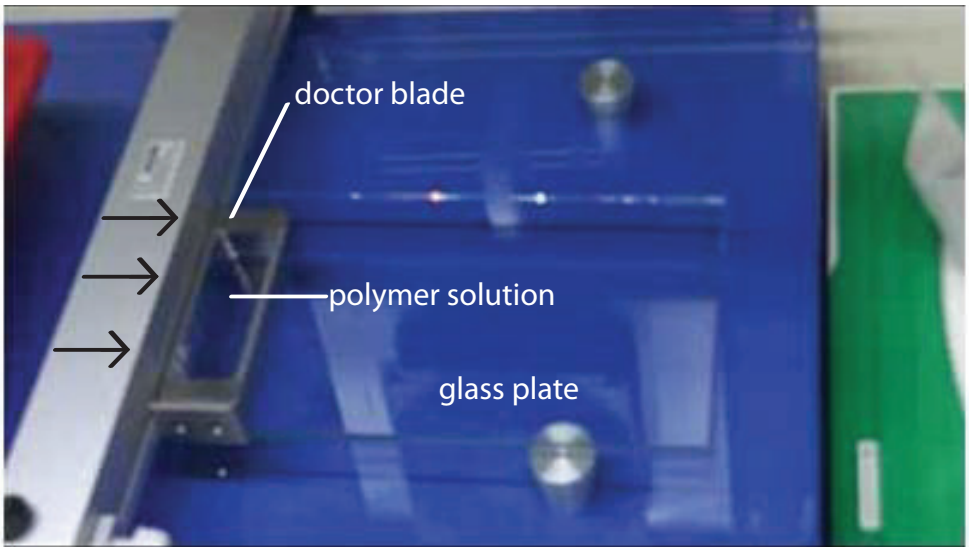

Figure 6.2 Setup of the film casting *via* a doctor blade with the Coatmaster 510.

PDMS Stamp Preparation

PDMS stamps were prepared by mixing poly(dimethylsiloxane) and curing agent (Sylgard 184, Dow Corning) in a 10 to 1 ratio and casting this mixture on a patterned silicon master. The PDMS mixture was cured at 80 ℃ overnight. Patterned stamps were cut out with a knife and put into a UV ozonizer (PSD-UV, Novascan Technologies Inc.) for

55 min prior to use. If not used immediately, the PDMS stamps were stored in distilled water.

Protein Adsorption

Micropatterned polymer surfaces were covered with tetramethylrhodamine labeled peanut agglutinin (50 µg mL^{-1}) in HEPES buffer (20 mM HEPES, 150 mM NaCl, 1 mM $CaCl_2$, 1 mM $MnCl_2$, pH 7.5) for 20 min. Next, the substrates were carefully washed with HEPES-buffer and ultrapure water by exposing the surfaces for 5 min in beakers with the corresponding wash solutions and gentle shaking. After drying the substrates in a slow stream of Ar, the samples were analyzed by fluorescence microscopy.

6.4 Synthesis Protocols

Synthesis of 3-((2-bromo-2-methylpropanoyl)oxy)propyl 2-(((dodecylthio)carbonothioyl)thio)-2-methylpropanoate (DMP-Br; CTA-1)

DMP (3.12 g, 8.56 mmol), DMAP (0.11 g, 0.86 mmol) and 3-hydroxypropyl 2-bromo-2-methylpropanoate (3.85 g, 17.1 mmol) were dissolved in DCM (20 mL) and cooled to 0 ℃ using an ice bath. After addition of a solution of DCC (1.77 g, 8.58 mmol) in DCM (10 mL), the cooling bath was removed and the mixture was stirred overnight at ambient temperature. Subsequently, the white precipitate was filtered off, the solution was diluted with DCM (70 mL), extracted with 0.5 M aqueous HCl (2×100 mL) and washed with saturated $NaHCO_3$ solution (1×100 mL). The organic layer was dried over $MgSO_4$ and concentrated under vacuum. The crude product was purified by column chromatography on silica with *n*-hexane/ethyl acetate (19:1, v/v, R_f 0.23) as solvent and subsequently dried under high vacuum to give a yellow liquid (3.08 g, 63 %). ^{1}H NMR (500 MHz, $CDCl_3$) δ (ppm): 4.22–4.18 (m, 4H, **b**), 3.26 (t, J^3 = 7.4 Hz, 2H, **e**), 2.04–1.99 (m, 2H, **c**), 1.93 (s, 6H, **a**), 1.69 (s, 6H, **d**), 1.70–1.62 (m, 2H, **f**), 1.40–1.33 (m, 2H, **g**), 1.33–1.20 (m, 16H, **h**), 0.86 (t, J^3 = 6.9 Hz, 3H, **i**). ^{13}C NMR (125 MHz, $CDCl_3$, depicted in Figure 6.3) δ (ppm): 221.64 (C=S), 172.90, 171.49, 62.33, 62.13, 55.88, 66.68, 36.97, 31.91, 30.74, 29.63, 29.62, 29.55, 29.45, 29.34, 29.10, 28.96, 27.83, 25.36, 22.69, 22.65, 14.12. ESI-MS: m/z calculated for $C_{24}H_{43}BrO_4S_3$ $[M + Na]^+$, 593.14; found, 593.17.

Copolymerization of Styrene and Isoprene ($P1_a$, $P2_a$)

Copolymerization of styrene and isoprene ($\mathbf{P1}_a$, $\mathbf{P2}_a$). The polymerizations were conducted in the bulk in a pressure stable flask. Styrene (80 mol%), isoprene (20 mol%), the RAFT agent **CTA-1** and the initiator VAm-110 were placed in the flask and the polymerization mixture was purged 45 min with N_2 to remove oxygen. To obtain $\mathbf{P1}_a$, the ratio of monomer/CTA/initiator was 300/1/0.2 and for $\mathbf{P2}_a$ the ratio was 1500/1/0.2. After purging, the reaction mixture was immersed in an oil bath (110 ℃) to start the

polymerization. The reaction time for $\mathbf{P1}_a$ was 8.5 h and 24 h for $\mathbf{P2}_a$. Afterwards the polymerizations were quenched *via* rapid cooling and exposure to air. Subsequently, the polymers were recovered by repeated precipitation in cold methanol and dried under vacuum. $\mathbf{P1}_a$: 30 % conversion, M_n = 9100 g mol^{-1}(PS calibration), $Đ$ = 1.19. $\mathbf{P2}_a$: 39 % conversion, M_n = 49 000 g mol^{-1}(PS calibration), $Đ$ = 1.32.

Nucleophilic Substitution of Bromine with Cyclopentadienyl ($\mathbf{P1}_b$, $\mathbf{P2}_b$)

The following procedure is valid for both polymers. Polymer $\mathbf{P1}_a$: under inert atmosphere, 3 g $\mathbf{P1}_a$ (0.33 mmol), 0.54 g triphenylphosphine (2 mmol), 0.76 g $NiCp_2$ (4 mmol) and 0.90 g NaI (6 mmol) were dissolved in 75 mL dry THF and stirred over night at ambient temperature. Afterwards 200 mL DCM were added and all solids were removed *via* centrifugation. Subsequently, the solution was concentrated under vacuum and precipitated in methanol. The obtained polymer was dissolved again in THF and then passed through a column of basic aluminum oxide. Repeated precipitation in methanol and drying under vacuum provided a clean yellow polymer ($\mathbf{P1}_b$: M_n = 9200 g mol^{-1}(PS calibration), $Đ$ = 1.22; $\mathbf{P4}_b$: M_n = 50 000 g mol^{-1}(PS calibration), $Đ$ = 1.36).

Polymerization of Triethylene Glycol Methyl Ether Acrylate (P3, P4, P12)

Dioxane (**P3**: 8.35 mL; **P5** and **P12**: 25 mL), triethylene glycol methyl ether acrylate (**P3**: 6.53 mL, 7.12 g, 32.6 mmol; **P4** and **P12**: 19.56 mL, 21.32 g, 97.70 mmol), AIBN (**P3**: 8.2 mg, 50 µmol; **P4** and **P12**: 7.1 mg, 43 µmol) and **CTA-2** (**P3**: 70.6 mg, 0.25 mmol; **P4** and **P12**: 61.1 mg, 0.22 mmol) were placed in a Schlenk-flask and the polymerization mixture was degassed *via* three consecutive freeze-pump-thaw cycles. Next, the flask was placed in a 70 ℃ oil bath to commence the polymerization. After 3 h (for **P3**; for **P4** 2.25 h and **P12** 1 h) the reaction was stopped *via* rapid cooling and exposure to air. The polymer was obtained by repeated precipitation in *n*-hexane (**P3**:

19 % conversion, M_n = 6600 g mol^{-1}(PMMA calibration), $Đ$ = 1.12; **P4**: 37 % conversion, M_n = 35 000 g mol^{-1}(PMMA calibration), $Đ$ = 1.30; **P12**: 20 % conversion, M_n = 18 000 g mol^{-1}(PS calibration), $Đ$ = 1.16).

Polymerization of Hydroxyethyl Acrylate (P5)

Ethanole (9.5 mL), hydroxyethyl acrylate (9.5 mL, 9.60 g, 82.71 mmol), AIBN (45.3 mg, 275 µmol) and 2-cyanopropan-2-yl(diethoxy-phosphoryl)methane-dithioate (155.1 mg, 551 µmol) were placed in a round-bottom flask and the polymerization mixture was purged 45 min with N_2 to remove oxygen. Next, the flask was placed in a 60 ℃ oil bath to commence the polymerization. After 5 h the reaction was stopped *via* rapid cooling and exposure to air. The polymer was obtained by repeated precipitation in *n*-hexane (7 % conversion, M_n = 1500 g mol^{-1} (PS calibration), $Đ$ = 1.09).

Polymerization of Acrylic Acid (P6)

Dioxane (25 mL), acrylic acid (13.7 mL, 14.39 g, 199.6 mmol), AIBN (82.0 mg, 499 µmol) and 2-cyanopropan-2-yl(diethoxy-phosphoryl)methane-dithioate (280.8 mg, 1.00 mmol) were placed in a round-bottom flask and the polymerization mixture was purged 60 min with N_2 to remove oxygen. Next, the flask was placed in a 70 ℃ oil bath to commence the polymerization. After 4 h the reaction was stopped *via* rapid cooling and exposure to air. The polymer was obtained by repeated precipitation in ether (30 % conversion, M_n = 4000 g mol^{-1} (NMR calculation)).

Synthesis of the Amphiphilic Block Terpolymers (P7, P8, P13)

Equimolar amounts of **P1**$_b$ and **P3** (respectively **P2**$_b$ and **P4** or **P12**) were dissolved in ethyl acetate (total concentration: 50 g L^{-1} polymer) and a catalytic amount of $ZnCl_2$ (5 g L^{-1}) was added. The reaction mixture was stirred for 16 h over night (respectively two days for **P8** and **P13**) at ambient temperature. Next, the solvent was removed under reduced pressure and the polymer was dissolved again in THF. Subsequently, the polymer was precipitated in water to remove the residual catalyst (**P7**: M_n = 16 000 g mol^{-1}(PS calibration), $Đ$ = 1.15; **P8**: M_n = 68 000 g mol^{-1}(PS calibration), $Đ$ = 1.32; **P13**: M_n = 60 000 g mol^{-1}(PS calibration), $Đ$ = 1.33).

Macroscopic Separation of the Building Blocks from the Amphiphilic Block Terpolymer (P2$_b$*, P4*).

To form an aqueous dispersion, 20 mg of the block copolymer **P**8 was dissolved in a small amount of THF and then precipitated in 7 mL water. The THF was removed under reduced pressure. The dispersion was subsequently heated to 90 °C for 30 min and then cooled to ambient temperature. Subsequently, the white solid (**P2**$_b$*) and the aqueous solution (**P4***) were separated *via* centrifugation. The water was removed under reduced pressure and both polymers were dried under vacuum.

Synthesis of the RAFT-Agent Precursor 2-((4-(1-Bromoethyl)benzyl)oxy)-6-methyl Benzaldehyde (4)

Vinyl benzyl photoenol (645 mg, 2.556 mmol) and 6 g of dry silica were placed in a flask and suspended in 12 mL of dichloromethane. The reaction mixture was cooled to −21 °C, and 0.344 mL (522 mg, 3.834 mmol) of oxalyl bromide dissolved in 3 mL of dichloromethane was added drop wise. After stirring for 3 h at −21 °C, 1 mL of triethylamine was added, and stirring was continued overnight at ambient temperature. Afterward, the silica was removed by filtration, and the dichloromethane solution was washed consecutively with aq. $NaHCO_3$ (25 mL), water (25 mL), and brine (25 mL). The

organic layer was dried over $MgSO_4$ and concentrated under vacuum. The crude product was purified by column chromatography on silica with *n*-hexane/ethyl acetate/triethyl amine (19:1:0.5, v/v) as solvent and subsequently dried under high vacuum to give a yellow oil (342 mg, 40 %). ^{1}H NMR (500 MHz, $CDCl_3$, see Figure 6.10) δ (ppm): 10.73 (s, 1H, **a**), 7.52–7.32 (m, 3H, **g**, **h**, **d**), 6.89 (d, J^3 = 8.3 Hz, 1H, **e**), 6.84 (d, J^3 = 7.5 Hz, 1H, **c**), 5.23 (q, J^3 = 6.9 Hz, 1H, **i**), 5.15 (s, 2H, **f**), 2.99 (s, 3H, **b**), 2.06 (d, J^3 = 6.9 Hz, **j**). ^{13}C NMR (125 MHz, $CDCl_3$, see Figure 6.11) δ (ppm): 192.30 (s, 1C, **a**), 162.29 (s, 1C, **h**), 143.38 (s, 1C, **d**), 142.31 (s, 1C, **m**), 136.54 (s, 1C, **j**), 134.54 (s, 1C, **f**), 127.67 (s, 2C, **k**), 127.30 (s, 2C, **l**), 124.63 (s, 1C, **e**), 123.75 (s, 1C, **b**), 110.45 (s, 1C, **g**), 70.25 (s, 1C, **i**), 49.07 (s, 1C, **n**), 26.89 (s, 1C, **c**), 21.64 (s, 1C, **o**). ESI-MS: m/z calculated for $C_{17}H_{17}BrO_2$ $[M + Na]^+$, 355.0310; found, 355.0306.

Synthesis of the Dual Functional RAFT-Agent 1-(4-((2-Formyl-3-methyl phenoxy)methyl)phenyl)ethyl (Diethoxyphosphoryl) Methane Dithioate (CTA-3)

Under Ar atmosphere, a solution of diethyl phosphite (1.1 mL, 1.18 g, 8.529 mmol) in 1 mL of dry THF was added slowly to a suspension of NaH (206.75 mg, 8.615 mmol) in dry THF (9 mL). After being refluxed for 5 min, the reaction mixture was cooled to −83 °C, and carbon disulfide (2.6 mL, 3.3 g, 43.43 mmol) was added. The solution was allowed to warm to ambient temperature and stirred for an additional 2 h. After cooling to −21 °C, a solution of **4** (2.8 g, 11.39 mmol) in 5 mL of dry THF was added to the reaction mixture, and stirring was continued overnight. Subsequently, 20 mL of dichloromethane was added, and the resulting precipitate was filtered off. The solvent was removed under reduced pressure, and the residue was purified by column chromatography on silica using *n*-hexane/ethyl acetate (6:4, v/v) as eluent. After drying under high vacuum a pink oil was received (1.3 g, 33 %). ^{1}H NMR (500 MHz, $CDCl_3$) δ (ppm): 10.72 (s, 1H, **a**), 7.52–7.32 (m, 3H, **g**, **h**, **d**), 6.88 (d, J^3 = 8.4 Hz, 1H, **e**), 6.84 (d, J^3 = 7.5 Hz, 1H, **c**), 5.21 (q, J^3 = 7.1 Hz, 1H, **i**), 5.14 (s, 2H, **f**), 4.32–4.16 (m, 4H, **k**), 2.58 (s, 3H, b), 1.73 (d, J^3 = 7.1 Hz, **j**), 1.39–1.31 (m, 6H, **l**). ^{13}C NMR (125 MHz, $CDCl_3$, see Figure 6.12) δ (ppm): 226.92 (d,

1C, **p**), 192.22 (s, 1C, **a**), 162.17 (s, 1C, **h**), 142.22 (s, 1C, **d**), 140.14 (s, 1C, **m**), 136.10 (s, 1C, **j**), 134.44 (s, 1C, **f**), 128.19 (s, 1C, **k**), 127.65 (s, 1C, **l**), 124.53 (s, 1C, **e**), 123.62 (s, 1C, **b**), 110.34 (s, 1C, **g**), 70.15 (s, 1C, **i**), 64.78 (s, 1C, **q**), 48.12 (s, 1C, **n**), 21.51 (s, 1C, **c**), 20.13 (s, 1C, **r**), 16.30 (s, 1C, **o**). ESI-MS: *m*/*z* calculated for $C_{22}H_{27}O_5PS_2$ $[M + Na]^+$, 489.0935; found, 489.0937.

Synthesis of Poly(Ethyl Acrylate)(PEA, P9)

Ethyl acrylate (7.5 mL, 6.885 g, 8.77 mmol) the RAFT-agent (**CTA-3**) (213.9 mg, 0.46 mmol) and the initiator AIBN (15.1 mg, 91.0 µmol) were placed in a flask and purged with Ar for 45 min. Subsequently, the reaction mixture was placed in a 70 °C hot oil bath and stirred for 7 h. The polymerization was stopped by cooling with liquid nitrogen and exposure to atmosphere. The polymer was recovered by 3 times precipitation in a methanol/water mixture (1/1; v/v) and dried under high vacuum (4 % conversion, M_n = 1200 g mol^{-1}(PS calibration), $Đ$ = 1.24).

Reaction of P9 with Cyclopentadienyl ($P9_a$)

25 mg (22.7 µmol) polymer **P9** and 7.5 µL (5.9 mg, 89.2 µmol) cyclopentadiene were dissolved in 0.8 mL dichloromethane and stirred over night. Subsequently the solvent was removed under reduced pressure and the polymer was recovered *via* precipitation from THF into a mixture of acetonitrile/water (1/1, v/v) and dried under high vacuum (M_n = 1200 g mol^{-1}(PS calibration), $Đ$ = 1.30).

Reaction of $P9_a$ with Diethyl Fumarate ($P9_b$)

31.2 mg (26 µmol) polymer $\mathbf{P9}_a$ and 50 µL (52.6 mg) diethyl fumarate were dissolved in 6 mL acetonitrile and the solution was purged with Ar for 15 min. Subsequently, the reaction mixture was exposed to UV-light for 2.5 h. Next, 6 mL water was added to the solution and the polymer was recovered *via* centrifugation and dried under high vacuum (M_n = 1500 g mol^{-1}(PS calibration), $Đ$ = 1.27).

Synthesis of the Diblock Terpolymer P(I-*co*-S)-*b*-PEA (P10)

271.8 mg (30.2 µmol) **P1**, 50 mg (45.5 µmol) **P9**, and 6.2 mg (45.5 µmol) $ZnCl_2$ were dissolved in ethyl acetate and stirred for 24 h. Precipitation in methanol and drying under high vacuum yielded the diblock terpolymer P(I-*co*-S)-*b*-PEA (**P10**; M_n = 10 500 g mol^{-1}(PS calibration), $Đ$ = 1.26).

Synthesis of the Triblock Quaterpolymer P(I-*co*-S)-*b*-PEA-*b*-PEO (P11)

43 mg (4.3 µmol, 1.0 eq) diblock copolymer (**P10**) and 86 mg (43 µmol) fumarate end-capped PEO were dissolved in 8.6 mL dichloromethane and purged with Ar for 15 min. Subsequently, the reaction mixture was exposed to UV-light (370 nm) for 2.5 h. Next, the dichloromethane was reduced under vacuum to a volume of approximately 1 mL and 3 mL THF were added to the solution. To this mixture 5 mL of water was added and the organic solvents were removed under reduced pressure. The precipitated polymer was recovered *via* centrifugation and the procedure was repeated. Subsequent drying under high vacuum yields the pure triblock quaterpolymer P(I-*co*-S)-*b*-PEA-b-PEG (**P11**; M_n = 12 500 g mol^{-1}(PS calibration), $Đ$ = 1.37).

Preparation of Br Functional Surfaces

Silicon wafers were first cleaned by sonication for 3 min in pentane, acetone and water. Next, the wafers were activated in piranha solution (H_2SO_4(conc.):H_2O_2(30 %) = 2:1) for 30 min, rinsed with copious amounts of water, dried in a stream of Ar and transferred into a solution of 11-bromoundecyltrichlorosilane (0.1 vol% in toluene (analytical grade)). After stirring the solution for 45 min at room temperature, the samples were taken out and rinsed with dichloromethane, ethanol and water and dried in a stream of argon.

Preparation of Cp Functional Surfaces

Sodium cyclopentadienide (0.8 g) was dissolved in dry THF (30 mL) and the Br functionalized silicon wafers were immersed. The solution was stirred overnight at ambient temperature. Afterwards, the samples were taken out, sonicated in water (10 min) and rinsed with water, ethanol and acetone and dried in a stream of argon. The Cp functional wafers were stored in a schlenk tube, if not used immediately.

Preparation of Polymer Patterned Surfaces

Aqueous solutions of the three polymers (**P3**, **P5** and **P6**) were prepared. The concentration for all solutions was set to 30 g L^{-1}. Oxidized PDMS stamps were placed on Cp functional silicon wafers and 5 µL of polymer solution was poured at the open end of the capillaries with a pipette. The surfaces were placed in a sealable petri dish with a wet tissue to provide a humid atmosphere, which prevents the aqueous solution from evaporating before the reaction is over. After 90 min the samples were taken out of the petri dish and the stamp was removed from the Cp SAM while holding the surface in a beaker with water. Next, the samples were washed with water, ethanol and acetone, sonicated and dried.

Non patterned surfaces were prepared for XPS and contact angle measurements.

6.5 Additional Figures

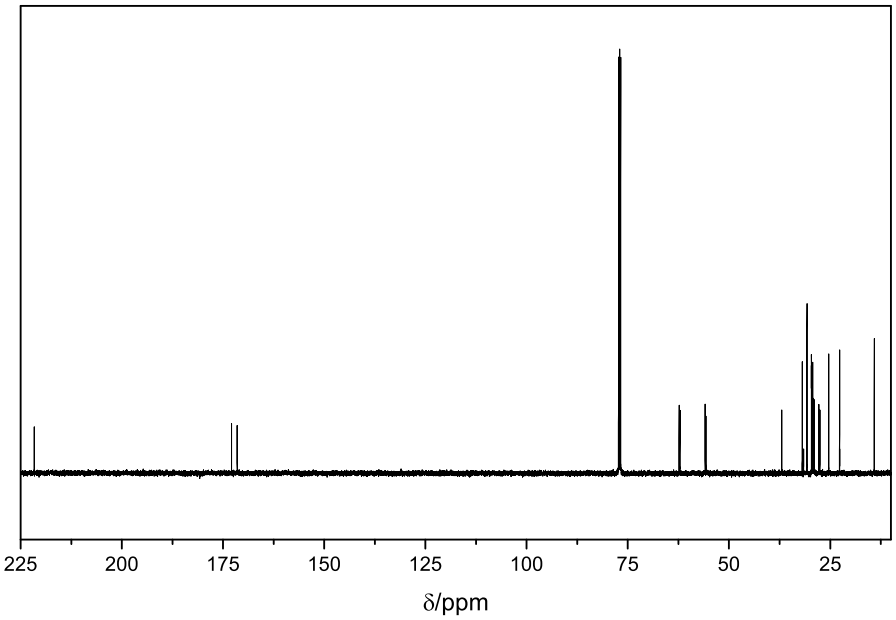

Figure 6.3 ^{13}C NMR spectrum (125 MHz) of the Br-functional RAFT agent **CTA-1** in $CDCl_3$ at ambient temperature.

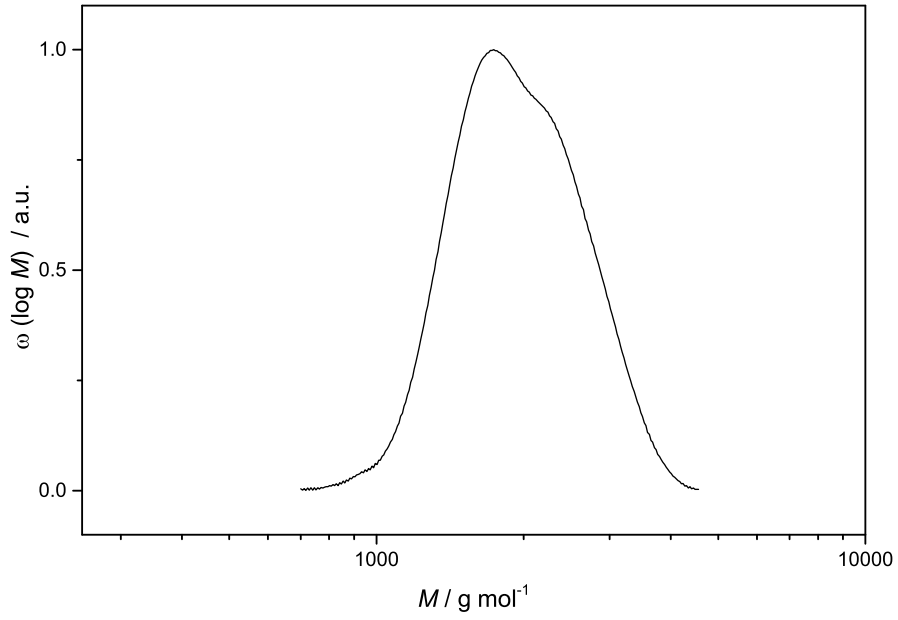

Figure 6.4 SEC trace of **P5**, measured in THF (M_n = 1500 g mol^{-1} (PS calibration), $Đ$ = 1.09).

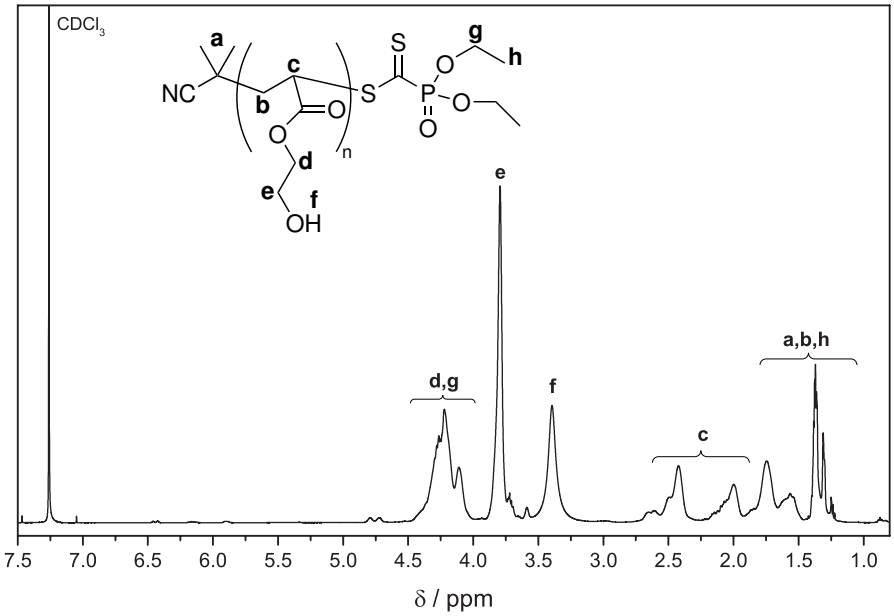

Figure 6.5 ^{1}H NMR spectrum (500 MHz) of the polymer **P5** in $CDCl_3$.

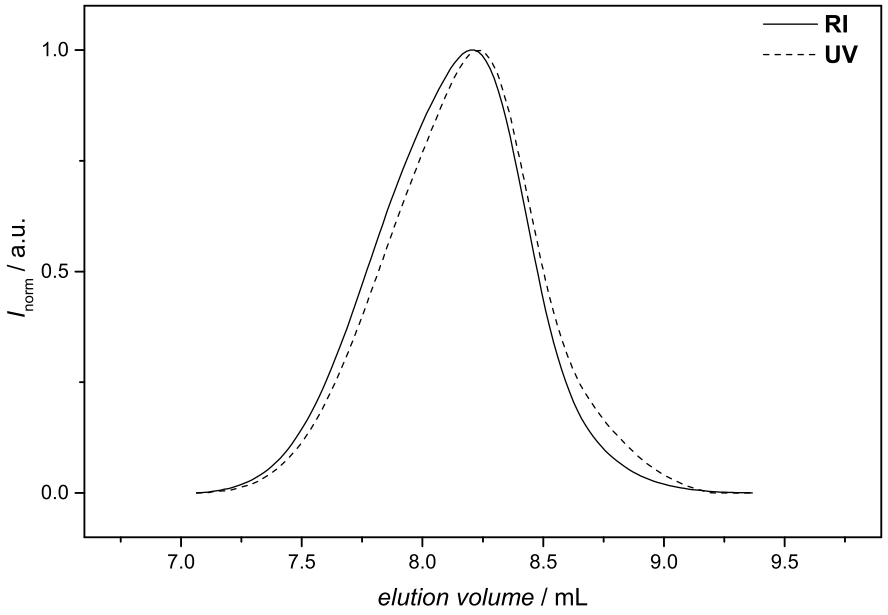

Figure 6.6 SEC trace of **P6**, measured in Na_2HPO_4 buffer. The good overlap of the RI- (mass distribution) and the UV-signal (number distribution) indicate a small $Đ$.

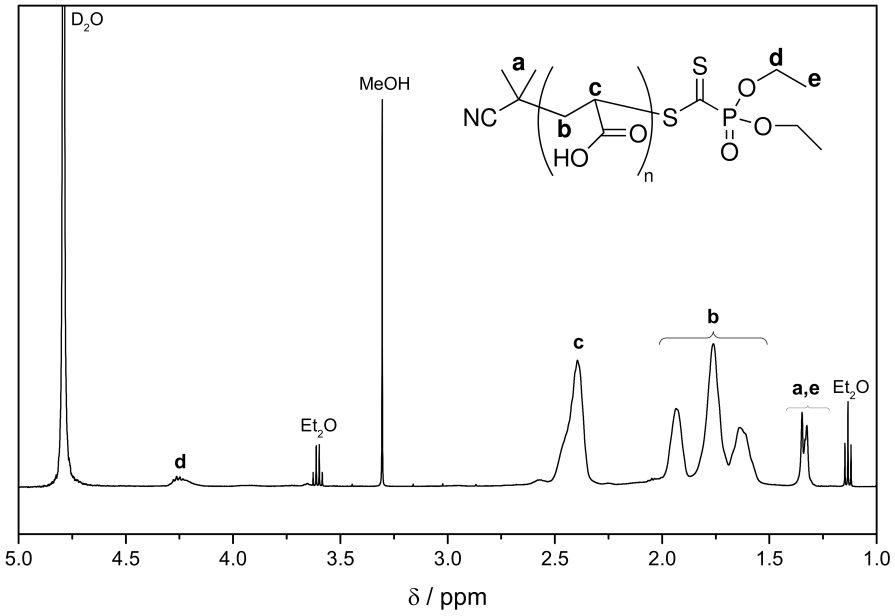

Figure 6.7 ^{1}H NMR spectrum (500 MHz) of **P6** in D_2O at ambient temperature.

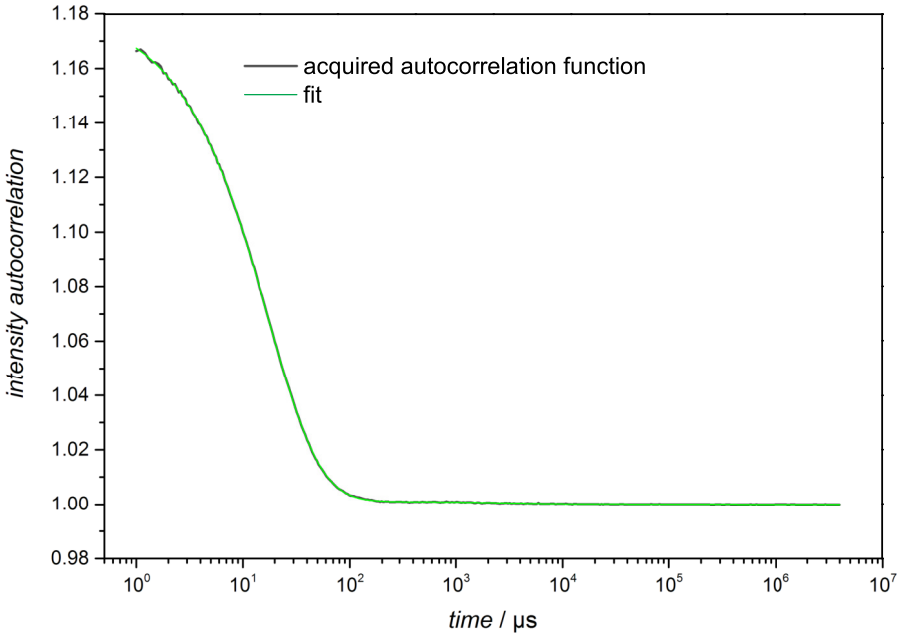

Figure 6.8 Exemplary autocorrelation function from the DLS measurements of the block terpolymer **P7** in 80 % DMAc and 20 % toluene (containing 2.75 g L^{-1} $ZnCl_2$) at 30 °C. The black line depicts the experimentally recorded function, whereas the green line shows the mathematical fit with excellent agreement.

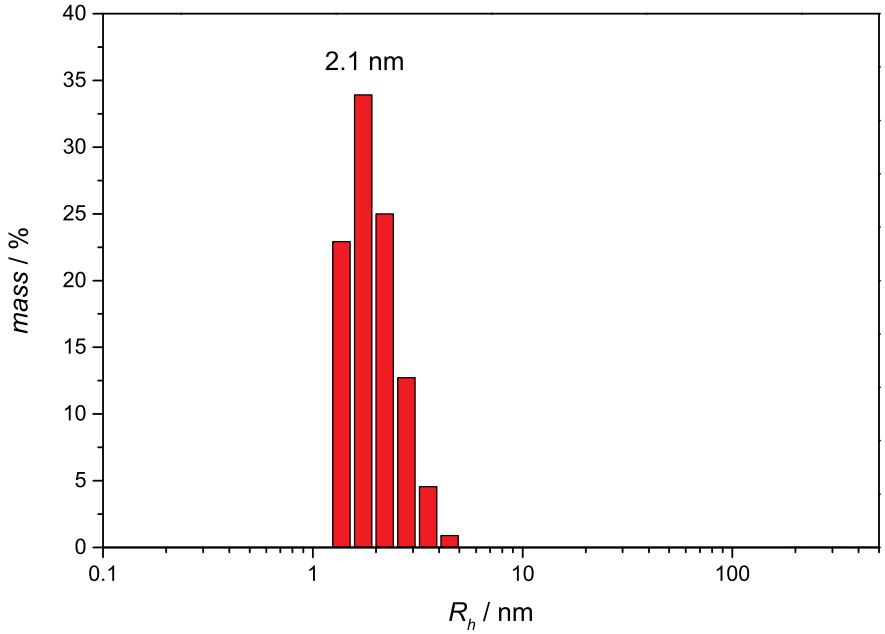

Figure 6.9 Exemplary experimental size distribution obtained from the DLS measurements of the block terpolymer **P7** in 80 % DMAc (containing 2.75 g L^{-1} $ZnCl_2$) and 20 % toluene at 30 °C as a result of the fit depicted in Figure 6.8.

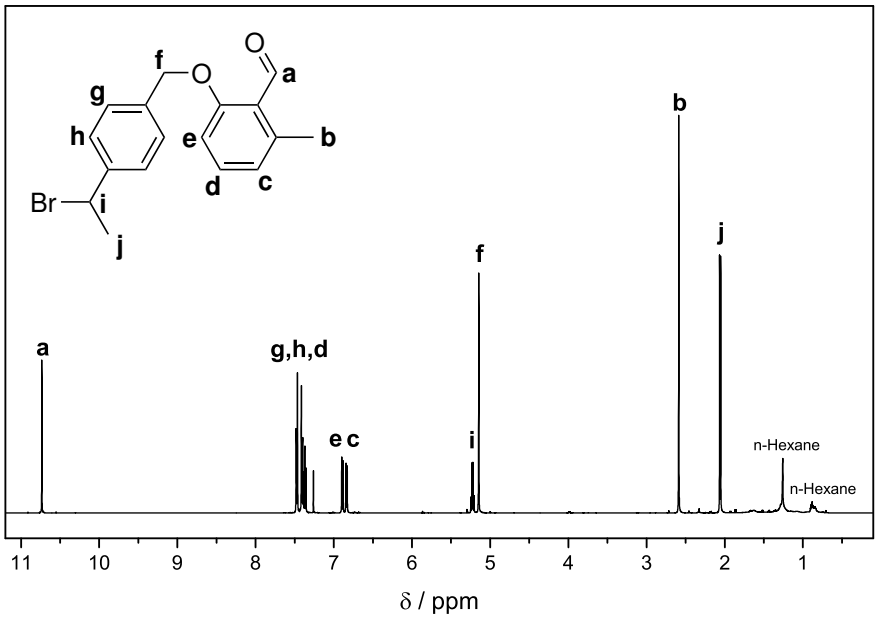

Figure 6.10 ^{1}H NMR spectrum (500 MHz, $CDCl_3$) of the CTA precursor **4**.

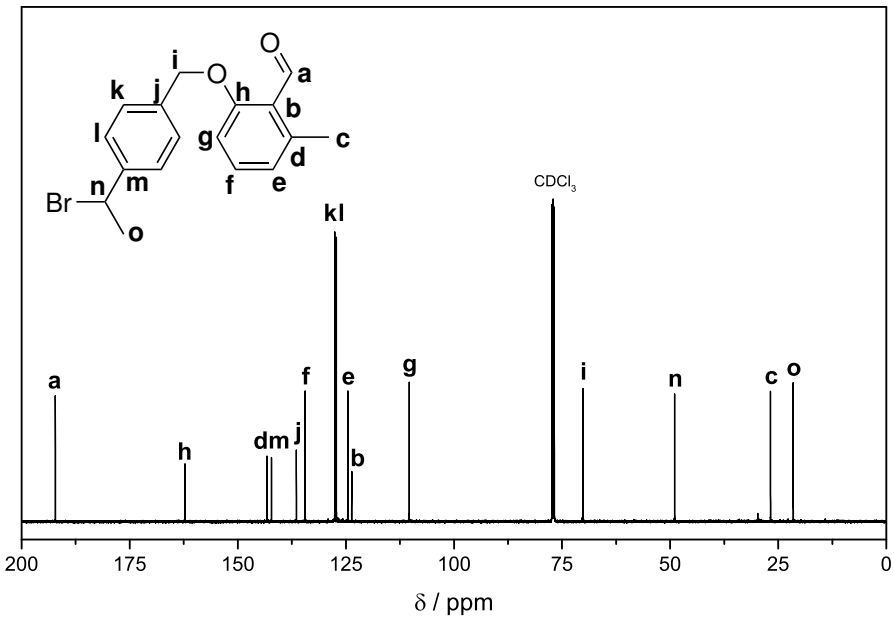

Figure 6.11 ^{13}C NMR spectrum (500 MHz, $CDCl_3$) of the CTA precursor **4**.

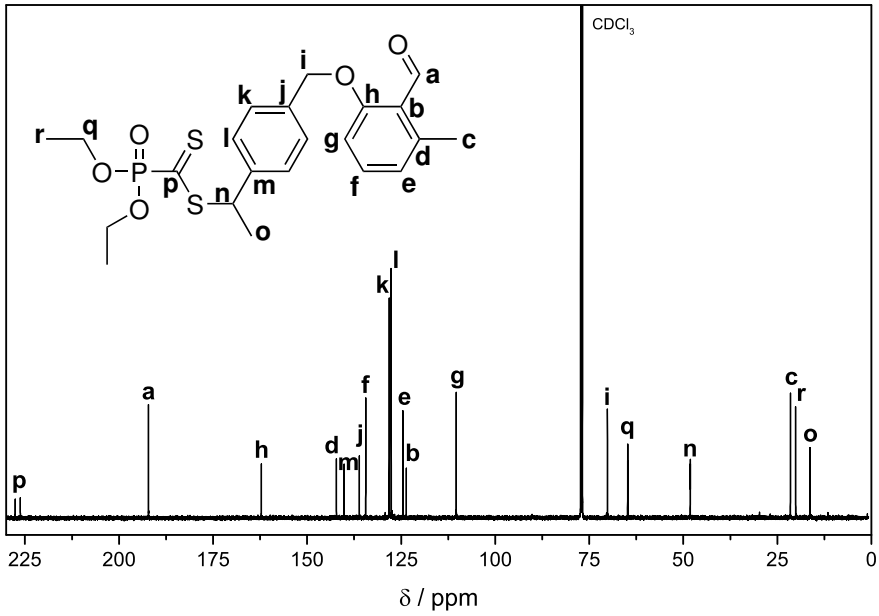

Figure 6.12 ^{13}C NMR spectrum (125 MHz, $CDCl_3$) of the **CTA-3**.

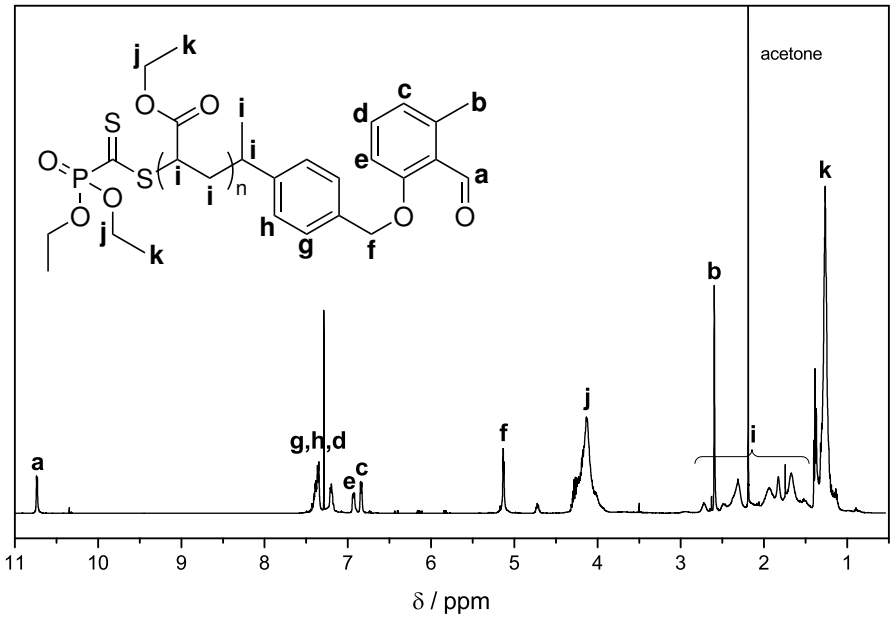

Figure 6.13 ^{1}H NMR spectrum (500 MHz, $CDCl_3$) of the building block **P9**.

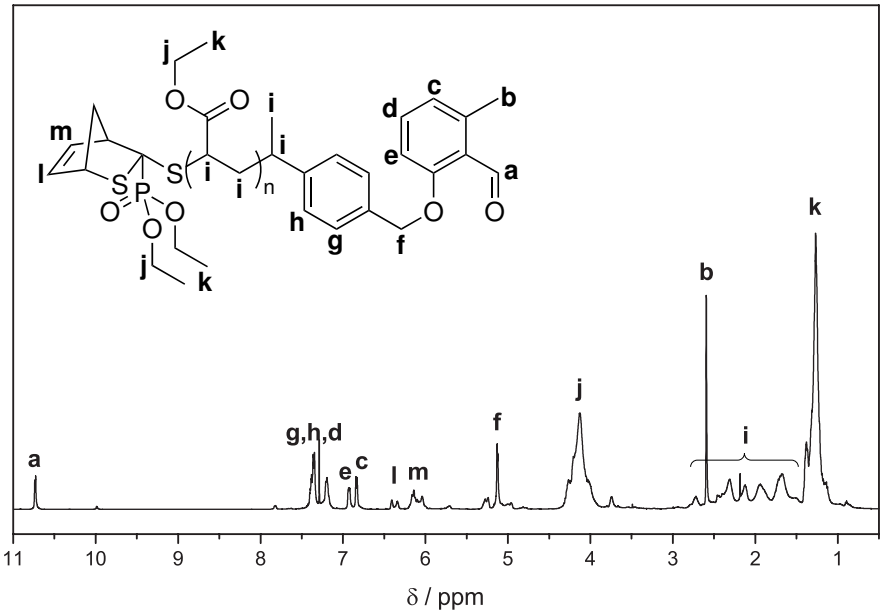

Figure 6.14 ^{1}H NMR spectrum (500 MHz, $CDCl_3$) of the building block **P9**$_a$.

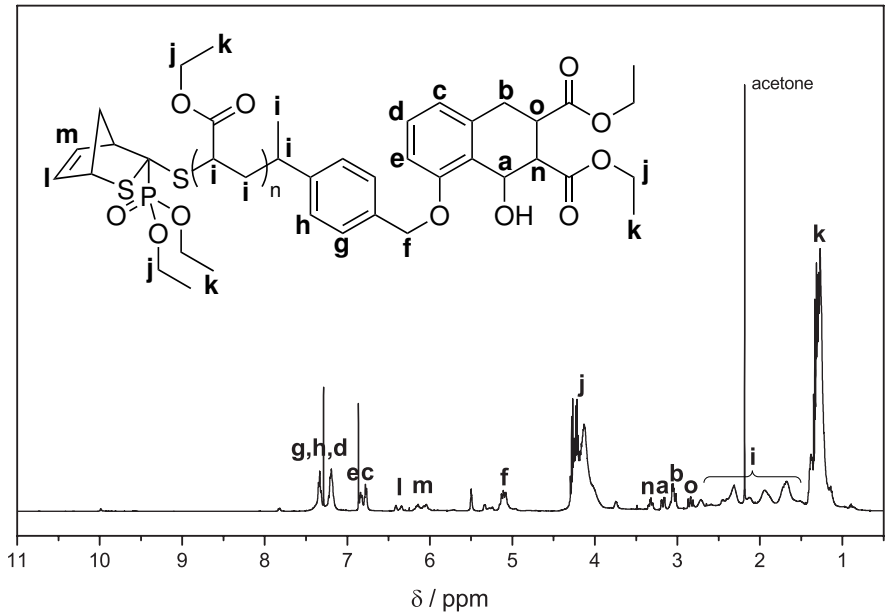

Figure 6.15 ^{1}H NMR spectrum (500 MHz, $CDCl_3$) of the building block **P9**$_b$.

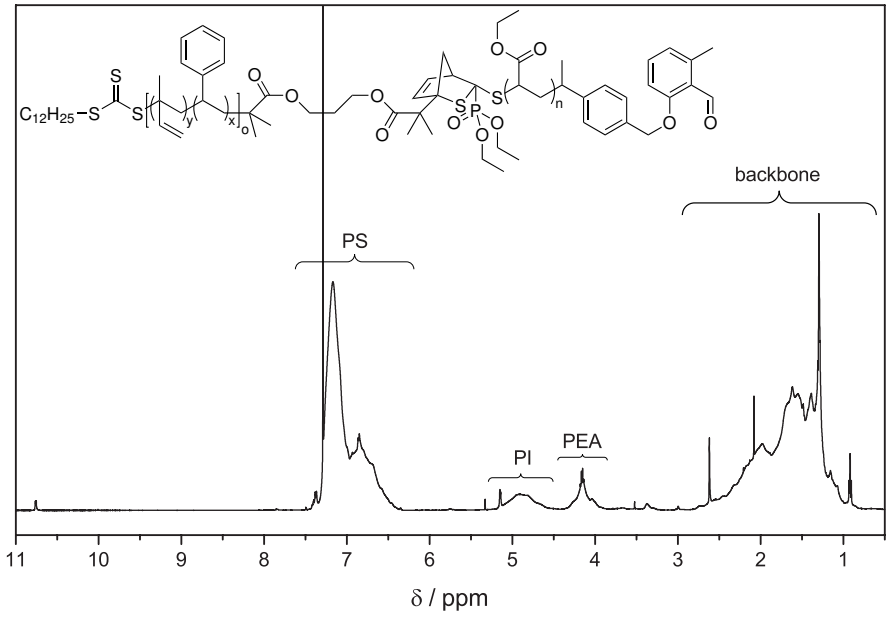

Figure 6.16 ^{1}H NMR spectrum (500 MHz, $CDCl_3$) of the diblock terpolymer **P10**.

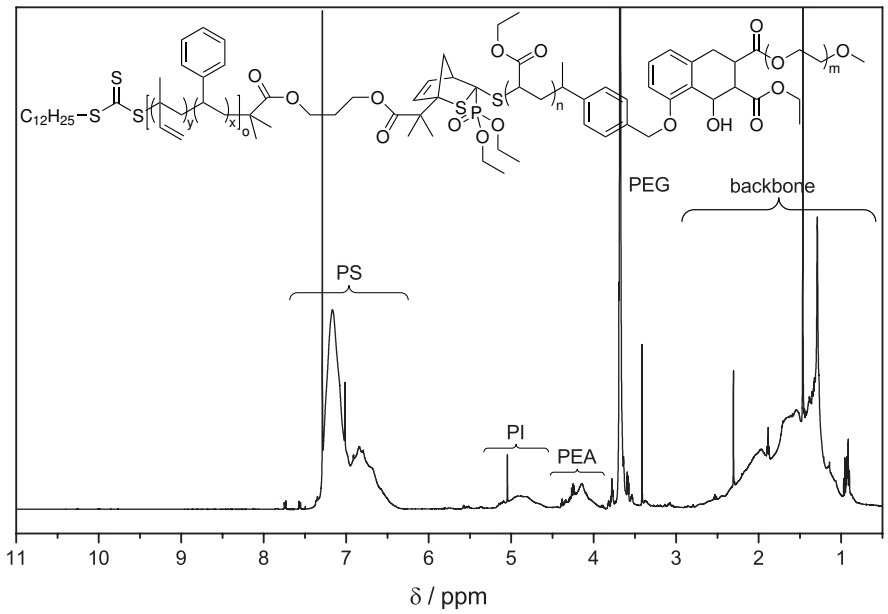

Figure 6.17 ^{1}H NMR spectrum (500 MHz, $CDCl_3$) of the triblock quaterpolymer **P11**.

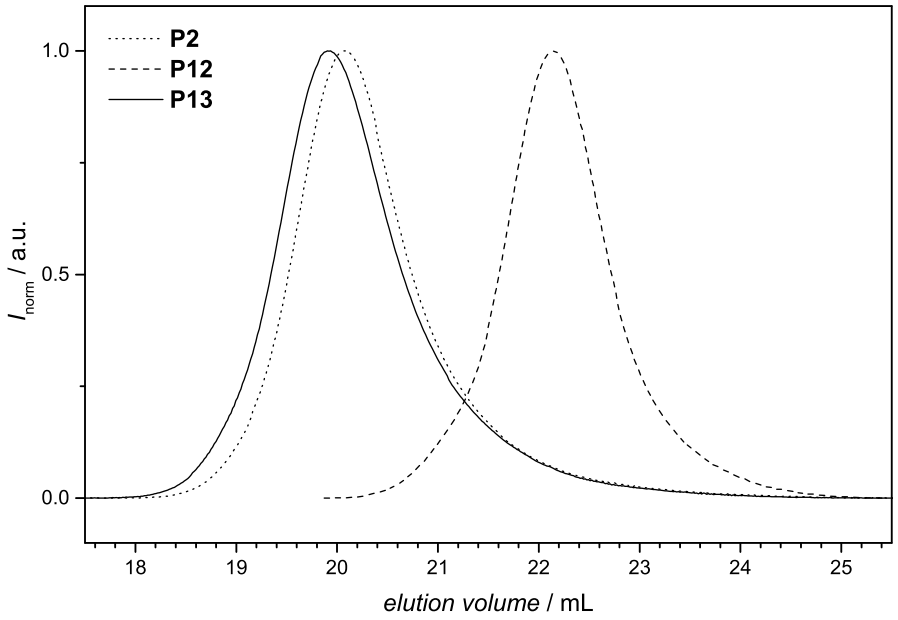

Figure 6.18 SEC traces of the polar building block PTEGA (**P12**, dashed line, M_n = 18 000 g mol^{-1} (PS calibration), $Đ$ = 1.16), the unpolar building block P(I-*co*-S) (**P2**, dotted line, M_n = 50 000 g mol^{-1} (PS calibration), $Đ$ = 1.36) and the resulting block terpolymer P(I-*co*-S)-*b*-PTEGA (**P13**, solid line, M_n = 60 000 g mol^{-1} (PS calibration), $Đ$ = 1.33).

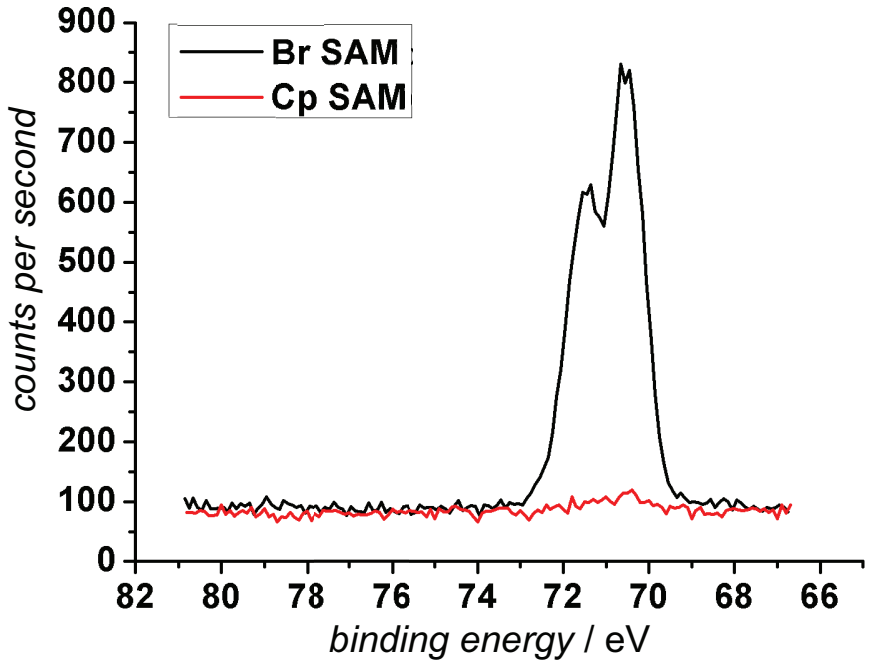

Figure 6.19 High resolution XPS scan of Br3d for the Br (black line) and Cp (red line) functional surface.

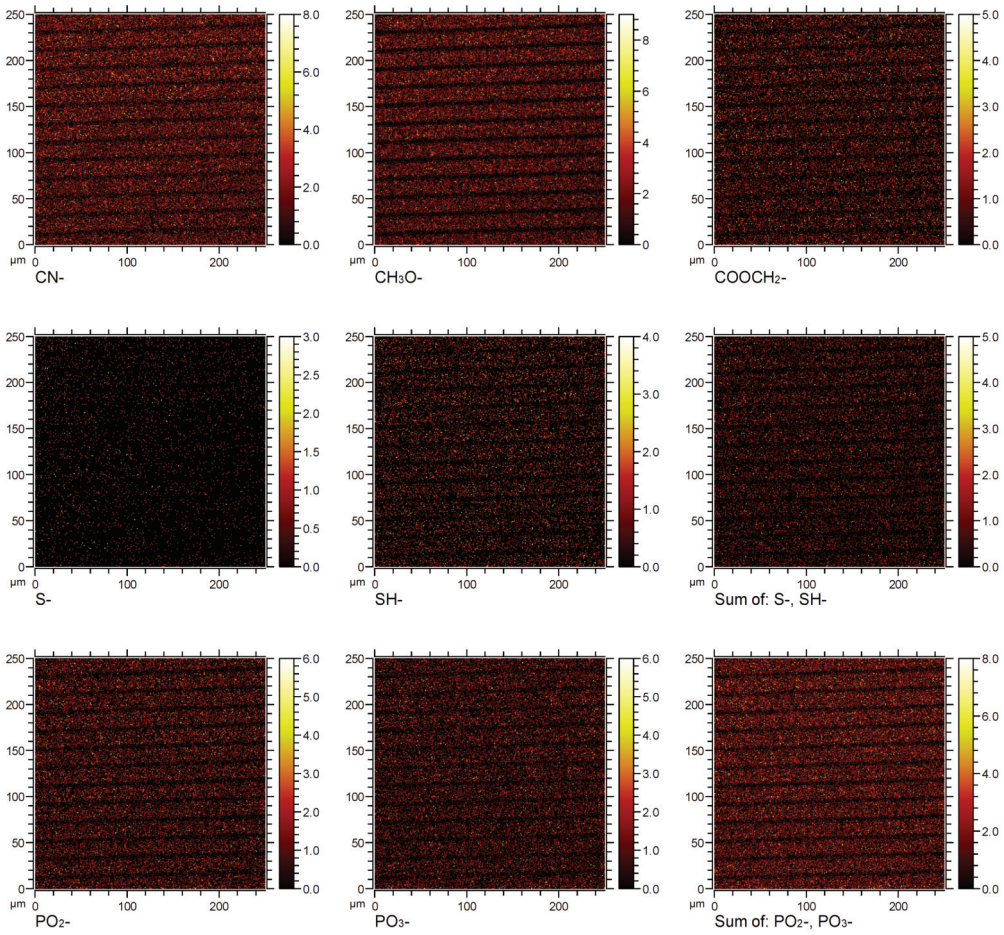

Figure 6.20 Characteristic fragments of **P3** (PTEGA) detected in the negative ion mode (stamp pattern: 5 µm contact area spaced by 15 µm).

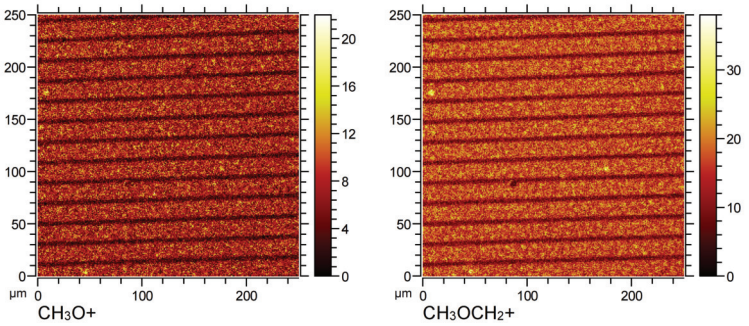

Figure 6.21 Characteristic fragments of **P3** (PTEGA) detected in the positive ion mode (stamp pattern: 5 µm contact area spaced by 15 µm).

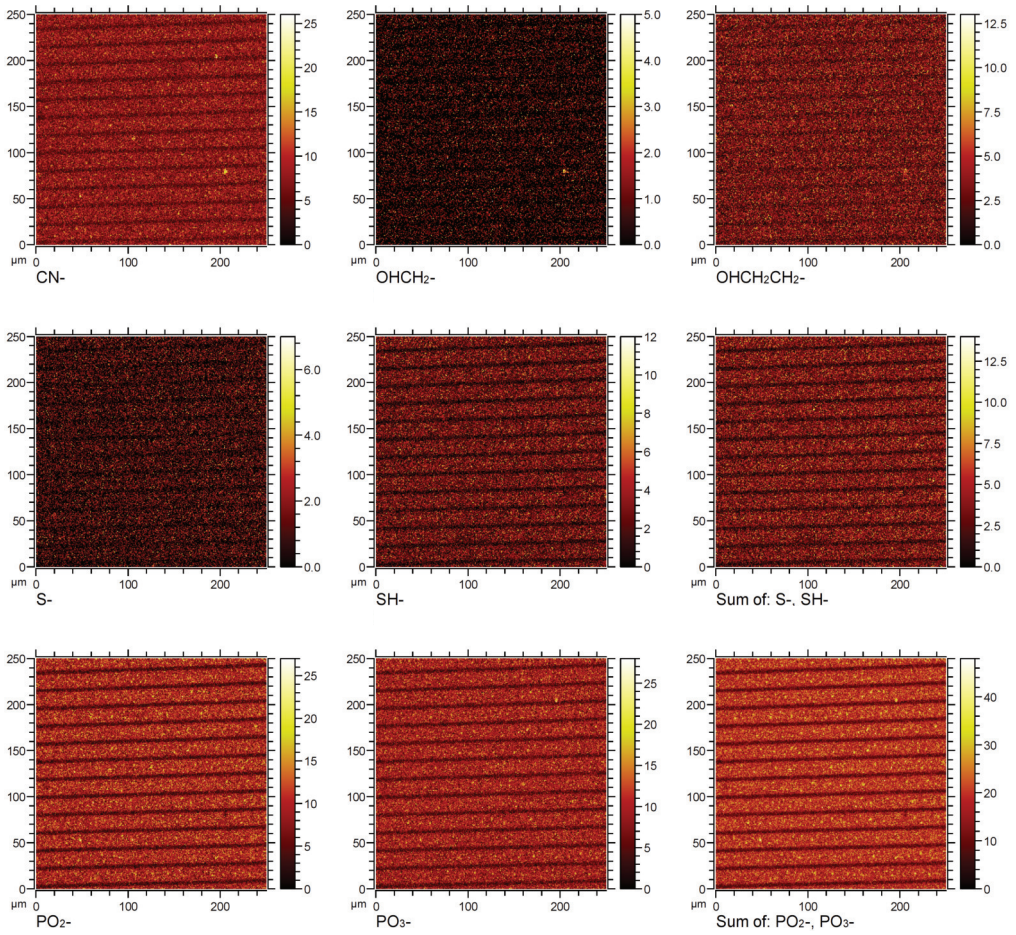

Figure 6.22 Characteristic fragments of **P5** (PHEA) detected in the negative ion mode (stamp pattern: 5 µm contact area spaced by 15 µm).

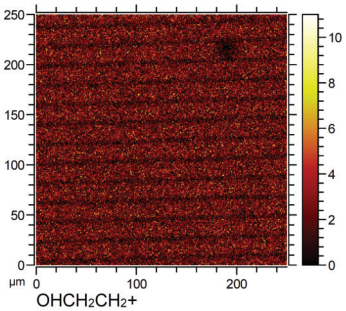

Figure 6.23 Characteristic fragments of **P5** (PHEA) detected in the positive ion mode (stamp pattern: 5 µm contact area spaced by 15 µm).

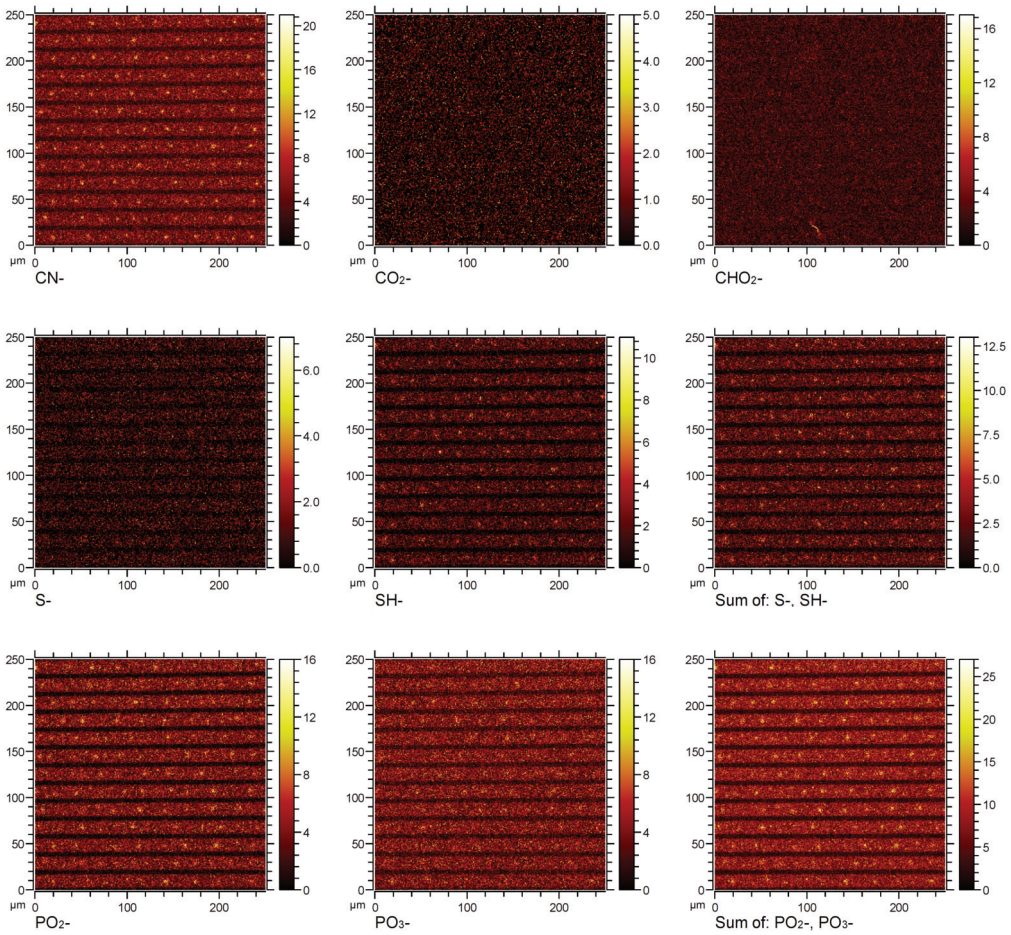

Figure 6.24 Characteristic fragments of **P6** (PAA) detected in the negative ion mode (stamp pattern: 5 µm contact area spaced by 15 µm).

Bibliography

[1] E. M. V. Hoek, V. V. Tarabara, *Encyclopedia of Membrane Science and Technology*, Wiley, **2013**.

[2] M. M. Pendergast, E. M. Hoek, *Energy & Environmental Science* **2011**, *4*, 1946–1971.

[3] E. K. Yanful et al., *Appropriate technologies for environmental protection in the developing world*, Springer, **2009**, pp. 151–168.

[4] M. Elimelech, W. A. Phillip, *Science* **2011**, *333*, 712–717.

[5] M. A. Shannon, P. W. Bohn, M. Elimelech, J. G. Georgiadis, B. J. Mariñas, A. M. Mayes, *Nature* **2008**, *452*, 301–310.

[6] Y. Zhang, J. L. Sargent, B. W. Boudouris, W. A. Phillip, *J. Appl. Polym. Sci.* **2015**, *132*.

[7] D. M. Dotzauer, J. Dai, L. Sun, M. L. Bruening, *Nano Lett.* **2006**, *6*, 2268–2272.

[8] A. Asatekin, S. Kang, M. Elimelech, A. M. Mayes, *J. Membr. Sci.* **2007**, *298*, 136–146.

[9] I. Banerjee, R. C. Pangule, R. S. Kane, *Adv. Mater.* **2011**, *23*, 690–718.

[10] J. B. Schlenoff, *Langmuir* **2014**, *30*, 9625–9636.

[11] D. Rana, T. Matsuura, *Chem. Rev.* **2010**, *110*, 2448–2471.

[12] S. Jiang, Z. Cao, *Adv. Mater.* **2010**, *22*, 920–932.

[13] S. Krishnan, C. J. Weinman, C. K. Ober, *J. Mater. Chem.* **2008**, *18*, 3405–3413.

[14] E. Ostuni, R. G. Chapman, R. E. Holmlin, S. Takayama, G. M. Whitesides, *Langmuir* **2001**, *17*, 5605–5620.

[15] M. Gu, A. J. Vegas, D. G. Anderson, R. S. Langer, J. E. Kilduff, G. Belfort, *Biomaterials* **2013**, *34*, 6133–6138.

[16] M. Gu, J. E. Kilduff, G. Belfort, *Biomaterials* **2012**, *33*, 1261–1270.

[17] M. Zhou, H. Liu, A. Venkiteshwaran, J. Kilduff, D. G. Anderson, R. Langer, G. Belfort, *J. Mater. Chem.* **2011**, *21*, 693–704.

[18] A. J. Inglis, M. H. Stenzel, C. Barner-Kowollik, *Macromol. Rapid Commun.* **2009**, *30*, 1792–1798.

[19] M. Glassner, G. Delaittre, M. Kaupp, J. P. Blinco, C. Barner-Kowollik, *J. Am. Chem. Soc.* **2012**, *134*, 7274–7277.

[20] J. P. Blinco, V. Trouillet, M. Bruns, P. Gerstel, H. Gliemann, C. Barner-Kowollik, *Adv. Mater.* **2011**, *23*, 4435–4439.

[21] K. Hong, D. Uhrig, J. W. Mays, *Curr. Opin. Solid State Mater. Sci.* **1999**, *4*, 531–538.

[22] N. Hadjichristidis, H. Iatrou, S. Pispas, M. Pitsikalis, *J. Polym. Sci. Part A: Polym. Chem.* **2000**, *38*, 3211–3234.

[23] W. A. Braunecker, K. Matyjaszewski, *Prog. Polym. Sci.* **2007**, *32*, 93–146.

[24] D. H. Solomon, E. Rizzardo, P. Cacioli, *European Patent*, EP 135280, **1985**.

[25] M. K. Georges, R. P. Veregin, P. M. Kazmaier, G. K. Hamer, *Macromolecules* **1993**, *26*, 2987–2988.

[26] D. Bertin, F. Chauvin, S. Marque, P. Tordo, *Macromolecules* **2002**, *35*, 3790–3791.

[27] D. Benoit, S. Grimaldi, S. Robin, J.-P. Finet, P. Tordo, Y. Gnanou, *J. Am. Chem. Soc.* **2000**, *122*, 5929–5939.

[28] D. Benoit, V. Chaplinski, R. Braslau, C. J. Hawker, *J. Am. Chem. Soc.* **1999**, *121*, 3904–3920.

[29] A. Studer, K. Harms, C. Knoop, C. Müller, T. Schulte, *Macromolecules* **2004**, *37*, 27–34.

[30] A. Studer, T. Schulte, *The Chemical Record* **2005**, *5*, 27–35.

[31] E. Yoshida, *Colloid Polym. Sci.* **2008**, *286*, 1663–1666.

[32] E. Yoshida, *Colloid Polym. Sci.* **2013**, *291*, 2733–2739.

[33] F. Minisci, *Acc. Chem. Res.* **1975**, *8*, 165–171.

[34] J.-S. Wang, K. Matyjaszewski, *J. Am. Chem. Soc.* **1995**, *117*, 5614–5615.

[35] M. Kato, M. Kamigaito, M. Sawamoto, T. Higashimura, *Macromolecules* **1995**, *28*, 1721–1723.

[36] P. Krys, T. G. Ribelli, K. Matyjaszewski, A. Gennaro, *Macromolecules* **2016**, *49*, 2467–2476.

[37] Y. A. Kabachii, S. Y. Kochev, L. M. Bronstein, I. B. Blagodatskikh, P. M. Valetsky, *Polym. Bull.* **2003**, *50*, 271–278.

[38] J. A. Brandts, P. van de Geijn, E. E. van Faassen, J. Boersma, G. van Koten, *J. Organomet. Chem.* **1999**, *584*, 246–253.

[39] Y. Kotani, M. Kamigaito, M. Sawamoto, *Macromolecules* **1999**, *32*, 2420–2424.

[40] K. Matyjaszewski, M. Wei, J. Xia, N. E. McDermott, *Macromolecules* **1997**, *30*, 8161–8164.

[41] W. A. Braunecker, Y. Itami, K. Matyjaszewski, *Macromolecules* **2005**, *38*, 9402–9404.

[42] V. Percec, B. Barboiu, A. Neumann, J. C. Ronda, M. Zhao, *Macromolecules* **1996**, *29*, 3665–3668.

[43] B. Wang, Y. Zhuang, X. Luo, S. Xu, X. Zhou, *Macromolecules* **2003**, *36*, 9684–9686.

[44] C. Granel, P. Dubois, R. Jérôme, P. Teyssié, *Macromolecules* **1996**, *29*, 8576–8582.

[45] P. Lecomte, I. Drapier, P. Dubois, P. Teyssié, R. Jérôme, *Macromolecules* **1997**, *30*, 7631–7633.

[46] A. Kaur, T. G. Ribelli, K. Schröder, K. Matyjaszewski, T. Pintauer, *Inorg. Chem.* **2015**, *54*, 1474–1486.

[47] W. Jakubowski, K. Min, K. Matyjaszewski, *Macromolecules* **2006**, *39*, 39–45.

[48] W. Jakubowski, K. Matyjaszewski, *Angew. Chem.* **2006**, *118*, 4594–4598.

[49] N. Jasinski, A. Lauer, P. J. Stals, S. Behrens, S. Essig, A. Walther, A. S. Goldmann, C. Barner-Kowollik, *ACS Macro Lett.* **2015**, *4*, 298–301.

[50] J. Wootthikanokkhan, M. Peesan, P. Phinyocheep, *Eur. Polym. J.* **2001**, *37*, 2063–2071.

[51] J. Chiefari, Y. Chong, F. Ercole, J. Krstina, J. Jeffery, T. P. Le, R. T. Mayadunne, G. F. Meijs, C. L. Moad, G. Moad, E. Rizzardo, S. H. Thang, *Macromolecules* **1998**, *31*, 5559–5562.

[52] D. Charmot, P. Corpart, D. Michelet, S. Zard, T. Biadatti, *PCT Int. Appl.* WO 9858974 A1, **1998**.

[53]). Y. Chong, J. Krstina, T. P. Le, G. Moad, A. Postma, E. Rizzardo, S. H. Thang, *Macromolecules* **2003**, *36*, 2256–2272.

[54] J. Chiefari, R. T. Mayadunne, C. L. Moad, G. Moad, E. Rizzardo, A. Postma, M. A. Skidmore, S. H. Thang, *Macromolecules* **2003**, *36*, 2273–2283.

[55] G. Moad, J. Chiefari, Y. Chong, J. Krstina, R. T. A. Mayadunne, A. Postma, E. Rizzardo, S. H. Thang, *Polymer International* **2000**, *49*, 993–1001.

[56] S. Perrier, C. Barner-Kowollik, J. F. Quinn, P. Vana, T. P. Davis, *Macromolecules* **2002**, *35*, 8300–8306.

[57] Y. Kwak, A. Goto, T. Fukuda, *Macromolecules* **2004**, *37*, 1219–1225.

[58] M. Buback, P. Vana, *Macromol. Rapid Commun.* **2006**, *27*, 1299–1305.

[59] C. Barner-Kowollik, P. Vana, J. F. Quinn, T. P. Davis, *J. Polym. Sci. Part A: Polym. Chem.* **2002**, *40*, 1058–1063.

[60] Y. Kwak, A. Goto, Y. Tsujii, Y. Murata, K. Komatsu, T. Fukuda, *Macromolecules* **2002**, *35*, 3026–3029.

[61] C. Barner-Kowollik, J. F. Quinn, D. R. Morsley, T. P. Davis, *J. Polym. Sci. Part A: Polym. Chem.* **2001**, *39*, 1353–1365.

[62] M. J. Monteiro, H. de Brouwer, *Macromolecules* **2001**, *34*, 349–352.

[63] P. Geelen, B. Klumperman, *Macromolecules* **2007**, *40*, 3914–3920.

[64] E. Chernikova, V. Golubev, A. Filippov, E. Garina, *Polymer Science Series C* **2015**, *57*, 94–109.

[65] A. Goto, K. Sato, Y. Tsujii, T. Fukuda, G. Moad, E. Rizzardo, S. H. Thang, *Macromolecules* **2001**, *34*, 402–408.

[66] J. B. McLeary, M. P. Tonge, B. Klumperman, *Macromol. Rapid Commun.* **2006**, *27*, 1233–1240.

[67] J. McLeary, F. Calitz, J. McKenzie, M. Tonge, R. Sanderson, B. Klumperman, *Macromolecules* **2004**, *37*, 2383–2394.

[68] M. Drache, G. Schmidt-Naake, M. Buback, P. Vana, *Polymer* **2005**, *46*, 8483–8493.

[69] F. Calitz, J. McLeary, J. McKenzie, M. Tonge, B. Klumperman, R. Sanderson, *Macromolecules* **2003**, *36*, 9687–9690.

[70] F. Calitz, M. Tonge, R. Sanderson, *Macromolecules* **2003**, *36*, 5–8.

[71] M. Buback, P. Hesse, T. Junkers, P. Vana, *Macromol. Rapid Commun.* **2006**, *27*, 182–187.

[72] K. Ranieri, G. Delaittre, C. Barner-Kowollik, T. Junkers, *Macromol. Rapid Commun.* **2014**, *35*, 2023–2028.

[73] E. Chernikova, V. Golubev, A. Filippov, C. Y. Lin, M. L. Coote, *Polym. Chem.* **2010**, *1*, 1437–1440.

[74] W. Meiser, M. Buback, *Macromol. Rapid Commun.* **2011**, *32*, 1490–1494.

[75] W. Meiser, M. Buback, *Macromol. Rapid Commun.* **2012**, *33*, 1273–1279.

[76] C. Li, J. He, Y. Liu, Y. Zhou, Y. Yang, *Aust. J. Chem.* **2012**, *65*, 1077–1089.

[77] D. Konkolewicz, B. S. Hawkett, A. Gray-Weale, S. Perrier, *Macromolecules* **2008**, *41*, 6400–6412.

[78] D. Konkolewicz, B. S. Hawkett, A. Gray-Weale, S. Perrier, *J. Polym. Sci. Part A: Polym. Chem.* **2009**, *47*, 3455–3466.

[79] D. Konkolewicz, M. Siauw, A. Gray-Weale, B. S. Hawkett, S. Perrier, *J. Phys. Chem. B* **2009**, *113*, 7086–7094.

[80] S. S. Ting, T. P. Davis, P. B. Zetterlund, *Macromolecules* **2011**, *44*, 4187–4193.

[81] T. Junkers, G. Delaittre, R. Chapman, F. Günzler, E. Chernikova, C. Barner-Kowollik, *Macromol. Rapid Commun.* **2012**, *33*, 984–990.

[82] C. Barner-Kowollik, T. Junkers, *J. Polym. Sci. Part A: Polym. Chem.* **2011**, *49*, 1293–1297.

[83] M. L. Coote, L. Radom, *J. Am. Chem. Soc.* **2003**, *125*, 1490–1491.

[84] M. L. Coote, *Macromolecules* **2004**, *37*, 5023–5031.

[85] T. Junkers, C. Barner-Kowollik, M. L. Coote, *Macromol. Rapid Commun.* **2011**, *32*, 1891–1898.

[86] B. Klumperman, E. T. van den Dungen, J. Heuts, M. J. Monteiro, *Macromol. Rapid Commun.* **2010**, *31*, 1846–1862.

[87] M. Benaglia, J. Chiefari, Y. K. Chong, G. Moad, E. Rizzardo, S. H. Thang, *J. Am. Chem. Soc.* **2009**, *131*, 6914–6915.

[88] C. Barner-Kowollik, *Handbook of RAFT polymerization*, John Wiley & Sons, **2008**.

[89] D. A. Schlüter, C. Hawker, J. Sakamoto, *Synthesis of Polymers: New Structures and Methods*, John Wiley & Sons, **2012**.

[90] W. Zhang, F. D'Agosto, O. Boyron, J. Rieger, B. Charleux, *Macromolecules* **2011**, *44*, 7584–7593.

[91] H. S. Köllisch, C. Barner-Kowollik, H. Ritter, *Chem. Commun.* **2009**, 1097–1099.

[92] M. Hetzer, B. V. Schmidt, C. Barner-Kowollik, H. Ritter, *J. Polym. Sci. Part A: Polym. Chem.* **2013**, *51*, 2504–2517.

[93] Y. Wang, H. Xu, X. Zhang, *Adv. Mater.* **2009**, *21*, 2849–2864.

[94] F. S. Bates, G. H. Fredrickson, *Annu. Rev. Phys. Chem.* **1990**, *41*, 525–557.

[95] K. Koo, H. Ahn, S.-W. Kim, D. Y. Ryu, T. P. Russell, *Soft Matter* **2013**, *9*, 9059–9071.

[96] N. A. Lynd, A. J. Meuler, M. A. Hillmyer, *Prog. Polym. Sci.* **2008**, *33*, 875–893.

[97] F. H. Schacher, H. Sugimori, S. Hong, H. Jinnai, A. H. Müller, *Macromolecules* **2012**, *45*, 7956–7963.

[98] F. H. Schacher, T. Rudolph, M. Drechsler, A. H. Müller, *Nanoscale* **2011**, *3*, 288–297.

[99] H. Jinnai, T. Kaneko, K. Matsunaga, C. Abetz, V. Abetz, *Soft Matter* **2009**, *5*, 2042–2046.

[100] A. Böker, H. Elbs, H. Hänsel, A. Knoll, S. Ludwigs, H. Zettl, A. Zvelindovsky, G. Sevink, V. Urban, V. Abetz, A. Müller, G. Krausch, *Macromolecules* **2003**, *36*, 8078–8087.

[101] K. Letchford, H. Burt, *Eur. J. Pharm. Biopharm.* **2007**, *65*, 259–269.

[102] P. Alexandridis, J. F. Holzwarth, T. A. Hatton, *Macromolecules* **1994**, *27*, 2414–2425.

[103] A. Martin, *Physical pharmacy: physical chemical principles in the pharmaceutical sciences*, BI Waverly. Pvt Ltd, **1993**.

[104] C. Allen, D. Maysinger, A. Eisenberg, *Colloids Surf. B* **1999**, *16*, 3–27.

[105] R. Gref, Y. Minamitake, M. T. Peracchia, V. Trubetskoy, V. Torchilin, R. Langer, *Science* **1994**, *263*, 1600–1603.

[106] R. Gref, A. Domb, P. Quellec, T. Blunk, R. Müller, J. Verbavatz, R. Langer, *Adv. Drug Delivery Rev.* **2012**, *64*, 316–326.

[107] K. S. Soppimath, T. M. Aminabhavi, A. R. Kulkarni, W. E. Rudzinski, *J. Controlled Release* **2001**, *70*, 1–20.

[108] T. Ameller, V. Marsaud, P. Legrand, R. Gref, G. Barratt, J.-M. Renoir, *Pharm. Res.* **2003**, *20*, 1063–1070.

[109] T. Riley, S. Stolnik, C. Heald, C. Xiong, M. Garnett, L. Illum, S. Davis, S. Purkiss, R. Barlow, P. Gellert, *Langmuir* **2001**, *17*, 3168–3174.

[110] M. Teixeira, M. J. Alonso, M. M. Pinto, C. M. Barbosa, *Eur. J. Pharm. Biopharm.* **2005**, *59*, 491–500.

[111] D. E. Discher, A. Eisenberg, *Science* **2002**, *297*, 967–973.

[112] M. L. Adams, A. Lavasanifar, G. S. Kwon, *J. Pharm. Sci.* **2003**, *92*, 1343–1355.

[113] G. Gaucher, M.-H. Dufresne, V. P. Sant, N. Kang, D. Maysinger, J.-C. Leroux, *J. Controlled Release* **2005**, *109*, 169–188.

[114] F. H. Schacher, P. A. Rupar, I. Manners, *Angew. Chem. Int. Ed.* **2012**, *51*, 7898–7921.

[115] H.-C. Kim, S.-M. Park, W. D. Hinsberg, *Chem. Rev.* **2009**, *110*, 146–177.

[116] C. J. Hawker, T. P. Russell, *MRS Bull.* **2005**, *30*, 952–966.

[117] J. M. Leiston-Belanger, T. P. Russell, E. Drockenmuller, C. J. Hawker, *Macromolecules* **2005**, *38*, 7676–7683.

[118] P. Mansky, C. Harrison, P. Chaikin, R. Register, N. Yao, *Appl. Phys. Lett.* **1996**, *68*, 2586–2588.

[119] J. Bang, S. H. Kim, E. Drockenmuller, M. J. Misner, T. P. Russell, C. J. Hawker, *J. Am. Chem. Soc.* **2006**, *128*, 7622–7629.

[120] H.-Y. Hsueh, H.-Y. Chen, M.-S. She, C.-K. Chen, R.-M. Ho, S. Gwo, H. Hasegawa, E. L. Thomas, *Nano Lett.* **2010**, *10*, 4994–5000.

[121] M. Zhang, L. Yang, S. Yurt, M. J. Misner, J.-T. Chen, E. B. Coughlin, D. Venkataraman, T. P. Russell, *Adv. Mater.* **2007**, *19*, 1571–1576.

[122] H. Zhao, W. Gu, E. Sterner, T. P. Russell, E. B. Coughlin, P. Theato, *Macromolecules* **2011**, *44*, 6433–6440.

[123] R. A. Mulvenna, J. L. Weidman, B. Jing, J. A. Pople, Y. Zhu, B. W. Boudouris, W. A. Phillip, *J. Membr. Sci.* **2014**, *470*, 246–256.

[124] S. P. Nunes, A. R. Behzad, K.-V. Peinemann, *J. Mater. Res.* **2013**, *28*, 2661–2665.

[125] K.-V. Peinemann, V. Abetz, P. F. Simon, *Nat. Mater.* **2007**, *6*, 992–996.

[126] D. S. Marques, R. M. Dorin, U. Wiesner, D.-M. Smilgies, A. R. Behzad, U. Vainio, K.-V. Peinemann, S. P. Nunes, *Polymer* **2014**, *55*, 1327–1332.

[127] W. A. Phillip, R. Mika Dorin, J. Werner, E. M. Hoek, U. Wiesner, M. Elimelech, *Nano Lett.* **2011**, *11*, 2892–2900.

[128] A. Jung, V. Filiz, S. Rangou, K. Buhr, P. Merten, J. Hahn, J. Clodt, C. Abetz, V. Abetz, *Macromol. Rapid Commun.* **2013**, *34*, 610–615.

[129] J. Hahn, V. Filiz, S. Rangou, J. Clodt, A. Jung, K. Buhr, C. Abetz, V. Abetz, *J. Polym. Sci. Part B: Polym. Phys.* **2013**, *51*, 281–290.

[130] A. Jung, S. Rangou, C. Abetz, V. Filiz, V. Abetz, *Macromol. Mater. Eng.* **2012**, *297*, 790–798.

[131] C. Hörenz, C. Pietsch, A. S. Goldmann, C. Barner-Kowollik, F. H. Schacher, *Adv. Mater. Interfaces* **2015**, *2*.

[132] J. Hahn, V. Filiz, S. Rangou, B. Lademann, K. Buhr, J. I. Clodt, A. Jung, C. Abetz, V. Abetz, *Macromol. Mater. Eng.* **2013**, *298*, 1315–1321.

[133] S. P. Nunes, R. Sougrat, B. Hooghan, D. H. Anjum, A. R. Behzad, L. Zhao, N. Pradeep, I. Pinnau, U. Vainio, K.-V. Peinemann, *Macromolecules* **2010**, *43*, 8079–8085.

[134] H. C. Kolb, M. Finn, K. B. Sharpless, *Angew. Chem. Int. Ed.* **2001**, *40*, 2004–2021.

[135] C. J. Hawker, V. V. Fokin, M. Finn, K. B. Sharpless, *Aust. J. Chem.* **2007**, *60*, 381–383.

[136] C. Barner-Kowollik, A. J. Inglis, *Macromol. Chem. Phys.* **2009**, *210*, 987–992.

[137] C. Barner-Kowollik, F. E. Du Prez, P. Espeel, C. J. Hawker, T. Junkers, H. Schlaad, W. Van Camp, *Angew. Chem. Int. Ed.* **2011**, *50*, 60–62.

[138] M. Meldal, C. W. Tornøe, *Chem. Rev.* **2008**, *108*, 2952–3015.

[139] R. Huisgen, G. Szeimies, L. Möbius, *Chem. Ber.* **1967**, *100*, 2494–2507.

[140] V. V. Rostovtsev, L. G. Green, V. V. Fokin, K. B. Sharpless, *Angew. Chem.* **2002**, *114*, 2708–2711.

[141] H. C. Kolb, K. B. Sharpless, *Drug Discovery Today* **2003**, *8*, 1128–1137.

[142] G. von Maltzahn, Y. Ren, J.-H. Park, D.-H. Min, V. R. Kotamraju, J. Jayakumar, V. Fogal, M. J. Sailor, E. Ruoslahti, S. N. Bhatia, *Bioconjugate Chem.* **2008**, *19*, 1570–1578.

[143] X.-L. Sun, C. L. Stabler, C. S. Cazalis, E. L. Chaikof, *Bioconjugate Chem.* **2006**, *17*, 52–57.

[144] S. K. Mamidyala, M. Finn, *Chem. Soc. Rev.* **2010**, *39*, 1252–1261.

[145] H. Nandivada, X. Jiang, J. Lahann, *Adv. Mater.* **2007**, *19*, 2197–2208.

[146] R. K. Iha, K. L. Wooley, A. M. Nystrom, D. J. Burke, M. J. Kade, C. J. Hawker, *Chem. Rev.* **2009**, *109*, 5620–5686.

[147] G. J. Brewer, *Chem. Res. Toxicol.* **2009**, *23*, 319–326.

[148] L. M. Gaetke, C. K. Chow, *Toxicology* **2003**, *189*, 147–163.

[149] A. Bernardin, A. Cazet, L. Guyon, P. Delannoy, F. Vinet, D. Bonnaffé, I. Texier, *Bioconjugate Chem.* **2010**, *21*, 583–588.

[150] N. J. Agard, J. A. Prescher, C. R. Bertozzi, *J. Am. Chem. Soc.* **2004**, *126*, 15046–15047.

[151] J. M. Baskin, J. A. Prescher, S. T. Laughlin, N. J. Agard, P. V. Chang, I. A. Miller, A. Lo, J. A. Codelli, C. R. Bertozzi, *Proceedings of the National Academy of Sciences* **2007**, *104*, 16793–16797.

[152] N. J. Agard, J. M. Baskin, J. A. Prescher, A. Lo, C. R. Bertozzi, *ACS Chem. Biol.* **2006**, *1*, 644–648.

[153] X. Ning, J. Guo, M. A. Wolfert, G.-J. Boons, *Angew. Chem. Int. Ed.* **2008**, *47*, 2253–2255.

[154] M. F. Debets, S. S. van Berkel, S. Schoffelen, F. P. Rutjes, J. C. van Hest, F. L. van Delft, *Chem. Commun.* **2010**, *46*, 97–99.

[155] A. Kuzmin, A. Poloukhtine, M. A. Wolfert, V. V. Popik, *Bioconjugate Chem.* **2010**, *21*, 2076–2085.

[156] C. E. Hoyle, C. N. Bowman, *Angew. Chem. Int. Ed.* **2010**, *49*, 1540–1573.

[157] C. E. Hoyle, T. Y. Lee, T. Roper, *J. Polym. Sci. Part A: Polym. Chem.* **2004**, *42*, 5301–5338.

[158] A. B. Lowe, *Polym. Chem.* **2010**, *1*, 17–36.

[159] P. J. Roth, C. Boyer, A. B. Lowe, T. P. Davis, *Macromol. Rapid Commun.* **2011**, *32*, 1123–1143.

[160] S. P. Koo, M. M. Stamenović, R. A. Prasath, A. J. Inglis, F. E. Du Prez, C. Barner-Kowollik, W. Van Camp, T. Junkers, *J. Polym. Sci. Part A: Polym. Chem.* **2010**, *48*, 1699–1713.

[161] D. Konkolewicz, A. Gray-Weale, S. Perrier, *J. Am. Chem. Soc.* **2009**, *131*, 18075–18077.

[162] B. M. Rosen, G. Lligadas, C. Hahn, V. Percec, *J. Polym. Sci. Part A: Polym. Chem.* **2009**, *47*, 3931–3939.

[163] H. Li, B. Yu, H. Matsushima, C. E. Hoyle, A. B. Lowe, *Macromolecules* **2009**, *42*, 6537–6542.

[164] C. R. Becer, K. Babiuch, D. Pilz, S. Hornig, T. Heinze, M. Gottschaldt, U. S. Schubert, *Macromolecules* **2009**, *42*, 2387–2394.

[165] J. S. Clovis, A. Eckell, R. Huisgen, R. Sustmann, *Chem. Ber.* **1967**, *100*, 60–70.

[166] P. Lederhose, K. N. Wüst, C. Barner-Kowollik, J. P. Blinco, *Chem. Commun.* **2016**, *52*, 5928–5931.

[167] R. K. Lim, Q. Lin, *Acc. Chem. Res.* **2011**, *44*, 828–839.

[168] D. C. Sherrington, K. A. Taskinen, *Chem. Soc. Rev.* **2001**, *30*, 83–93.

[169] G. Armstrong, M. Buggy, *J. Mater. Sci.* **2005**, *40*, 547–559.

[170] C. Burd, M. Weck, *Macromolecules* **2005**, *38*, 7225–7230.

[171] K. Pahnke, O. Altintas, F. G. Schmidt, C. Barner-Kowollik, *ACS Macro Lett.* **2015**, *4*, 774–777.

[172] R. Dobrawa, F. Würthner, *J. Polym. Sci. Part A: Polym. Chem.* **2005**, *43*, 4981–4995.

[173] C.-A. Fustin, P. Guillet, U. S. Schubert, J.-F. Gohy, *Adv. Mater.* **2007**, *19*, 1665–1673.

[174] R. Hoogenboom, U. S. Schubert, *Chem. Soc. Rev.* **2006**, *35*, 622–629.

[175] I. Dance, *New J. Chem.* **2003**, *27*, 1–2.

[176] B. G. Lohmeijer, U. S. Schubert, *Angew. Chem. Int. Ed.* **2002**, *41*, 3825–3829.

[177] B. V. Schmidt, M. Hetzer, H. Ritter, C. Barner-Kowollik, *Prog. Polym. Sci.* **2014**, *39*, 235–249.

[178] G. Chen, M. Jiang, *Chem. Soc. Rev.* **2011**, *40*, 2254–2266.

[179] J. Zhou, H. Ritter, *Polym. Chem.* **2010**, *1*, 1552–1559.

[180] M. Nakahata, Y. Takashima, H. Yamaguchi, A. Harada, *Nat. Commun.* **2011**, *2*, 511.

[181] Y. Chen, Y. Liu, *Chem. Soc. Rev.* **2010**, *39*, 495–505.

[182] B. V. Schmidt, M. Hetzer, H. Ritter, C. Barner-Kowollik, *Macromolecules* **2013**, *46*, 1054–1065.

[183] Q. Yan, Y. Xin, R. Zhou, Y. Yin, J. Yuan, *Chem. Commun.* **2011**, *47*, 9594–9596.

[184] O. Diels, K. Alder, *Justus Liebigs Ann. Chem.* **1928**, *460*, 98–122.

[185] R. Brückner, *Reaktionsmechanismen: organische Reaktionen, Stereochemie, moderne Synthesemethoden*, Springer-Verlag, **2014**.

[186] I. Fleming, *Pericyclic reactions*, Oxford University Press, USA, **2015**.

[187] F. Fringuelli, A. Taticchi, *The Diels-Alder reaction: selected practical methods*, John Wiley & Sons, **2002**.

[188] K. C. Nicolaou, S. A. Snyder, T. Montagnon, G. Vassilikogiannakis, *Angew. Chem. Int. Ed.* **2002**, *41*, 1668–1698.

[189] L. F. Tietze, G. Kettschau in *Stereoselective Heterocyclic Synthesis I*, Springer, **1997**, pp. 1–120.

[190] K. P. C. Vollhardt, N. E. Schore, *Organische chemie*, John Wiley & Sons, **2011**.

[191] R. Hoffmann, R. Woodward, *J. Am. Chem. Soc.* **1965**, *87*, 2046–2048.

[192] I. Flemig, *Molecular Orbitals and Organic Chemical Reactions*, John Wiley & Sons Ltd: London, UK, **2009**.

[193] R. Hoffmann, R. Woodward, *J. Am. Chem. Soc.* **1965**, *87*, 4388–4389.

[194] J. I. García, J. A. Mayoral, L. Salvatella, *Acc. Chem. Res.* **2000**, *33*, 658–664.

[195] V. Eschenbrenner-Lux, K. Kumar, H. Waldmann, *Angew. Chem. Int. Ed.* **2014**, *53*, 11146–11157.

[196] M. A. Tasdelen, *Polym. Chem.* **2011**, *2*, 2133–2145.

[197] M. L. Szalai, D. V. McGrath, D. R. Wheeler, T. Zifer, J. R. McElhanon, *Macromolecules* **2007**, *40*, 818–823.

[198] X. Chen, M. A. Dam, K. Ono, A. Mal, H. Shen, S. R. Nutt, K. Sheran, F. Wudl, *Science* **2002**, *295*, 1698–1702.

[199] A. Gandini, *Prog. Polym. Sci.* **2013**, *38*, 1–29.

[200] S. Sinnwell, A. J. Inglis, T. P. Davis, M. H. Stenzel, C. Barner-Kowollik, *Chem. Commun.* **2008**, 2052–2054.

[201] A. J. Inglis, S. Sinnwell, M. H. Stenzel, C. Barner-Kowollik, *Angew. Chem. Int. Ed.* **2009**, *48*, 2411–2414.

[202] R. Breslow, *Acc. Chem. Res.* **1991**, *24*, 159–164.

[203] A. J. Inglis, S. Sinnwell, T. P. Davis, C. Barner-Kowollik, M. H. Stenzel, *Macromolecules* **2008**, *41*, 4120–4126.

[204] S. Sinnwell, M. Lammens, M. H. Stenzel, F. E. Du Prez, C. Barner-Kowollik, *J. Polym. Sci. Part A: Polym. Chem.* **2009**, *47*, 2207–2213.

[205] A. Bousquet, C. Barner-Kowollik, M. H. Stenzel, *J. Polym. Sci. Part A: Polym. Chem.* **2010**, *48*, 1773–1781.

[206] M. Kaupp, A. P. Vogt, J. C. Natterodt, V. Trouillet, T. Gruendling, T. Hofe, L. Barner, C. Barner-Kowollik, *Polym. Chem.* **2012**, *3*, 2605–2614.

[207] A. S. Goldmann, T. Tischer, L. Barner, M. Bruns, C. Barner-Kowollik, *Biomacromolecules* **2011**, *12*, 1137–1145.

[208] S. Sinnwell, C. V. Synatschke, T. Junkers, M. H. Stenzel, C. Barner-Kowollik, *Macromolecules* **2008**, *41*, 7904–7912.

[209] T. Paulöhrl, A. J. Inglis, C. Barner-Kowollik, *Adv. Mater.* **2010**, *22*, 2788–2791.

[210] N. K. Guimard, J. Ho, J. Brandt, C. Y. Lin, M. Namazian, J. O. Mueller, K. K. Oehlenschlaeger, S. Hilf, A. Lederer, F. G. Schmidt, M. L. Coote, C. Barner-Kowollik, *Chem. Sci.* **2013**, *4*, 2752–2759.

[211] K. Pahnke, J. Brandt, G. Gryn'ova, P. Lindner, R. Schweins, F. G. Schmidt, A. Lederer, M. L. Coote, C. Barner-Kowollik, *Chem. Sci.* **2015**, *6*, 1061–1074.

[212] K. Pahnke, J. Brandt, G. Gryn'ova, C. Y. Lin, O. Altintas, F. G. Schmidt, A. Lederer, M. L. Coote, C. Barner-Kowollik, *Angew. Chem. Int. Ed.* **2016**, *55*, 1514–1518.

[213] A. J. Inglis, L. Nebhani, O. Altintas, F. G. Schmidt, C. Barner-Kowollik, *Macromolecules* **2010**, *43*, 5515–5520.

[214] M. Glassner, K. K. Oehlenschlaeger, A. Welle, M. Bruns, C. Barner-Kowollik, *Chem. Commun.* **2013**, *49*, 633–635.

[215] T. Tischer, T. K. Claus, K. K. Oehlenschlaeger, V. Trouillet, M. Bruns, A. Welle, K. Linkert, A. S. Goldmann, H. G. Börner, C. Barner-Kowollik, *Macromol. Rapid Commun.* **2014**, *35*, 1121–1127.

[216] T. Pauloehrl, A. Welle, K. K. Oehlenschlaeger, C. Barner-Kowollik, *Chem. Sci.* **2013**, *4*, 3503–3507.

[217] S. Mellows, P. Sammes, *J. Chem. Soc. D* **1971**, 21–22.

[218] T. Gruendling, K. K. Oehlenschlaeger, E. Frick, M. Glassner, C. Schmid, C. Barner-Kowollik, *Macromol. Rapid Commun.* **2011**, *32*, 807–812.

[219] M. Glassner, K. K. Oehlenschlaeger, T. Gruendling, C. Barner-Kowollik, *Macromolecules* **2011**, *44*, 4681–4689.

[220] M. Winkler, J. O. Mueller, K. K. Oehlenschlaeger, L. Montero de Espinosa, M. A. Meier, C. Barner-Kowollik, *Macromolecules* **2012**, *45*, 5012–5019.

[221] O. Altintas, J. Willenbacher, K. N. Wuest, K. K. Oehlenschlaeger, P. Krolla-Sidenstein, H. Gliemann, C. Barner-Kowollik, *Macromolecules* **2013**, *46*, 8092–8101.

[222] T. Josse, O. Altintas, K. K. Oehlenschlaeger, P. Dubois, P. Gerbaux, O. Coulembier, C. Barner-Kowollik, *Chem. Commun.* **2014**, *50*, 2024–2026.

[223] T. Josse, J. De Winter, O. Altintas, P. Dubois, C. Barner-Kowollik, P. Gerbaux, O. Coulembier, *Macromol. Chem. Phys.* **2015**, *216*, 1227–1234.

[224] T. Pauloehrl, G. Delaittre, V. Winkler, A. Welle, M. Bruns, H. G. Börner, A. M. Greiner, M. Bastmeyer, C. Barner-Kowollik, *Angew. Chem. Int. Ed.* **2012**, *51*, 1071–1074.

[225] C. M. Preuss, T. Tischer, C. Rodriguez-Emmenegger, M. M. Zieger, M. Bruns, A. S. Goldmann, C. Barner-Kowollik, *J. Mater. Chem. B* **2014**, *2*, 36–40.

[226] T. Tischer, T. K. Claus, M. Bruns, V. Trouillet, K. Linkert, C. Rodriguez-Emmenegger, A. S. Goldmann, S. Perrier, H. G. Börner, C. Barner-Kowollik, *Biomacromolecules* **2013**, *14*, 4340–4350.

[227] D. S. Germack, K. L. Wooley, *J. Polym. Sci. Part A: Polym. Chem.* **2007**, *45*, 4100–4108.

[228] X. Yin, A. S. Hoffman, P. S. Stayton, *Biomacromolecules* **2006**, *7*, 1381–1385.

[229] C. W. Scales, A. J. Convertine, C. L. McCormick, *Biomacromolecules* **2006**, *7*, 1389–1392.

[230] S. R. Gondi, A. P. Vogt, B. S. Sumerlin, *Macromolecules* **2007**, *40*, 474–481.

[231] E. A. Grulke, E. Immergut, J. Brandrup, *Polymer handbook*, John Wiley & Sons, **1999**.

[232] M. D. Rausch, W. P. Hart, D. U. Macomber, *J. Macromol.Sci. Chem.* **1981**, *16*, 243–250.

[233] M. T. Blankenbuehler, J. P. Selegue, *J. Organomet. Chem.* **2002**, *642*, 268–274.

[234] A. J. Inglis, T. Pauloehrl, C. Barner-Kowollik, *Macromolecules* **2009**, *43*, 33–36.

[235] D. J. am Ende, D. C. Whritenour, J. W. Coe, *Organic Process Research & Development* **2007**, *11*, 1141–1146.

[236] I. Lacík, M. Stach, P. Kasák, V. Semak, L. Uhelská, A. Chovancová, G. Reinhold, P. Kilz, G. Delaittre, B. Charleux, I. Chaduc, F. D'Agosto, M. Lansalot, M. Gaborieau, P. Castignolles, R. G. Gilbert, Z. Szablan, C. Barner-Kowollik, P. Hesse, M. Buback, *Macromol. Chem. Phys.* **2015**, *216*, 23–37.

[237] R. Gilbert, M. Hess, A. Jenkins, R. Jones, P. Kratochvil, R. Stepto, *Pure Appl. Chem.* **2009**, *81*, 351–353.

[238] C. Barner-Kowollik, *Macromol. Rapid Commun.* **2009**, *30*, 1625–1631.

[239] C. M. Preuss, C. Barner-Kowollik, *Macromol. Theory Simul.* **2011**, *20*, 700–708.

[240] J. Brandt, K. K. Oehlenschlaeger, F. G. Schmidt, C. Barner-Kowollik, A. Lederer, *Adv. Mater.* **2014**, *26*, 5758–5785.

[241] A. F. Hirschbiel, B. V. Schmidt, P. Krolla-Sidenstein, J. P. Blinco, C. Barner-Kowollik, *Macromolecules* **2015**, *48*, 4410–4420.

[242] P. J. Kropp, K. A. Daus, S. D. Crawford, M. W. Tubergen, K. D. Kepler, S. L. Craig, V. P. Wilson, *J. Am. Chem. Soc.* **1990**, *112*, 7433–7434.

[243] E. Kim, Y. Xia, G. M. Whitesides, *J. Am. Chem. Soc.* **1996**, *118*, 5722–5731.

[244] W. J. Brittain, S. Minko, *J. Polym. Sci. Part A: Polym. Chem.* **2007**, *45*, 3505–3512.

[245] G. Beamson, D. Briggs, et al., *High resolution XPS of organic polymers*, Wiley, **1992**.

[246] M. Kaupp, T. Tischer, A. F. Hirschbiel, A. P. Vogt, U. Geckle, V. Trouillet, T. Hofe, M. H. Stenzel, C. Barner-Kowollik, *Macromolecules* **2013**, *46*, 6858–6872.

[247] G. Mantovani, F. Lecolley, L. Tao, D. M. Haddleton, J. Clerx, J. J. Cornelissen, K. Velonia, *J. Am. Chem. Soc.* **2005**, *127*, 2966–2973.

[248] C. N. Urbani, C. A. Bell, M. R. Whittaker, M. J. Monteiro, *Macromolecules* **2008**, *41*, 1057–1060.

[249] J. T. Lai, D. Filla, R. Shea, *Macromolecules* **2002**, *35*, 6754–6756.

[250] F. Hua, X. Jiang, D. Li, B. Zhao, *J. Polym. Sci. Part A: Polym. Chem.* **2006**, *44*, 2454–2467.

[251] J. O. Mueller, F. G. Schmidt, J. P. Blinco, C. Barner-Kowollik, *Angew. Chem. Int. Ed.* **2015**, *54*, 10375–10375.

[252] A. Alberti, M. Benaglia, M. Laus, K. Sparnacci, *J. Org. Chem.* **2002**, *67*, 7911–7914.

[253] T. K. Panda, M. T. Gamer, P. W. Roesky, *Organometallics* **2003**, *22*, 877–878.

Abbreviations

AA	acrylic acid
ADIBO	aza-dibenzocyclooctyne
AFM	atomic-force microscopy
ARGET	activator regenerated by electron transfer
ATRA	atom transfer radical addition
ATRP	atom transfer radical polymerization
CD	cyclodextrin
CMC	critical micelle concentration
Cp	cyclopentadienyl
CRP	controlled radical polymerization
CSIRO	Commonwealth Scientific and Industrial Research Organization
CTA	chain transfer agent
CuAAC	cooper(I)-catalized azide-alkine cycloaddition
DCC	*N*,*N*'-dicyclohexylcarbodiimide
DCM	dichloromethane
DLS	dynamic light scattering
DMAc	*N*,*N*-dimethylacetamide
DMAEMA	*N*,*N*-dimethylaminoethyl methacrylate
DMAP	4-(dimethylamino)pyridine
DMP	2-(((dodecylthio)carbonothioyl)thio)-2-methyl-propanoic acid
DP	degree of polymerization
dRI	differential refractive index
EA	ethylacetate
ESI-MS	electrospray ionisation mass spectrometry
EWG	electron withdrawing group

FMO	frontier molecule orbital
FRP	free radical polymerization
HDA	hetero Diels-Alder
HEA	hydroxyethyl acrylate
HEPES	4-(2-hydroxyethyl)-1-piperazineethanesulfonic acid
HOMO	highest occupied molecular orbital
HT	high temperature
IUPAC	International Union of Pure and Applied Chemistry
k_a	activation rate coefficient
k_{add}	addition rate coefficient
k_β	β-scission rate coefficient
k_{da}	deactivation rate coefficient
k_{frag}	fragmentation rate coefficient
k_p	polymerization rate coefficient
k_t	termination rate coefficient
DIBO	dibenzocyclooctyne
DIFO	difluorinated cyclooctyne
L	ligand
LCST	lower critical solution temperature
LUMO	lowest unoccupied molecular orbital
MIMIC	micromolding in capillaries
MO	molecular orbitals
MS	mass spectrometry
NaCp	sodium cyclopentadienyl
NIPAM	*N*-isopropyl acrylamide
NITEC	nitrile imine mediated tetrazole-ene cycloaddition
NMP	nitroxide mediated polymerization
NMR	nuclear magnetic resonance
P4VP	poly(4-vinylpyridine)

PAA	poly(acrylic acid)
PDMS	poly(dimethylsiloxane)
PEA	poly(ethyl acrylate)
PEO	poly(ethylene oxide)
PHEA	poly(hydroxyethyl acrylate)
P(I-*co*-S)	poly(isoprene-*co*-styrene)
PLLA	poly(*L*-lactide)
PMMA	poly(methyl methacrylate)
PS	polystyrene
PNA	peanut agglutinin
PTEGA	poly(triethylene glycol methyl ether acrylate)
RAFT	reversible addition-fragmentation chain transfer
rDA	retro Diels–Alder
RDRP	reversible-deactivation radical polymerization
R_h	hydrodynamic radius
SEC	size exclusion chromatography
SEM	scanning electron microscopy
SNIPS	self-assembly and nonsolvent induced phase separation
SPAAC	strain-promoted azide-alkine cycloaddition
TCB	1,2,4-trichlorobenzene
TEGA	triethylene glycol methyl ether acrylate
TEMPO	2,2,6,6-tetramethyl-1-piperidynyl-*N*-oxy
TFA	trifluoroacetic acid
THF	tetrahydrofuran
ToF-SIMS	time-of-flight secondary ion mass spectrometry
UV-Vis	ultraviolet-visible
wt	weight
XPS	X-ray photoelectron spectroscopy

List of Figures

List of Tables

List of Schemes

Curriculum Vitae

The Curriculum Vitae is not shown in the online version of the document.

Publications and Conference Contributions

Peer Reviewed Publications

1. *Amphiphilic Block Copolymers Featuring a Reversible Hetero Diels–Alder Linkage*

   Langer, M.; Brandt, J.; Lederer, A.; Goldmann, A. S.; Schacher, F. H.; Barner-Kowollik, C. *Polym. Chem.* **2014**, *5*, 5330–5338.

2. *Fast and Simple Preparation of Patterned Surfaces with Hydrophilic Polymer Brushes by Micromolding in Capillaries*

   Vonhören, B.;[*] Langer, M.;[*] Abt, D.; Barner-Kowollik, C.; Ravoo, B. J. *Langmuir* **2015**, *31*, 13625–13631.

3. *α, ω-Reactive Building Blocks Based on a Dual Functional RAFT Agent for Thermal and Light-Induced Ligation*

   Langer, M.; Mueller, J. O.; Goldmann, A. S.; Schacher, F. H; Barner-Kowollik, C. *ACS Macro Lett.* **2016**, *5*, 597–601.

Conference Contribution

1. *A Novel Concept for the Design of Block Copolymer Membranes via a Modular Chemical Ligation Approach*

   M. Langer, C. Hörenz, C. Pietsch, A. S. Goldmann, F. H. Schacher, C. Barner-Kowollik **The International Chemical Congress of Pacific Basin Societies 2015**, Honolulu, Hawaii, **USA**. Poster presentation.

[*] V. B. and M. L. contributrd equally.

Acknowledgements

Zu erst gilt mein Dank natürlich meinem Doktorvater, Prof. Dr. Christopher Barner-Kowollik. Neben der Tatsache, dass er mir ermöglicht hat, in seiner Gruppe zu promovieren, bin ich vor allem für das entgegengebrachte Vertrauen in meine eigenen Fähigkeiten dankbar und die Freiheit eigene Ideen in die Forschungsprojekte einzubringen und zu verwirklichen. In diesem Zuge möchte ich mich auch noch für das Vermitteln der Kontakte danken, die zu meiner zukünftigen Postdoc-Stelle an der RTWH Aachen geführt haben.

Diese Arbeit wurde durch das Bundesministerium für Bildung und Forschung (BMBF) unter der Fördernummer 31P7233 finanziell gefördert und entstand im Rahmen des Kooperationsprojektes *BioCoBra* vom AK Barner-Kowollik und dem AK Schacher (Universität Jena). In diesem Zusammenhang möchte ich mich bei Prof. Dr. Felix Schacher (Jena), Dr. Anja Goldmann (KIT), Dr. Christian Pietsch (Jena) und Christoph Hörenz (Jena) für die fruchtbaren wissenschaftlichen Diskussionen bedanken. Außerdem danke ich allen Jenanos für die tolle Gasfreundschaft während meines Aufenthalts in ihrem Arbeitskreis.

Bei den Kooperationspartnern außerhalb der *BioCoBra* bedanke ich mich ebenfalls für die hervorragende Zusammenarbeit. Namentlich sind das Josef Brandt und Dr. Albena Lederer vom Leibniz-Institut für Polymerforschung in Dresden, Banjamin Vonhören und Prof. Dr. Bart Jan Ravoo von der Westfälischen Wilhelms-Universität Münster und Doris Abt und Dr. Jan Ole Müller aus unserer eigenen Gruppe.

Ein besonderer Dank gilt Dr. Sylvain Grosjean, Dr. Elise Deniau, Dr. Mirela Zamfir, Dr. Nicolas Zydziak, Dr. Hatice Mutlu, Birgit Huber und Florian Feist, die mich während meiner Zeit im Soft Matter Synthesis Lab begleitet und mit Rat und Tat unterstützt haben. Ein großes Dankeschön geht auch an Dr. Leonie Barner, die immer für bestmögliche Arbeitsbedingungen im Soft Matter Synthesis Lab gekämpft hat (schade, dass ich den

ersten Sommer mit funktionierender Klimaanlage nicht miterleben konnte) und meine Dissertation Korrektur gelesen hat.

In der letzten Phase meiner Doktorarbeit (dem Zusammenschreiben) wurde ich herzlichst von Tanja Claus, Carolin Heiler, Paul Lederhose, Rouven Müller, Kai Pahnke und Markus Zieger in der Westhochschule aufgenommen, vielen Dank dafür. Noch mal besonders möchte ich mich bei Rouven für die Unterstützung beim Einrichten von meinem LaTeX-Dokument und den sonstigen Tipps und Tricks bedanken.

Allen ehemaligen und gegenwärtigen macroarc-Mitarbeitern möchte ich für die vielen wissenschaftlichen Anregungen und Diskussionen danken. Aber noch mehr, für die vielen geselligen Abende bei den BBQs, den Geburtstagen oder beim Doktorwagenbau. Es war mir eine Freude mit Euch zusammengearbeitet zu haben.

Zu guter Letzt will ich mich auch bei all jenen bedanken, die abseits der Arbeit immer für mich da waren und mich unterstützt haben. Bei meiner Familie, bei meinen Freunden, bei den Kollegen, die zu Freunden wurden, aber vor allem bei Dir, Sofia. Du hast mich schon seit dem Studium durch alle Höhen und Tiefen begleitet und nie an Mir gezweifelt. Dir allein gilt mein größter Dank.

Declaration

Ich erkläre hiermit, dass ich die vorliegende Arbeit im Rahmen der Betreuung durch Prof. Dr. Christopher Barner-Kowollik selbstständig verfasst und keine anderen als die angegebenen Quellen und Hilfsmittel verwendet habe. Wörtlich oder inhaltlich übernommene Stellen sind als solche kenntlich gemacht und die Satzung des Karlsruher Instituts für Technologie (KIT) zur Sicherung guter wissenschaftlicher Praxis wurde beachtet. Die elektronische Version der Arbeit stimmt mit der schriftlichen überein und die Abgabe und Archivierung der Primärdaten gemäß Abs. A (6) der Regeln zur Sicherung guter wissenschaftlicher Praxis des KIT ist beim Institut gesichert. Des weiteren erkläre ich, dass ich mich derzeit in keinem weiteren laufenden Promotionsverfahren befinde und auch keine vorausgegangenen Promotionsversuche unternommen habe.

Ort, Datum

Unterschrift